INAUGURAL-DISSERTATION

Zur
Erlangung der Doktorwürde
der
Naturwissenschaftlich-Mathematischen
Gesamtfakultät
der
Ruprecht-Karls-Universität
Heidelberg

Vorgelegt von
Julia Ricken (M. Sc.)
aus Göttingen

Tag der mündlichen Prüfung:
25. Januar 2019

Photo-Switchable Proteins for Cell-Matrix Adhesion

Gutachter:

Prof. Dr. Joachim P. Spatz
Prof. Dr. Dirk-Peter Herten

Abstract

The adhesion of cells to each other and to a scaffolding matrix is a major feature of multi-cellular organisms. Since misregulation can have fatal consequences, thereto related biological processes, such as wound healing, differentiation and embryogenesis, are tightly regulated in space and time. To get an understanding in these systems it is of big interest to generate dynamically regulated platforms. In order to dynamically and spatiotemporally control integrin-mediated cell adhesion to the extracellular matrix (ECM) several systems have been establish, which can be controlled by an outer stimulus. Nevertheless, these methods are limited by a variety of drawbacks like low resolution, the use of photo-toxic UV-light or tedious synthesis of chemical building blocks.

In this thesis, I present a novel optogenetic tool to control cell-matrix adhesion, combining in a new manner the approaches from material science with optogenetics. By incorporation of naturally occurring ligands for cell-matrix receptors, namely intergrins, like the RGD-sequence or the PHSRN-sequence into optogenetic proteins, they can be applied to mediated cell-surface adhesion. Surfaces coated with the engineered proteins can be switched either once or reversibly, by visible light in their ability to mediate cell adhesion.

First, I employed the green light switchable protein CarH from *T. thermophilus* in order to switch surfaces from an adhesive to a non-adhesive state. The protein monomers form tetramers when the cofactor Cobalamin is incorporated and disassemble into dimers upon green light illumination. By incorporation of the RGD motif into the protein a cell adhesive building block was generated that can be immobilized on surfaces. Upon disassembly of the tetramer, the monomers presenting the RGD motif to the cell are removed and the surface is switched to the non-adhesive state. In this work, I showed the immobilization of proteins on the surfaces as well as their ability to bind integrin and disassemble under green light in vitro. Further, I confirmed these results in cell adhesion experiments. For the first time, I designed and implemented a green light-switchable system for cell-surface adhesion based on altered ligand presentation.

In the second part of my thesis, I employed the blue light-switchable protein domain LOV2 from *A. sativa* to build a reversible system. This protein domain consists of a small protein core with a long C-terminal Jα-helix, which reversibly unwinds, when illuminated with blue-light. I generated a library of 40 LOV2RGD mutants by insertion of the RGD motif at different positions in the Jα-helix and by combination with further complementing mutations, like the PHSRN motif. The RGD peptide is caged by the helical conformation in dark and is presented to cells upon unwinding of the Jα-helix under blue light illumination. I have narrowed the library to 8 promising mutants through characterization of the ability of the LOV2RGD mutants to bind integrin in dark and under blue light illumination in fluorescence anisotropy measurements. The selected mutants were evaluated for their ability to mediate cell adhesion depending on their switching state, showing significant difference in the

spreading area of the cells. Additionally, I determined the reversibility of cell adhesion on such substrates. Finally, the most promising two candidates were evaluated in live cell experiments, showing a significant decrease in the spreading area in dark but not under blue light illumination.

In summary, I have designed and implemented two protein-based approaches for the dynamic control of cell adhesion using light of two different wavelengths. The green light-dependent CarH based system can be used to capture and release cells on command, whereas the LOV2 domain-based approach resembles natural timescales for adhesion and can therefore be used in investigations of signaling cascades or other processes involved in cell-matrix adhesion. In conclusion, the herein presented systems can overcome most of the existing drawbacks due to their sensitivity to visible light, their facile way to get produced in high amounts and their high spatial and temporal control.

Zusammenfassung

Die Adhäsion von Zellen zur extrazellulären Matrix (EZM) ist essentiell für die störungsfreie Funktion vieler Zellen. Daher ist die Interaktion von Zellen und ihrer Umgebung zeitlich und räumlich streng reguliert und unterliegt in Prozessen wie Wundheilung, Stammzelldifferenzierung und Embryogenese ständiger dynamischer Veränderungen. Fehlregulationen dieser Zell-Matrix Interaktionen können verheerende Folgen haben, wie z.B. die Entstehung von Krebs oder anderer unheilbarer Krankheiten. Aufgrund dessen sind für die Erforschung dieser pathologischen Prozesse synthetische EZM Systeme mit extern steuerbaren Eigenschaften interessant, die so einen Einblick in die zugrundeliegenden biologischen Prozesse ermöglichen. Zur dynamischen Steuerung der Zell-Matrix Adhäsion wurden bereits Systeme entwickelt, welche auf einen externen Stimulus wie z.B. Licht, Temperatur, Spannung oder pH reagieren. Vor allem Licht ist ein besonders geeigneter Stimulus, da es eine hohe zeitliche und räumliche Auflösung bietet, bioorthogonal ist und die Intensität variabel reguliert werden kann. Die Verwendung von photo-toxischem UV-Licht oder eine fehlende Reversibilität der Systeme sind immer noch große Herausforderungen in der aktuellen Forschung von extern-steuerbaren synthetischen EZM Systemen.

In dieser Arbeit habe ich durch die Kombination von Ansätzen aus der Materialwissenschaft und der Optogenetik Proteine entwickelt, mit denen sich die Zell-Matrix Adhäsion lichtgesteuert kontrollieren lässt. Die generelle Entwicklungsstrategie beruht auf dem Einbau von natürlich vorkommenden EZM Adhäsionspeptiden, wie die RGD-Sequenz oder die PHSRN-Sequenz, in optogenetische Proteine. Diese Proteine reagieren intrinsisch entweder mit Dimerisierung oder Konformationsänderung auf Licht. Dadurch wird die Interaktion

der Adhäsionspeptide in den Proteinen mit Rezeptoren der Zellen, den sogenannten Integrinen, abhängig von der Wellenlänge des Lichts.

Im ersten Teil meiner Thesis habe ich das lichtempfindliche Protein CarH aus *T. thermophilus* benutzt, um Zelladhäsion durch grünes Licht auszuschalten. Dafür habe ich die RGD-Sequenz an unterschiedliche Stellen in CarH eingefügt, welches im Dunklen eine tetramere Konformation einnimmt und durch Bestrahlung mit grünem Licht zerfällt. Zellen können an Oberflächen, die mit dem Tetramer beschichtet wurde, adhärieren und werden abgelöst, wenn das Protein, induziert durch grünes Licht, wieder zerfällt. Dieses System ist die erste synthetische EZM, die durch grünem Licht in ihrer Fähigkeit Zelladhäsion zu vermitteln schaltbar ist und stellt eine Alternative zu Systemen dar, die auf der UV-Licht spaltbaren Nitrobenzylgruppe basieren.

Im zweiten Teil meiner Thesis habe ich ein System entwickelt, welches reversibel zwischen einem adhäsiven und einen nicht-adhäsiven Zustand geschaltet werden kann. Dafür habe ich das blau-licht schaltbare Protein LOV2 aus *Avena sativa* verwendet. Dieses Protein besteht aus einem kleinen Proteinkern und einer langen C-terminalen Jα-Helix, welche sich reversibel unter blauem Licht entwindet. Durch Einbau von Zelladhäsion-Sequenzen in verschiedenen Kombinationen und Positionen innerhalb des Proteins habe ich 40 verschiedene licht-sensitive Mutanten zur Zelladhäsion generiert. Im Dunkeln sind die Bindesequenzen durch die helikale Konformation versteckt und können nicht von Zellen zur Adhäsion genutzt werden, während die entsprechenden Sequenzen durch die blau-licht induzierte Entwindung der Helix zur Adhäsion zugänglich werden. Durch die Bestimmung der Bindekonstanten der einzelnen Protein-Mutanten zu Integrin, im Dunklen und unter blauem Licht, konnten die Mutanten auf acht vielversprechende Variationen eingegrenzt werden. Zelladhäsionsstudien auf den jeweilig beschichteten Oberflächen zeigen in Bezug auf die Zelladhäsionsfläche eine signifikant bessere Zelladhäsion unter blauem Licht. Zusätzlich konnte die Adhäsion der Zellen im Dunklen verringert werden. Diese Ergebnisse demonstrieren die Möglichkeit, mit einem entsprechend veränderten optogenetischen Protein Zelladhäsion reversibel durch sichtbares Licht zu kontrollieren.

Zusammenfassend habe ich in dieser Arbeit basierend auf optogenetischen Proteinen zwei Systeme entwickelt, welche sich mit sichtbarem Licht schalten lassen. Dadurch lässt sich die Zell-Matrix Adhäsion reversibel mit hoher zeitlicher und räumlicher Auflösung steuern und viele der Nachtteile der bereits existierenden Systeme konnten überwunden werden.

Acknowledgments

I like to express my gratitude Prof. Joachim P. Spatz for giving me the opportunity to do my PhD in his group with all these wonderful members. I felt very comfortable here and always like a part of the group, especially at the group retreats in Antholz, which were always excellent in both perspectives, academically and personal. I am very thankful to Prof. Spatz and Dr. Seraphine Wegener that I was allowed to stay in Heidelberg, even when my sub-group moved to Mainz. Many thanks to Dr. Seraphine Wegner for the attractive topic of research, her supervision and guidance with the projects. Your faith in me to let me stay in Heidelberg without direct supervision meant a lot to me. Many thanks to PD Ada Cavalcanti-Adam to let me participate in her group seminars, which were a precious opportunity to get input from people around.

Many thanks to the actual and the former Mainz colleagues (Simge, Lisa, Solveig, Samaneh, Ilke, Tanya, Fei, DongDong and Marc) for letting me feel as an equal part of the wegner-group. Thank you for good scientific discussions, your help with the local administration and for your friendship.

I like to thank the colleagues from Stuttgart: even when we didn't meet often enough, I enjoyed your company during Antholz, the group seminars and the Wasen very much!

I like to thank the whole HD-Spatz with all its present and former members for amazing 4 years! I enjoyed having coffee or lunch breaks together, to fool around in the lab, have after work beer, barbecues in the sun and of course amazing times in Antholz! Thank you, officemates for updating me in sports, have "Doppelkekse" for the hangry times, having basketball challenges and answering my endless questions. But besides having these wonderful officemates, I made really good friends. Tina, Dirk, Chiara, Silvia, Rebecca, Maria and Marian, I will miss the time we spent together. And a special thanks to Rebecca for always having an open ear for everything, no matter if in personal or scientific matters, for proofreading the paper and a whole lot of the thesis. Your advice was and still is indispensable for me!

I also like to thank my interns Raoul, Anna, Mareike and Svenja with whom I really enjoyed working together.

Many thanks to my "chemist" friends Baucis, Basti, JFS, Yuri, Saskia, Benni, Anki, Lena and Melissa. Thank you for spending all the time in the lab and in the library with me, having thrilling kicker tournaments, lunch breaks and uncounted perfect evenings. You made my chemistry study an unforgettable journey! In same way, I want to thank my friends from home and my dear flatmates for distracting me from studying and for being my compensatory family.

Last but not least I want to thank my family Ruth, Martin, Elena and my husband Fabian for endless support, help and love! Thank you all very, very much!

Content

I. Introduction

1. Cell - Matrix Adhesion

The interaction between cells and their microenvironment, the extracellular matrix (ECM), is crucial for the regulation of cellular processes such as adhesion,[1] migration,[2] differentiation,[3] proliferation[4] and apoptosis.[5] To characterize basic principles in cell biology and also for potential medical applications it is necessary to precisely control the extracellular environment of cells. Cells mostly adhere to ECM proteins such as fibronectin, collagen, laminin and vitronectin via integrins,[6] heterodimeric plasma membrane receptors. In the following sections the major key player in cell-surfaces adhesion will be introduced.

1.1 The Extracellular Matrix

The ECM operates as a scaffold. Through the presentation of chemical and mechanical cues, the ECM influences and modulates cellular behavior. It consists of a variety of different proteins subdivided in two classes. These classes are fibrous proteins, like collagen and elastin, and glycoproteins, like fibronectin, proteoglycans and laminin (Figure 1.1). The respective monomers bear a variety of binding motifs, which are either directly recognized by integrins or linked to the cell via other ECM components, as e.g. fibronectin. The ECM does not only present adhesion motifs for cell adhesion but also actively form the tissue, influences the elastic properties of the tissue and regulates the availability of soluble factors, such as growth factors. Adhesion motifs are short amino acid sequences embedded in the ECM proteins, which can be recognized by integrins. Cells like fibroblasts secret ECM proteins, thereby remodeling the microenvironment, whereas other cells types rearrange the microenvironment by cleaving the ECM proteins.[7,8] Hence, the interaction between the ECM and the cell is dynamic and reciprocal.

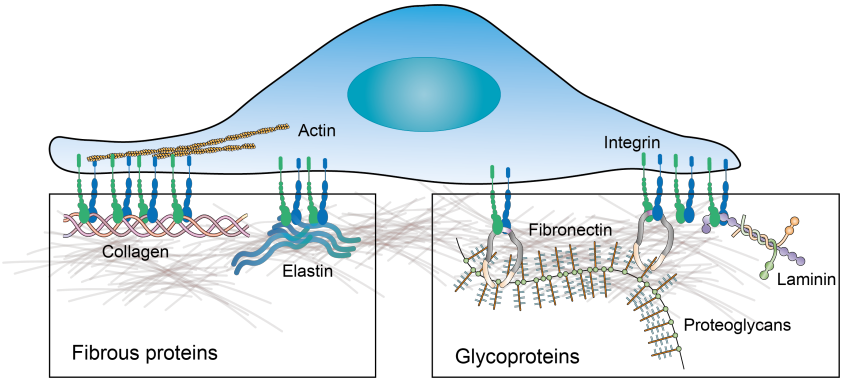

Figure 1.1: Cells and the ECM microenvironment. Cells adhere via integrins to two different classes of supramolecular polymers, the fibrous proteins and glycoproteins. Collagen, laminin, elastin and fibronectin directly interact with integrins, while proteoglycans are bound by fibronectin, connecting them to the cell. Intracellular parts of integrins link the ECM to the actin cytoskeleton. Parts adapted from Mouw et al.[1]

The major scaffolding protein is collagen but through the interplay with the other components, the ECM can dramatically change depending on the mechanic demands and functions of the tissue. Since fibronectin is a well-studied protein and features of

it will be used within this thesis,[9,10,37] the next section will focus on this protein and its characteristics enabling the adhesion of cell receptors.

1.2 Cellular Fibronectin

Cellular fibronectin (cFN) is encoded in a single gene, but due to alternative splicing 20 variants are known in human.[9] The protein is multivalent and has several binding sites for other ECM proteins, such as cellular fibronectin itself, growth factors and integrins.[9] Forming a folded dimer in solution, stabilized by disulfide bonds, it can be straightened into fibrils upon adhesion of fibroblasts. This exposes various additional binding motifs for ECM ligands (Figure 1.2a+c).[1] Cell-cFN interaction is driven by the binding of integrins to the III_{10} domain, containing the cell binding motif arginine-glycine-aspartic acid (RGD),[11,12] and to the synergistic site prolin-histidine-serin-arginine-asparagine (PHSRN) in domain III_9.[13,14] The latter, named the synergy peptide, is known to increase the affinity of integrin to RGD and thereby enhance cell-matrix adhesion.[15,16] The synergistic effect of PHSRN on integrin/RGD binding is highly dependent on the distance of the PHSRN motif to the RGD motif.[17-19] The highest synergistic effect is present at a distance of 35 Å (Figure 1.2b).[20-22]

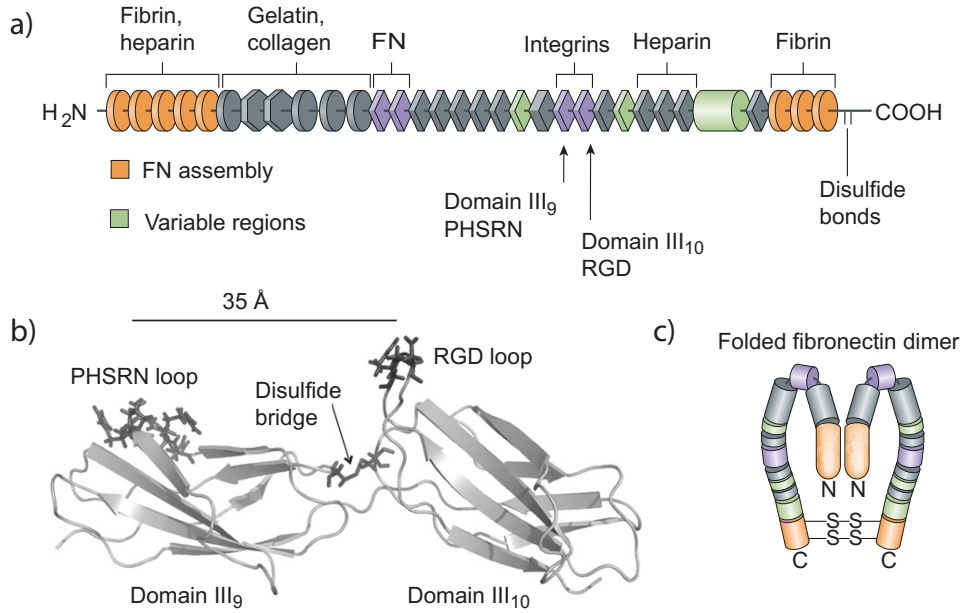

Figure 1.2: Sketch of fibronectin. a) Linear fibronectin monomer, showing binding sites for fibrin and heparin in organge, for gelatin, collagen and heparin in dark grey and for fibronectin and integrin in purple. The arrows indicated the regions of the PHSRN and the RGD motif. In light green the motifs which can be rendered by alternative splicing are shown. b) The binding motifs on the III_9 and III_{10} domain in cellular fibronectin exhibit a distance of 35 Å. c) Fibronectin exists in two conformations: As a stretched dimer by application of cellular forces driving fibril formation and as a globular dimer, hiding the fibrin and heparin binding sides. Adapted from Mouw et al.[23] and Kreiner et al.[24]

The cell and its respective microenvironment are in constant communication with each other, exchanging signals in both directions. These signals are transduced through cell-surface receptors, whereas the integrin family is the most prominent of them and will therefore be introduced in the following section.

1.3 Integrin-Mediated Cell-Matrix Adhesion

Integrins are transmembrane proteins, composed of two non-covalently associated subunits, α and β. From a pool of 18 α and 8 β subunits a family of 24 different integrins emerges upon heterodimerization in various combinations of the subunits.[6]

The subunits consist of a big extracellular domain, a transmembrane domain and a small but unstructured cytoplasmic domain. Both subunits have a single helix as the transmembrane domain, which are intersecting and forcing the integrin monomers in a bent, inactivated conformation (Figure 1.3, middle).[25,26] Upon binding of specific proteins, like talin, to the cytosolic tail of the β subunit, the interactions between the helices are overcome. Hence, the integrin take an upright, activated conformation (Figure 1.3).[27] This process is known as 'inside-out' signaling as the activation is achieved by the stimulus from the cytosol. Integrins can also be activated from the outside by binding of ECM proteins, Mn^{2+} ions,[28,29] and transmembrane proteins of other cells, as intercellular adhesion molecules (ICAMs) and E-Cadherins (titled as 'outside-in' signaling). So, integrins exhibit a bidirectional signaling function within the cell. Depending on the combination of the subunits, integrin binds to different adhesion motifs in the ECM proteins. The most prominent motif is the RGD sequence.[6]

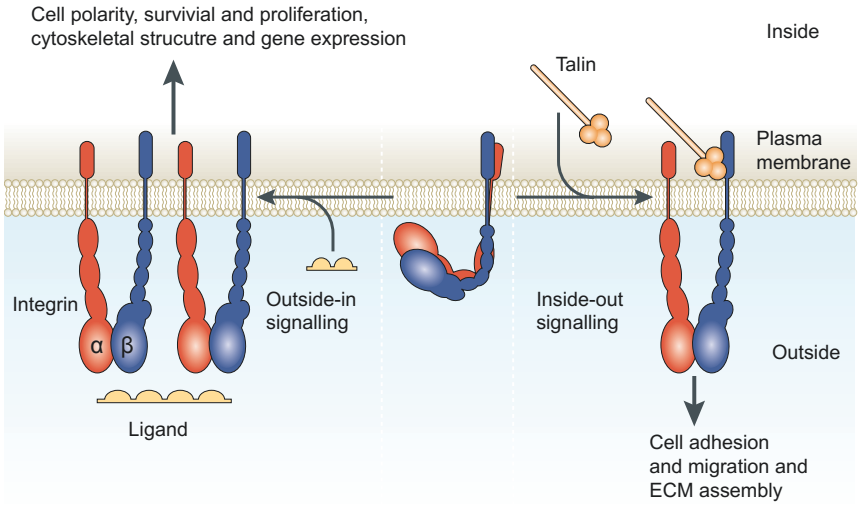

Figure 1.3: Bidirectional signalling of integrins. The Integrin heterodimer is deactive in its bent form (middle). Activation occurs via outside-in activation by binding respective ligands (left) or via inside-out activation through binding of talin to the cytosolic integrin tail (right). Scheme adapted from Shattil et al.[25]

1.4 The Clustering and Recycling of Focal Adhesions

To sense environmental stimuli, mechanical and chemical signals transduced by the ECM are converted into intracellular biochemical signals. Since integrins lack enzymatic activity, the signal needs to be transduced in other ways. This is achieved by the aforementioned conformational changes of integrins and by the thereby induced assembly of clustered adhesion complexes.[30] The formation of enlarged adhesion complexes called focal adhesions (FA) is induced upon outer stimuli. The first contact of a cell to an appropriate substrate induces small integrin clusters,

called nascent adhesions, with a lifetime of about 1 min. If the cell is able to strengthen these clusters, over 150 proteins can be recruited to the adhesion points, forming mature focal adhesions. These can exhibit a half-life of about 21 min. The entity of all enzymes and proteins involved are titled as the adhesome.[31] Because most of them are multi-domain ligands, they form a complex network of interacting proteins. Three major classes of proteins are assembled to the adhesome, or influenced by integrin-matrix binding. These are (1) cytoskeleton proteins, (2) adaptor proteins cross-linked with each other and (3) enzymes (Figure 1.4).[32] If the cell can form mature FA, polarize and migrate, the FA are in a continuous recycling. In the direction of migration new FA will emerge, whereas FA at the retracting cell site will be disassembled.

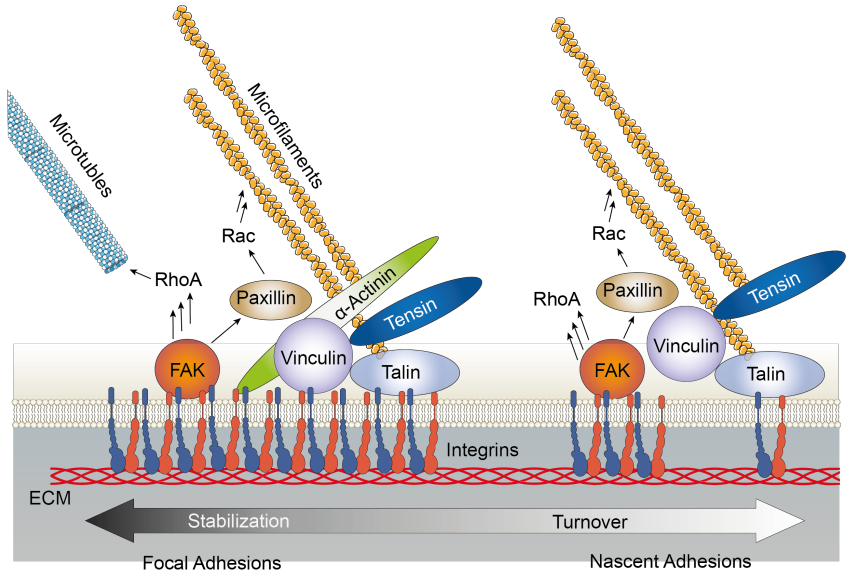

Figure 1.4: Sketch the equilibrium from nascent adhesions and the formation of mature focal adhesions with the simplified interplay of some FA-proteins. Adapted fromVicente-Manzanares et al.[33]

Not only ligand recognition alone is able to induce FA formation, but also mechanical input is recognized by integrins and transduced to the adhesome, initiating signaling cascades.[34] Talin is one of the earliest proteins localizing at the intracellular integrin tail during initial adhesion formation. When the adhesion sites assemble, cells apply endogenous tension to the ECM. If the forces thereby exceed a certain threshold value,[35] unfolding of talin can be initiated, which allows vinculin to bind and nascent adhesions can maturate.[36] The presence of vinculin can therefore be an indicator of the formation of FAs and transduction of cellular forces through integrins.[37] In mature FAs, zyxin is recruited among many other proteins to further strengthen the interactions with the actin cytoskeleton.[38] Since adhesion sites are highly dynamic, the turnover and recycling of integrins play an important role.[39] Recycling of integrins affects inactivated as well as activated integrins. It largely varies between cell types and integrin types,[39,40] but is a comparably fast process with an average half-life of less than 15 min.[41,42]

Loss of ECM contact induces in most cell types a special type of apoptosis, called anoikis.[43] This protecting mechanism is one of the key players for tissue integrity. Alterations in the expression levels, the recycling or in the distribution of integrins do often interfere with this mechanism, leading to a variety of diseases. Systems such

as the cardiovascular system, the dermatological system, the immune system, the muscle and the skeleton system can develop severe diseases by disturbance of the sensitive balance between the afore mentioned factors.[44] In addition, cancer metastasis[3] is highly dependent on the expression levels and types of integrins. Since the influence of integrins on the whole organism itself cannot be narrowed, their involvement in various pathways and malfunctions is of enormous interest to the scientific community and their potential as a therapeutic target is being investigated.[45,46]

1.5 The Regulation of Integrin-ECM Interactions

The regulation of integrin-ECM interactions play a major role in cell adhesion,[1] migration,[2] differentiation[3,47] and apoptosis.[5] Therefore, integrin to matrix adhesion is highly important in immune response,[48] wound healing[49,50] and cancer progression.[3] In wound healing the wounded site is plugged by a fibrin clot forming a provisional matrix. The migration of keratinocytes and fibroblast into the wound site is stimulated by soluble factors, but also by the ligands presented from the provisional ECM. Cells migrate upon signals of certain adhesion ligands and deposit new ECM proteins, leading to altered signaling patterns for following cells. These patterns are highly specific for different stages in the healing process.[51] To characterize influencing factors in processes like wound healing in detail, it is of utmost interest to generate minimal systems to specifically assess distinct signals.

The influence of ligand type and spacing[52-54] of the presented ligands on cell adhesion and migration has been studied in great detail.[15] These studies show that not only the spatial presentation of the ECM-cell interactions is important, also the time in which the cell can interact with specific ECM ligands is a crucial factor. Therefore dynamic systems able to tune ligand type or density in a spatiotemporal manner are of high interest.[55,56] This can be achieved by combination of stimuli-responsive building blocks (reacting to stimuli like voltage, light, heat or chemicals) with ligands for cell-surface interactions. In the next chapter a brief overview of surfaces applying external stimuli for alternation in ligand presentation in general, and a deeper insight into light-responsive systems, in particular is given.

2. Switchable Surfaces for Cell Adhesion

2.1 Stimuli-Responsive Surfaces

Synthetic biomaterials for biomedical applications have evolved from completely cell inert to more complex systems over the last decades to adequately model the natural ECM. Since, the effects of ligand composition, spacing, density and patterning was already investigated,[57,58] the dynamics of natural ECM is not yet achieved with synthetic systems. Especially the spatiotemporal changes of ligands within the ECM still lacks sufficient model systems. Therefore, surfaces responding to an external stimulus are becoming the main focus of tissue engineering approaches (Figure 2.1).[59,60]

To build efficient stimuli-responsive surfaces for cell adhesion, three elements are essential: i) an external stimulus, which function as a trigger like light, voltage, heat, or chemicals, ii) a recipient of the stimulus, which transforms or transduces the stimulus, iii) a building block mediating cell adhesion. To ensure an error free input-output correlation, surfaces conceived for stimulus-responsive cell adhesion have to present the chosen cell adhesion ligands but be cell inert otherwise. Self-assembled monolayers (SAMs) that are cell inert and can be functionalized with a ligand of choice is a broadly used to achieve a specific cellular response upon surface alteration. Alteration of the cell adhesion ligands or their exposure to the cells in response to stimuli, is the most direct and facile approach to control or modulate cell adhesion.

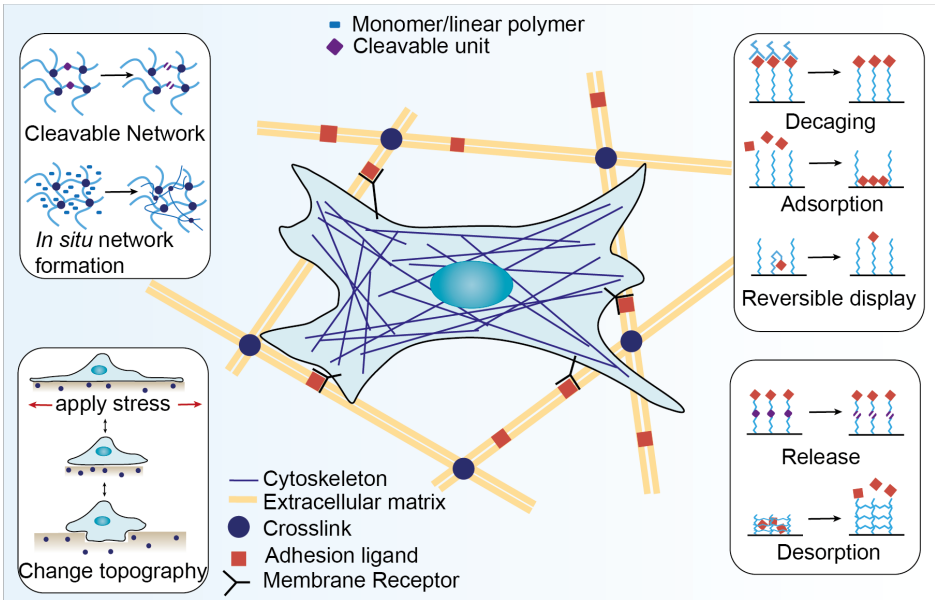

Figure 2.1: Overview of possible stimuli-responsive modifications of the ECM for altering cell adhesion. Alteration of meshsizes of gel based models of the ECM, altered ligand presentation, alteration of the force and/or stiffness of the synthetic ECM. Adapted from Kim et al.[61]

2.2 Light-Responsive Surfaces

Cell adhesion has been altered in response to voltage,[62,63] heat,[64,65] chemicals[66-68] and light,[56,69,70] but light as a stimulus provides outstanding advantages compared to other stimuli. First and most importantly, light is the only stimulus providing both high spatial and temporal resolution over the controlled interaction (Table 1). This feature makes light the most preferred stimulus for responsive surfaces to control cell-matrix adhesions. Beside the spatiotemporal control, light controlled interactions make it possible to tuned interactions by altering light intensities or illumination durations and to control them noninvasively for most wavelengths of light. Further, different wavelengths of light can be used to trigger different interactions orthogonally. Light-responsive systems to control cell adhesion are typically based on small photo-responsive molecules (with several exceptions). In the following chapter, the systems for light-induced control of cell adhesion will be reviewed and discussed for their potential and possible disadvantages.

Table 1: Possible external stimuli to alter stimuli-responsive surfaces. Red background color indicates no or little resolution, yellow indicates limited resolution and green indicates the possibility of subcellular resolution.

Stimulus	Spatial Resolution	Temporal Resolution
Heat	Limited to the nanorod size	Need relaxation time
Voltage	Limited to the electrode size	Yes
Chemicals	No	No
Light	Yes	Yes

2.2.1 Controlling Cell Adhesion with UV-light

Photo-Cleavable Systems to Control Cell Adhesion

One of the most widely integrated molecular building block as the stimuli recipient is the nitrobenzene moiety or related functional groups, which can be photo-cleaved upon UV-light illumination. By incorporating nitrobenzene groups into synthetic ECMs or surface coatings, their cell adhesive properties can be altered via light-induced transformation of the nitrobenzene moiety. Different designs allow to either render cell adhesive surfaces cell inert or vice versa.[71]

One design strategy is to use the nitrobenzyl group as a linker between the surface and a self-assembled monolayer carrying a cell-repellent poly(ethyleneglycol) (PEG). PEG is highly protein repellent and therefore prevents the adsorption of ECM proteins like fibronectin segregated by the cell and thereby the adhesion of the cell. Upon light illumination, the PEG group together with the nitrobenzyl is removed and the underlying surface is exposed. In cell culture, the newly exposed surface is likely to be covered by ECM proteins deposited by the cell. In addition, the surface can be functionalized through the unspecific adsorption of proteins from the serum,[72,73] or polylactic acid (PLA)[74] or the binding of His-tagged proteins to revealed nitrilotriacetic acid (NTA)[75] groups. As a result, the surface can be altered from a cell inert state to a cell adhesive state. The nitrobenzyl group can either be attached to

glass surfaces through a silane or to gold surfaces through a thiol group.[75] Such designs have been used to study the dependency of collective cell migration on geometric confinements and revealed that the geometry of the cell adhesive pattern influences the formation of leader cells.[76] Drawback of this design, where the nitrobenzene is used as a linker to remove a PEG group in response to light, is that the final composition of the exposed surface is not precisely controlled since it relies on secondary adsorption of molecules and can change with time (Figure 2.2).

A more defined way to turn on cell adhesion is by utilizing nitrobenzyl groups as caging groups on cell adhesion peptides. Several adhesion peptides including RGD peptide, the cyclic RGD[77,78] peptide and the laminin mimetic peptide have been photo-caged in this manner. In the first report by Petersen et al., the aspartic acid of the cRGD motif was photo-caged with an nitrobenzyl group, thereby blocking the cellular recognition by integrins. Upon UV-light illumination, the removal of the nitrobenzyl group resulted in the binding of integrins and the adhesion of cells. In the same study, confined cell patterns could be produced and retained for six hours.[79] Analysis of the photolytic reaction of the compound revealed that an illumination time of 15 min was needed to fully deprotect the peptide. The long UV exposure is a clear disadvantage for cell viability, but allows to alter the extend of uncaging depending on the illumination time. Although the affinity to integrin ($\alpha_v\beta_3$) increased six-fold upon decaging, surfaces already mediate cell adhesion in the caged state.[80] However, for some cell types, like Human umbilical vein endothelial cells (HUVEC), the caged compound exhibits sufficient protection from unspecific adhesion even after 24 hours. This allowed using this compound to study the migration of HUVEC cells in wound healing assays. Photo-caged surfaces for wound healing assays form an improved platform additionally to the standard techniques, since it avoids damaging of cells (like in the case for scratch assays).[81]

Photo-caged peptides were used to spatiotemporally modulate cell response through the dynamic remodelling of their microenvironments. For example, the cell adhesion ligand density at specific time points has a major influence on the differentiation of primary cell lines. C2C12 is a fast differentiating cell line, which enables the modeling and investigation of the role of adhesion in differentiation. Cells were cultured on surfaces coated with 20 % caged cRGD compound and 80 % normal cRGD linker. The level of basal cRGD was increased at different time points after cell seeding by uncaging of the protected groups and the degree of myogenic differentiation was measured. Decaging during the first six hours led to a significant increase in differentiation. Whereas decaging after six hours showed no myogenic differentiation of C2C12 cells.[82] Controlled differentiation of stem cells on surfaces was also achieved by Han et al. with a specific peptide (Pro-Phe-Ser-Ser-Thr-Lys-Thr-Cys; PFSSTKTC) instead of RGD for mesenchymal stem cells (MSCs) adhesion. Upon exposure of the ligand, induced by illumination, the peptide enabled osteogenic differentiation, which was confirmed by staining of the obtained tissue for calcification.[83] Specific caged ligands were not only synthesized for stem cell differentiation, but also for certain integrin types. A specific peptide for $\alpha_5\beta_1$ integrins was successfully caged and released, building a powerful tool to investigate the role and the dynamics of $\alpha_5\beta_1$ integrin in processes like migration.[84] Caging of laminin peptidomimetics led to directed neuronal growth on hydrogels

functionalized with the respective compound upon ligand activation.[85] Caged cRGD was also used in hydrogel patches implanted in mouse models, showing an increase in vascularization of biomaterials upon presentation of the adhesion peptide by UV-light illumination (Figure 2.2).[86] The photo-caged compound was not only successfully applied in hydrogels, but also in poly-L-Lysine films,[87] in peptide gels[88] and in PEG-based[89] hydrogel systems. This provides a versatile platform of substrates to build 2D and 3D scaffolds with the ability of light-tuned cell adhesion on softer tissues.

Switching surfaces from cell adhesive to inert is also possible by using nitrobenzyl groups as linkers between cell adhesive ligands and cell inert PEG coatings. Examples where the cell adhesive ligands were removed photo-chemically include cRGD,[90] antibodies[91] and biotin.[92] For instance, photo-patterned biotins were used to immobilize any kind of biotinylated antibody through a streptavidin linker. Thereby, specific immune cell types were immobilized via antibody-receptor interactions and released when the surface linker is decomposed by UV-light. In addition to the need of UV-light for decaging and the lack of reversibility, the decaging efficiency highly depends on the caged compound and the surrounding system. Therefore, all new compounds need to be elaborated for their decaging behavior.[93]

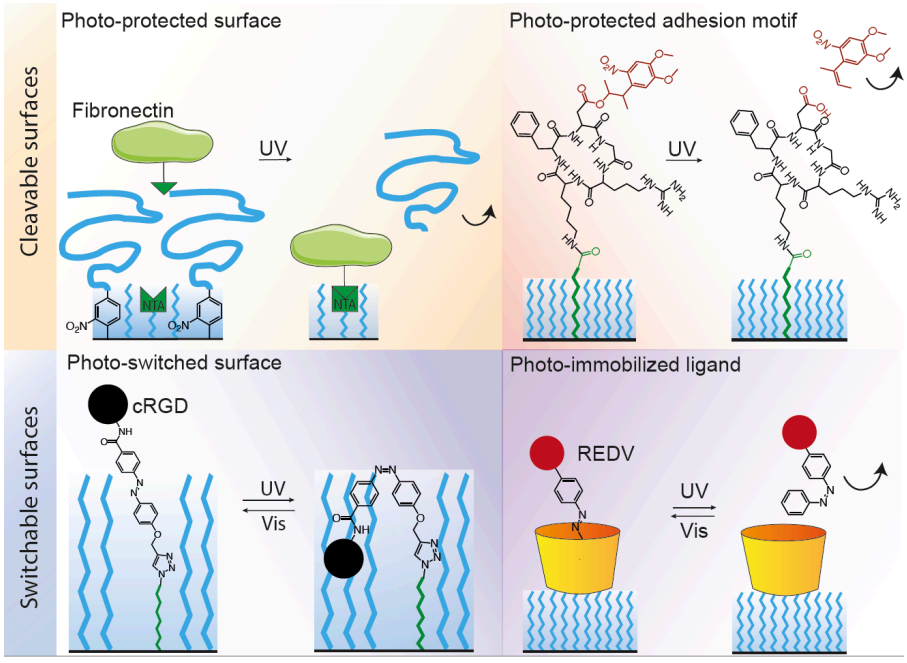

Figure 2.2: Exemplary UV-light responsive surfaces. Nitrobenzyl photo-protected surface linkers, with either a) PEG as a cell inert coating or b) caged cRGD. Photo-switchable surface coatings based on c) azobenzene switching alone or in combination with cyclodextrin as a d) host-guest complex. Adapted from Nakanishi et al.[75] Petersen et al.[79], Kadem et al.[94] and Ren et al.[95]

The systems mentioned above already provide a versatile toolbox to engineer light responsive surfaces to investigate cellular processes related with cell adhesion. One of their major drawbacks of photo-caging groups is the lack of reversibility. Surface properties can be altered only once between the cell inert and cell adhesive state in the direction of choice, which does not resemble the natural dynamics of cell to matrix adhesion.

Reversibly Switchable Systems to Control Cell-Matrix Adhesion

To overcome the drawback of photo-caging systems, reversibly photo-switchable functional groups can be used as light responsive building blocks. One of the most widely used molecules for photo-switching are azobenzenes, which as a core structure have two phenylrings bridged by two doubly bound nitrogen atoms. Most azobenzenes switch from the *trans* to the *cis* conformation under UV light illumination (365 nm) and relax back either thermally or under blue light (450 nm) illumination. The *cis* to *trans* conformational change induces a change of the end-to-end distance of the azobenzenes of about 3.5 Å.[96] Incorporation of the azobenzene moiety into polymer films allowed displacement of attached groups out of the surface plane by switching azobenzene into the *cis* state and thereby hiding the attached group in the polymer film.

Cell adhesion was successfully rendered photo-switchable by the incorporation of the azobenzene moiety into linkers between PEG films and RGD motifs.[97] Surfaces covered with a cRGD or linear RGD functionalized azobenzene, can be switched from the cell adhesive *trans* state to the cell inert *cis* state and back as shown in cell experiments.[98,99] Furthermore, atomic force microscopy (AFM) measurements showed that the cell adhesion force is different to the *cis* than to the *trans* state.[94] In a related study also modified azobenzenes that can be switched to the *cis* state with green light were used, which reduces photo-toxic effects on cells. It could be monitored that pulsed integrin activation by high frequency switching between the *cis* and *trans* state, upregulated the early expression of adhesion-associated protein encoding genes.[100] Similarly, the adhesion not through integrins but also other cell receptors can be controlled by changing the attached molecule. For instance, different cell types that express galactose and mannose specific receptors (asialoglycoprotein receptor and mannose receptor, respectively) could be specifically captured and released by attaching the respective sugars to the azobenzene linker. [101] In theory, other ligands, like antibodies, could also be switched with azobenzene as described above, but the efficiency is surely highly dependent on the size of the attached group and its incorporation into the polymer film.

An alternative strategy to overcome the problem of insufficient caged residues, is the use of host-guest interactions (Figure 2.2). The designs using host-guest interaction are based on the fact that the *trans* conformation of azobenzene can intercalate into large organic compounds like cyclodextrin (CD). Upon *cis* isomerization, the kinked azobenzene structure cannot be hosted by the cyclodextrin anymore and hence, it is released. When adhesive ligands are linked to *trans* azobenzene, they can be immobilized on a CD coated surface and thereby mediate cell adhesion. Upon UV-light illumination the azobenzene switches to the *cis* conformation and the adhesive ligand is displaced from the surface. Exemplarily linking the RGD motif to the azobenzene allowed to control the adhesion of Hela cells.[102,103] If more selective ligands are linked to the azobenzene, specific cell types can be captured out of a mixture of cell types, monitored and released on demand. Bian et al. utilized aptamer (molecule-selective DNA oligonucleotides) functionalized azobenzenes, to

specifically captured MCF-7 cells.[104] Likewise, Ren et al. attached the endothelia cell specific peptide, arginine-glutamic acid-aspartic acid-valine (REDV) to azobenzene and captured endothelia cells.[95] By light-induced stepwise release of the azobenzene ligand from the host-guest complex, the migration speed could be correlated to the ligand-density-dependent adhesion force to the surface.

Bulky ligands do not sterically hinder the immobilization of azobenzenes in host-guest complexes. However, upon displacement from the host, the azobenzene ligand is released and the surface needs to be recharged with the specific *trans*-azobenzene before it could be reused in cell experiments. This drawback was overcome by exchanging the location of the CD and the azobenzene linked adhesion ligand. Therefore, the azobenzene is immobilized covalently on the glass surface and the CD was attached via a lipid anchor to the cell membrane. This anchor is self-assembling within the cell membrane, coating the cells with a cyclodextrin shell. In the *trans*-conformation of azobenzene, the cells can be immobilized via the host-guest complex formation in the interface between the cell membrane and surface and released with UV-light induced ligand displacement.[105]

The introduced nitrobenzene and azobenzene based systems are already capable of controlling dynamically cell adhesion with light and the azobenzene based systems are even capable of doing so in a reversible manner. However, the employed wavelengths are almost exclusively UV-light bearing the risk of photo-toxicity to the cells. UV-light exhibit additionally low tissue penetration, making it impossible to employ these photo-switchable systems for medical applications. Therefore, it is of great interest to avoid UV-light and shift to longer wavelengths exhibiting deeper tissue penetration and less photo-toxicity.

2.2.2 Near Infrared (NIR)-Light Responsive Surfaces

In order to reduce the energy of the incident light, longer wavelengths combined with upconverting nanoparticles (UCNP) or surface coatings were employed. These materials can accept two or more photons of low energy light and emit a photon with high energy. Therefore, UCNP can be irradiated with NIR-light, which is then converted to light of shorter wavelengths, mostly UV-light, and emitted in a confined radius around the nanoparticle. The locally emitted UV-light can interact with photo-cleavable or other UV-light responsive groups without exposing the whole surface with UV-light, thereby reducing the risk of photo-toxic effects on cells.

By combination of UCNP with UV-light cleavable linkers, NIR-light induced photo-cleavable systems can be engineered. Based on this concept, Li et al. linked RGD-functionalized nitrobenzyl linkers to a gold nanorod functionalized surface. Fibroblast could recognize the RGD sequence and adhere to the surface. When the surface was illuminated with NIR-light, the light was upconverted by the nanorods to UV-light. Subsequently, the nitrobenzyl-linker was cleaved by the emitted UV-light and the number of adherent cells decreased five-fold. In contrast to the aforementioned photo-switchable systems, this system could be used in tissue

engineering since it exhibits a deeper tissue penetration of the used NIR-light compared to UV-light. At a tissue depth of 4 mm still 40 % of the original light intensity was retained whereas UV-light was only detectable with 10 % of the original intensity (Figure 2.3).[106]

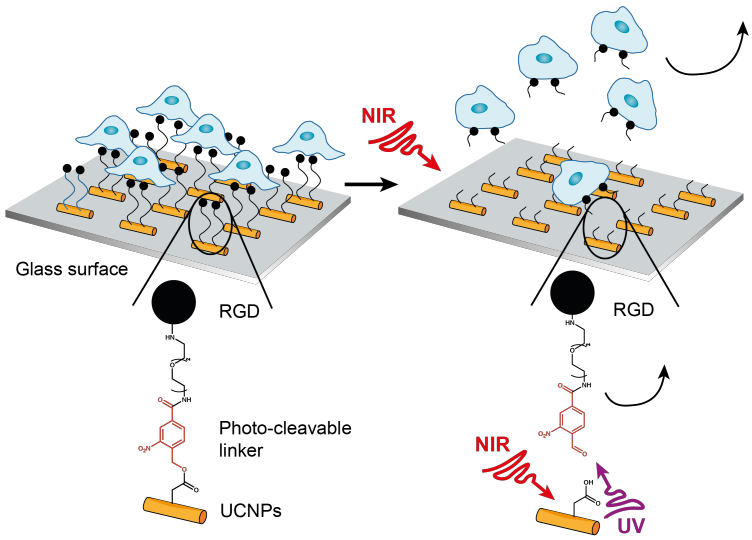

Figure 2.3: NIR-light photo-switchable surface with upconversion to confined UV-light illumination by gold nanorods. The UV-light cleaves the nitrobenzyl group and thereby the cell adhesion linker and the cells detaches from the surface. Adapted from Li et al.[106]

One of the main advantages of using light being its tunability, it can be applied in varying doses to the surface, leading to altered ligand density and thereby to changed signaling signals. Yan et al. used this features to control the adhesiveness of surfaces to directly regulate the differentiation of mesenchymal stem cells (MSCs) on photo-switchable surface. Therefore, they immobilized a photo-cleavable PEG combined with RGD-PEG on UCNP functionalized surfaces. The low density of RGD-PEG was enough to support the adhesion of MSCs. If the surfaces are kept in dark, the stem cells can interact with the RGD motif and thereby keep their multipotency. If the nanorods are illuminated with low power NIR-light, just some of the photo-cleavable PEG-groups are released, leading to higher number of cell adhesion points to the substrate in comparison to cell-inert PEG and thereby to a differentiation of the MSCs to adipocytes. When the surface is illuminated with high power NIR-light, all photo-cleavable PEGs are removed, revealing a very adhesive background. The exposure of the MSCs to a high percentage of adhesion molecules, induced the differentiation of the MSCs to osteoblasts.[107] This system already altered dynamically the exposure of different ligand densities to cells. However, the regulation is only possible in one direction since photo-cleavage of the linker can only occur once.

To circumvent this problem UV-light responsive photo-switchable linker can be combined with UCNP functionalized surfaces. Thereby the illumination with UV-light is avoided and a dynamically reversible system can be generated. Li et al. coupled a spiropyran terminated linker to upconverting nanoparticles in order to reversibly switch cell adhesion with long wavelength stimulation. Spiropyran is an

organic compound which exists in two polar isomerization forms, and can undergo reversible ring-closing and ring-opening interconversion. The closed-ring isoform is neutral and therefore lipophilic, whereas the open-ring isoform is a zwitterion and therefore hydrophilic. The interconversion to the open form can be initiated by UV-light, whereas light of longer wavelength lead to conversion to the closed form. Combination of this feature with UCNP coated surfaces, generates surfaces which can be reversibly switched between the two isomerization forms by application of NIR-light. The neutral, lipophilic form favors the deposition of ECM proteins from the cell or the serum and thereby cell adhesion. By irradiation with high energy NIR-light, resulting in surface material induced upconversion to UV-light, the spiropyron isomerizes back to the zwitterionic open ring, and therefore hydrophilic form. The hydrophilic form is protein repellent, which leads to detachment of adsorbed proteins and cells. The number of HeLa cells adhered to such surfaces decreased 5-fold upon conversion from the neutral to the zwitterionic isoform. It was shown that these surfaces can be switched about twenty times without efficiency loss, but since cell adhesion here depends on the deposition of proteins from the medium, the adhesion mediating layer is not characterized and therefore hard to control.[108]

Upconverting nanoparticles convert high energy NIR-light to short wavelength light. However, they also exhibit the capability of generating heat with low energy NIR-light, based on the photo-thermal effect. This can be used to indirectly alter cell adhesion with heat. Therefore, either the heat induced detachment of protein layers deposited of the cell or from the serum can be applied or specific heat responsive systems like DNA (and their assembly of the complementary strands) or the polymer poly(N-isopropylacrylamide) (pNIPAM) can be coupled to UCNP functionalized surfaces and thereby regulated indirectly with light.

If cells are cultured on glass surfaces they will segregate ECM proteins and thereby generate a matrix to adhere to. This is only possible if the surfaces are not protein repellent, as in the case of PEG coated glass. Not only the surface coating is important for deposition of ECM proteins, but also the temperature. High temperatures lead to detachment of the adsorbed protein layer from the surface and thereby to detachment of the adhered cells, as shown by Giner-Casares et al. They produced an anisotropic gold nanostructured surface by coating gold nanoparticles on the surface and subsequent growth of these seed crystals. The generated topographic features of an anisotropic gold nanostructured surface promote cell adhesion in comparison to flat substrates. Illumination of the gold structured surface with low intensity NIR-light, led to local heat generation and thereby to detachment of the covering proteins and cells.[109] The system can be used to detach cell sheets from the surface, but relatively long illumination times (up to 40 min) are needed to detach the cell layer.

To more precisely alter the ligand presentation to the cells, DNA strands can be used. DNA strands assemble with their complementary strand, but upon a specific temperature, called the melting temperature (T_m), the strands disassemble. This feature can be used to alter cell adhesion indirectly via heat by combination of DNA strands and UCNP. Therefore, one DNA strand is immobilized on UCNP coated surfaces, whereas to the complementary strand a ligand of choice is fused. The

complementary strand assembles with the immobilized DNA strand and thereby coat the surface with the respective ligand. The double strand was consequently disassembled by NIR-light induced local heat generation above the T_m, leading to release of the adhesion peptide and thereby of cells.[110,111] This solved the problem of nonspecific adhesion to ECM proteins deposited on the surface. However, the DNA complementary strands were diluted after release, causing the need of recharging the surface with the appropriate DNA before reuse.

Combination of upconverting substrates and immobilized thermal responsive building blocks can avoid ligand dilution. Polymers like PNIPAM react to heat with conformational changes. PNIPAM exhibit a brushed, hydrophilic conformation when kept below the critical solution temperature of 39 °C. When the temperature is increased above this critical solution temperature, the polymer collapses into a hydrophobic conformation. As aforementioned, proteins from cells or serum adsorb on lipophilic substrates, but not on hydrophilic. This effect was utilized by Cui et al. by functionalizing silicon nanowires covalently with the thermal responsive pNIPAM. If the surface is deactivated, the PNIPAM is hydrophilic and thereby protein and cell repellent. Upon NIR-light illumination, local heat will be generated by the photothermal effect of the silicon nanowires, leading to collapsed, hydrophobic pNIPAM. Upon hydrophobic-lipophilic interaction with the cell, cells were captured between the nanowires. Cells could be released when the surface was cooled below the critical temperature and the polymer take again the brushed, hydrophilic conformation. The surface could be switched twenty times effectively without performance reduction, but since the experiments were performed in fetal bovine serum (FBS) supplemented medium the deposition of ECM proteins cannot be excluded.[112] Also the cells are only captured by lipophilic interactions with the polymer, so no adhesion receptors are employed and cells cannot spread.

NIR-light responsive systems have the advantage to respond to long wavelengths but the systems are quite complex and the production of nanoparticles is not facile. In case of UV-light responsive systems the dose of UV-light can be reduced by employing upconverting materials, but not fully abandoned. Heat as a stimulus lack the advantages of the high spatial and temporal control of light and can have negative effects on cells when they are exposed too long. The development of facile, longer-wavelengths-of-light responsive surfaces, is therefore an ongoing research. Only a few systems responding to visible-light are contemporary known, which will be introduced in the following section.

2.2.3 Visible-Light Responsive Surfaces

There are only a few examples of controlling cell adhesion with visible light. One example is the aforementioned green-light switchable azobenzene covered surface, which was only established for push-pull activation of integrin,[100] and not tested for cell adhesion so far. The approaches to generate surfaces for visible light responsive cell-adhesion differ enormously and are facing still many drawbacks.

One possibility to alter cell adhesion with visible light was taken by Wang et al. They utilized, a boron doped silica surface, which was coated with collagen-I. Cells were grown on top, forming a cell sheet. Upon visible light illumination, the electron deficient boron enrich electrons, thereby gathering negative charge and consequently leading to desorption of the covering protein layer including adherent cells.[113]

Another light-responsive surface responding to visible light, is based on a dopamine related molecule, which can switch between a hydrophobic, open form and a zwitterionic, closed form by visible light. Surfaces functionalized with this compound can either be hydrophilic so that they are protein repellent and cell inert, or a hydrophobic so that cells seeded on top can segregate ECM proteins and adhere to the surface. Upon green light illumination, the compound switches to the hydrophilic form, leading to detachment of adsorbed proteins and cells. The compound can be switched back in dark it can and the cell attractive state can be recovered. The compound is stable for up to eight switching cycles. A major disadvantage is that the surface needs to be switched back to the lipophilic conformation in toluene, making it impossible to reversibly switch cell adhesion.[114]

Despite important progress in bio-instructive materials,[115] it remains a big challenge to spatiotemporally control cell adhesion in a reversible and noninvasive way. One of the most recently published studies employed photo-switchable proteins as a building block for light-mediated cell adhesion. In this study, two protein pairs that interact in a light dependent manner were used to mediate the interaction between cells and surfaces. Cryptochrome 2 (CRY2) interacts with N-truncated CRY-interaction basic helix-loop-helix protein 1 (CIBN) under blue light and phytochrome B (PhyB) interacts with phytochrome interacting factor 6 (PIF6) under red light. Both of these protein interactions reverse in dark. The proteins CRY2 or PhyB were expressed on the surfaces of MDA-MD-231 cells, which allowed them to attach to surfaces functionalized with their complementary interaction partners under blue or red light, respectively.[116,117] Further, in the dark the protein interactions reversed and the cells were released. It was shown that the cells can be captured and released reversibly several times on the same surface. Since the proteins are responding to orthogonal wavelengths, also specific immobilization of one cell type was be achieved in the presence of the other cell type (Figure 2.4). Besides that this approach requires the generation of stable cell lines, it does not employ natural adhesion molecules and does not connect the adhesions to the cellular signaling machinery.

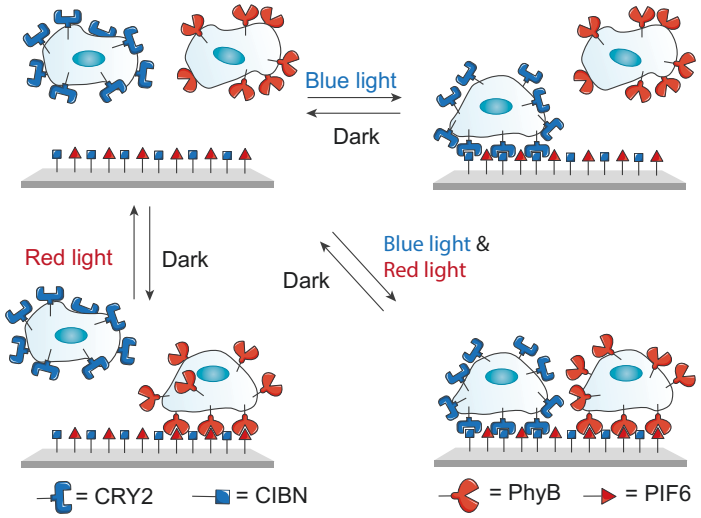

Figure 2.4: Schematic illustration of immobilization of specific cell types utilzing hetero-dimerizing protein pairs. Displayed in red: the red light induced heterodimerizing protein pair PhyB and PIF6; diplayed in blue: the blue light heterodimerizing protein pair CRY2 and CIBN. Adapted from Yüz et al.[116]

Photo-switchable proteins offer a great possibility to generate surfaces for light-induced reversibly switchable cell adhesion.[118] Besides, the bio-orthogonality and the facile way to generate the proteins by bacterial expression, a full library of proteins reacting in diverse manner to a broad range of wavelengths, is already accessible.

In the scope of this thesis photo-switchable proteins were engineered to mediate cell-matrix adhesion. Therefore, the optogenetic proteins CarH and LOV2 applied in this work will be introduced in the following section.

3. Optogenetic Building Blocks

The term optogenetics describes photo-responsive genetically encoded proteins. The tool box of optogenetic building blocks is equipped with a variety of different proteins, which can react to distinct wavelengths, covering the whole visible range of the electromagnetic spectrum.[119] Early examples were mostly used in neuronal science. However, the field of non-neuronal optogenetics has been growing over the last decade, offering powerful tools to investigate intracellular processes using light.[119,120] Within this thesis, two photo-responsive proteins were employed. The CarH from *Thermus thermophilus* and the LOV2 domain from *Avena sativa*, which are described more detailed in the following sections. The engineering principles of photo-responsive proteins[121,122] and applications of other photoreceptors is nicely discussed elsewhere[123] and will not be part of this section.

3.1 The Protein CarH

CarH is a transcription repressor in *Myxococcus xanthus* or *Thermus thermophilus,* but related variations exist in many different bacterial strains. CarH consists of three domains, a winged DNA-binding domain at the N-terminal, a four-helix bundle light-sensing domain and a C-terminal Rossmann-fold cofactor binding domain.[124] The cofactor for the CarH gene repressor family is adenosylcobalamin (AdoCbl, vitamin B12). AdoCbl assembles into the helix bundles, being coordinated by an axial 5'-deoxyadensosyl ligand. Upon cofactor incorporation, the CarH protein assembles into tetramers and binds to DNA at specific operons. Tetramers assemble first by head-to-tail dimer formation and latter formation of a dimer of dimers. If CarH from *T. thermophilus* is illuminated with green or blue light, the axial 5'-deoxyadensosyl ligand is exchanged by a histidine, resulting in a kinked conformation of the dimer and thereby in disassembly of the tetramer and DNA unbinding (Figure 3.1). Upon unbinding, the operon is again exposed and transcription of regulated genes is turned on.[125] In bacteria, CarH is involved in the genetic pathway of carotenogenisis, being an important molecule in oxidative stress suppression. The form of cobalamin is important for tetramer assembly since the isoform OHCbl binds the monomer but does not lead to tetramer assembly.

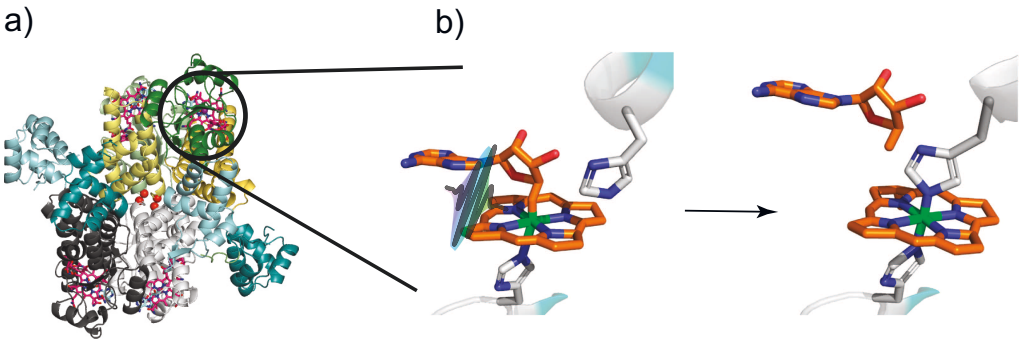

Figure 3.1: a) Tetramer of CarH and the AdoCbl cofactor, displayed in pink. b) Photoconversion of AdoCbl (orange) to HisCbl upon green light illumination, resulting in a kinked dimer formation and in temtramer dissassembly. Adapted from Jost et al.[125] and Kutta et al.[126]

First application of CarH as an optogenetic tool was performed by Kainrath et al. In the study a fusion protein of the cobalamin binding domain of CarH from *T. thermophilus* with the murine fibroblast growth factor receptor 1 (mFGFR1) was designed. In the dark, upon receptor clustering the downstream signaling pathway (MAPK/ERK) was activated, which was monitored with a luciferase reporter gene assay. The constructs were used in human embryonic kidney (HEK) cells, leading to an increase in luminescence due to CarH tetramer assembly induced by receptor clustering. By blue or green light illumination, but not under red light or in dark, receptor disassembly and a decrease of luminescence could be observed. The application of the optogenetic growth factor receptor 1 in zebrafish embryos showed that in dark, effective receptor clustering and a disturbed phenotype was obtained. Upon light illumination the larva development was undisturbed by silencing of the photo-inhibited signaling pathway.[127]

Another application of CarH as light sensitive building block was pursued by Wang et. al. by incorporation of CarH into protein hydrogels. For the preparation of hydrogels, CarH was included in a protein with a flexible elastin-like sequence and terminal SpyTag or SpyCatcher domains, which spontaneously form isopeptide bonds under mild conditions. The SpyTag/SpyCatcher reaction and AdoCbl induced assembly of CarH tetramers lead to a network formation and a hydrogel in dark (Figure 3.2).

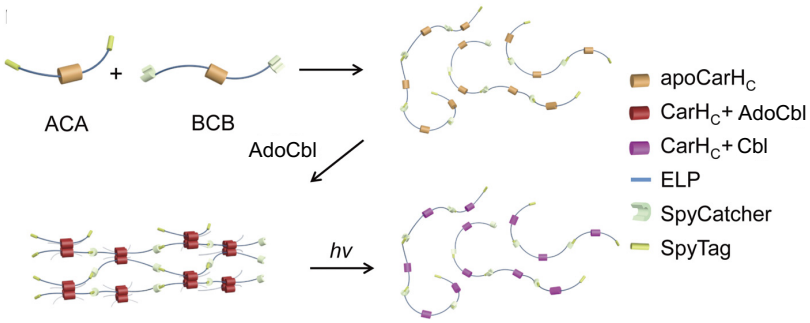

Figure 3.2: Building blocks used for assembly of green light-switchable hydrogels, the gelation in dark upon cofactor addition ($AdoB_{12}$), as well as the disassembly upon green light illumination. Adapted from Wang et al.[118]

Upon green light illumination, the CarH tetramer decomposes and the hydrogel liquefies. This light dependent decomposition of the hydrogel was used to release encapsulated cells without compromising cell viability.[118] Unlike other known optogenetic proteins, CarH is unique in its sensitivity to green light and fills a gap in the electromagnetic spectrum of optogenetic tools. Examples of its successfully use *in cellulo* and in material science, proves its versatility and makes it an attractive tool to control diverse systems externally with green light.

3.2 The LOV2 Domain

The light-oxygen-voltage (LOV) domain 2 is a 17 kDa domain of phototropin 1 from *Avena sativa.* Phototropin belongs to the Per-ARNT-Sim (PAS) superfamily and has two LOV domains, LOV1 and LOV2. In its organism of origin LOV2 is part of a blue light-activatable receptor kinase and phototropin is involved in the light-guided orientation of plants.[128]. The LOV2 domain consists of a small protein core, including five antiparallel β-sheets, and two α-helices, of which the one at the C-terminal is called Jα-helix (Figure 3.3). LOV2 binds to the chromophore and cofactor flavin mononucleotide (FMN), which absorbs blue light. Upon blue light illumination, a bond is formed between the cofactor and a conserved cysteine in the LOV2 domain. This reaction leads to an overall conformational change within the protein, including the unfolding of the Jα-helix.

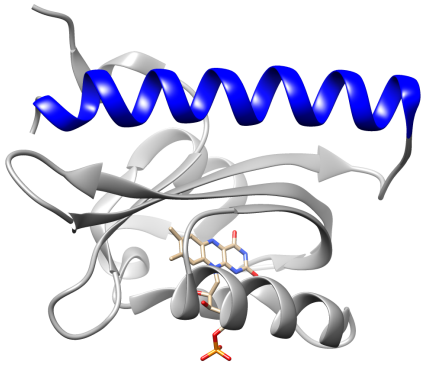

Figure 3.3: Sketch of the LOV2 domain. Displayed in blue the Jα-helix, in dark grey the protein core and in light brown the FMN cofactor.

The unfolding of the Jα-helix follows two separate steps with two different rate constants: first, the inner bond formation between the FMN and the cysteine and second, the unfolding of the Jα-helix. While the bond formation takes seconds to minutes, and can be easily monitored by the absorption spectrum of FMN, the unfolding of the helix follows within milliseconds, making it difficult to detect. Once illumination is stopped, protein thermally converts back to the dark state, during which bond between the FMN and the cysteine is broken and the Jα-helix docks to the β-sheet again. This unique feature of switching from a highly ordered structure to a disordered state bears high potential for utilizing the LOV2 domain as a molecular switch. Activity bearing amino acid sequences can be hidden in, or attached to the Jα-helix such that upon light-induced unfolding, they are be exposed and can interact with other binding partners. In general, the light controlled activity

in the protein can be subdivided into two parts; i) the photosensor, which is activated through the chromophore, and ii) an effector being induced by the active photosensor. Adapting this terminology to engineered LOV2 proteins, the LOV2 domain is the photosensor and peptides hidden in or attached to the helix are the effectors. Hence, to retain the photo-sensory function, it is important to preserve the interactions between the Jα-helix and the β-sheet during the incorporation of effectors.

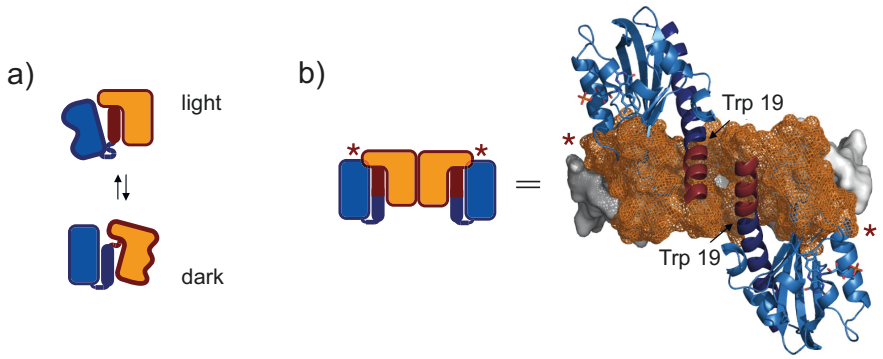

Figure 3.4: Sketch of the LOVTAP dimer system. Indicated in blue the LOV2 domain, in dark blue the Jα-helix of the protein and in orange the interface of the TrpR repressor and in dark red, the helix of the TrpR repressor. Adapted from Strickland et al.[129]

One of the first examples that use the LOV2 domain for photoreceptor engineering was reported by Strickland et al. In this study, the bacterial transcription repressor TrpR was incorporated into the LOV2 domain by fusing the terminal helix of the TrpR to the Jα-helix. The construct was named LOVTAP (Figure 3.4).[129] In the dark, the helix of TrpR is attached to the LOV2 domain, making it impossible for the transcription repressor to bind the respective DNA sequence as the TrpR binds DNA as a dimer in a specific conformation. Upon blue light illumination, the TrpR detaches from the LOV2 domain, forms the dimer and binds to its specific DNA, leading to a 6-fold increase in DNA binding.[129] Following similar design principles, a broad range of LOV2 based photoreceptors have been developed as optogenetic tools, enabling the

investigation of diverse cellular processes and their spatial and temporal control (Figure 3.5).

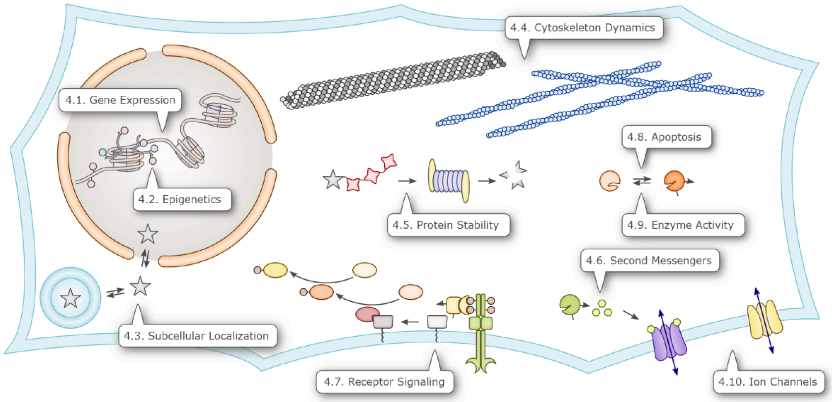

Figure 3.5: Overview of cellular processes that have been or can be regulated by blue light-switchable optogenetic tools employing the LOV2 domain. Adapted from Losi et al.[123]

For many other processes LOV2-based photoreceptors were engineered by direct incorporation of the effector into the photoreceptor. Not only apoptosis was induced by incorporation of degradation sequences into the LOV2 domain,[130,131] but also protein functionality could be rendered by combination of the LOV2 domain and split inteins. Inteins are peptides, which excise themselves posttranslational, connecting the C and the N-terminus of the attached protein parts, forming a new, modified protein. By combining a split intein with a photoreceptor, this splicing can be induced by light, resulting in the formation of an intact protein after blue light illumination.[132,133] The incorporation of nuclear localization sequences (NLS)[134,135] or nuclear export sequences (NES)[136,137] provide a versatile tool box of diverse blue light-switchable localization domains for the nucleus[138] or peroxisomes[139] (Figure 3.6).

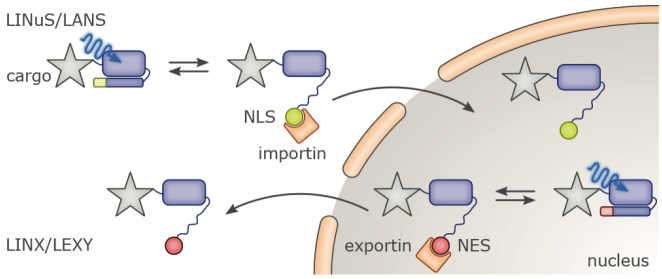

Figure 3.6: Sketch of blue light-induced nuclear import and export of proteins of interest with the LOV2 domain. Adapted from Losi et al.[123]

Besides the direct incorporation of the effectors in the Jα-helix, like described for the LOVTAP system, LOV2 based light dependent dimerizers have also been developed as general optogenetic platform. The general principle behind these designs is to include small dimerizing peptides in the Jα-helix, which are caged in dark. Upon blue light illumination, these peptides are exposed and can dimerize with the respective dimerization partner. Such light dependent dimerizers are of interest to control the localization of proteins; if one of the components is localized at a membrane, a protein of interest fused to the respective binding partner can be re-localized upon

blue light illumination. The altered localization leads to an increase of the local protein concentration and thereby photo-induced activity. Mainly three systems of LOV2 based dimerizers have gained strong interest within the optogenetic community, and many studies used these tools as discussed below.

Tunable, Light-Controlled Interacting Protein Tag (TULIP)

For the tunable, light-controlled interacting protein tag (TULIP), a small binding peptide was incorporated at the end of the LOV2 protein (LOVpep). The peptide binds to an engineered PDZ domain (ePDZ) in the lit state, leading to a dimerization of the two proteins (Figure 3.7). When LOVpep is localized to the cell membrane, proteins of interest, fused to the ePDZ domain, could be localized there as well upon blue light illumination, as initially shown with fluorescent proteins. By fusing proteins that are part of signaling cascades, the mating pathway in yeast could be activated upon membrane localization.[140] Likewise the TULIP dimerization pair was used to spatiotemporally control processes like organelles transport along microtubules,[141] the effect of localization/activation of the GTPases RhoA and Cdc42 on cytocynetic furrows,[142] stress fiber formation[143] and cell polarization.[144] Also, clathrin-mediated[145] endocytosis as well as specific integrin signaling[146] were photo-controlled employing the TULIP system.

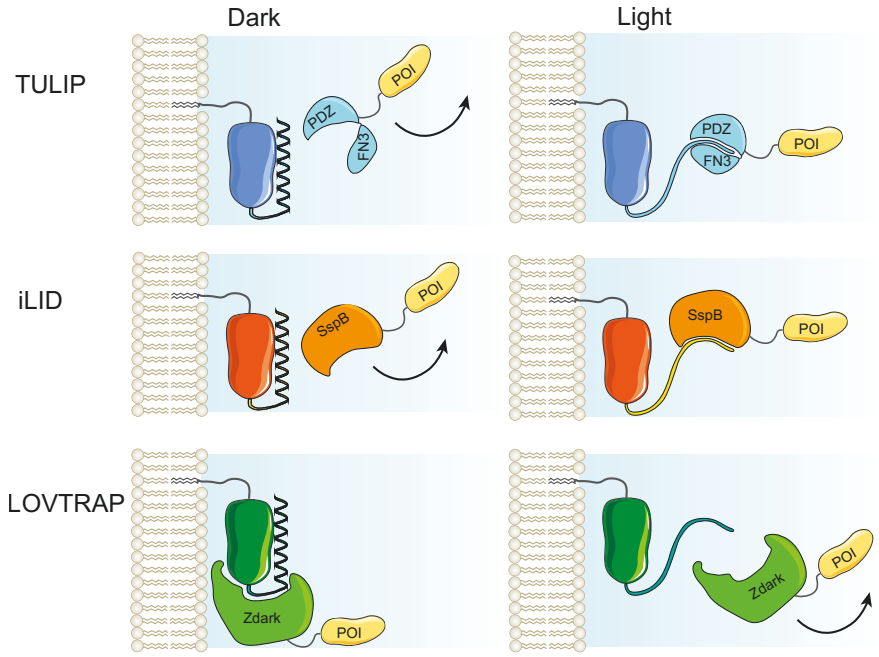

Figure 3.7: Three heterodimerzing LOV2-based optogenetic tools. a) Tunable, light-controlled interacting protein tag (TULIP), b) engineered light-inducible dimer (iLID) and c) LOVTRAP system based on dark state heterodimerization with an engineered Zdark protein and the LOV2 domain. Adapted from Strickland et al.[147] and Losi et al.[123]

Light-Inducible Dimers (LID)

In a related approach, the SsrA peptide from *E. coli* was introduced in the Jα-helix. This peptide dimerizes with a 13 kDa adaptor protein, called SspB. The original

approach exhibited a switching efficiency of 8-fold and an unusual fast dark relaxation. This protein pair, called original light-inducible dimer (oLID),[148] was further improved by combination of computational design and phage display, generating initially two light inducible dimerization pairs with different dynamic ranges. The improved LID (iLID) changes its affinity from 130 nM under blue light to 4.7 µM in the dark (36-fold, SspB was named Nano in the study). Similarly, iLID changes its affinity (due to a point mutant of Nano) from 800 nM to 47 µM in the dark (59-fold, SspB was consequently named Micro). Later a third protein pair, called iLID/Milli with a range from 3 µM to 125 µM was published.[149] The iLID/Nano(Micro) interaction has been used to control protein localization and activation of GTPase signaling by light-induced localization of the GTPase with Cdc42 at the cell membrane.[150] Depending on the kinetics and thermodynamics of the process of interest, the different dimerizing pair can be chosen accordingly.[151]

To determine the dynamic range of the proteins, fluorescence anisotropy measurements were used.[152] This method is based on the electronic features of fluorophores and their absorbance of polarized light. If a dye is excited with polarized light, also the emitted fluorescence is polarized in the same direction as the excitation. Given that the orientation of the fluorophore is not fixed between excitation and emission, it can move out of the polarization plane, leading to a decreased fluorescence signal in the original polarization direction. If the mobility of the fluorophore is decreased by binding of bulky compounds, the polarization direction of the excitation is retained to a higher degree. The anisotropy is a ratio between the vertical and perpendicular polarized emitted light and therefore a direct value of the mobility of the dye in the measured solution. From the motility of the dye the binding affinity of possible binding partners can be assessed.[153] Since it is a fast and easy method to determine binding affinities it is often used to characterize optogenetic tools.[149,154]

By blue light induced localization of Cdc42[155,156] or PIP_x phosphatase[157] at the plasma membrane, the downstream signals and cytoskeleton remodeling could be monitored. The iLID interaction pair has been used to generate a blue light-activatable calcium channel.[158] Furthermore, the iLID/Nano interaction has also been used in synthetic systems like giant unilamellar vesicles (GUVs) to control protein localization and patterns of proteins of interest[159] and the self-assembly of polystyrene beads in a light controlled manner.[160]

LOVTRAP

LOVTRAP system operates differently compared to the two previously described systems. Instead of incorporating a binding tag into the Jα-helix of the LOV2 domain, a small protein, Zdk, was engineered from the Z subunit of protein A, to bind the dark state of the LOV2 domain. Upon blue light illumination and subsequent helix unwinding, the ZdK protein detaches from LOV2 and diffuses to the region of action. This is a reverse system to further complete the toolbox of optogenetics. As proteins of interest the GTPases, RhoA and Rac1 as well as their upstream guanosine triphosphate (GTP) exchange factor Vav2 was utilized to control activity with light. For all three photo-regulated proteins light-induced changes in membrane ruffling,

spreading area and protrusion distribution of HeLa cells were observed.[161] Likewise, LOVTRAP was also used to control microtubule dynamics with blue light.[162]

Besides, incorporation of the effectors in the LOV2 domain, or the design of light controlled dimerizers, there is a third possibility to regulate protein function with light using the LOV2 domain. The insertion of the LOV2 domain into protein loops that are allosterically coupled to the active side, not conserved and accessible does not alter protein function in the dark state. However, upon blue light illumination the attached protein structure is disturbed, resulting in a loss of function. The small GTPases RhoA, Rac1, Src and Cdc42 and the Rac1 activator Vav2 were successfully inhibited by blue light-induced allosteric control with the LOV2 domain (Figure 3.8a).[163] The combination of protein design and computational selection of suited proteins was named Loopology.

One of the first approaches to control cellular functions with direct incorporation of the effector in the LOV2 domain, was shown by Wu et al. In this study the small GTPase Rac1, which regulates the actin cytoskeletal dynamics to the C-terminal Jα-helix, was fused to the end of the Jα-helix of the LOV2 domain. Thereby, the interaction of Rac1 with its effector the p21-activated kinase (PAK) was blocked. Upon blue light activation, the Rac1 interacts with its effector due to the helix unfolding. With the photo-switchable Rac1 construct (PA-Rac) transfected mouse embryonic fibroblast (MEF) were shown to migrate in the direction of activated PA-Rac (Figure 3.8b).[164] A follow up study could show that local Rac1 activation in *Drosophila* ovary led to clustered cell movement in direction of the highest Rac1 activity, like known in collective cell migration, which is an important process in morphogenesis.[165]

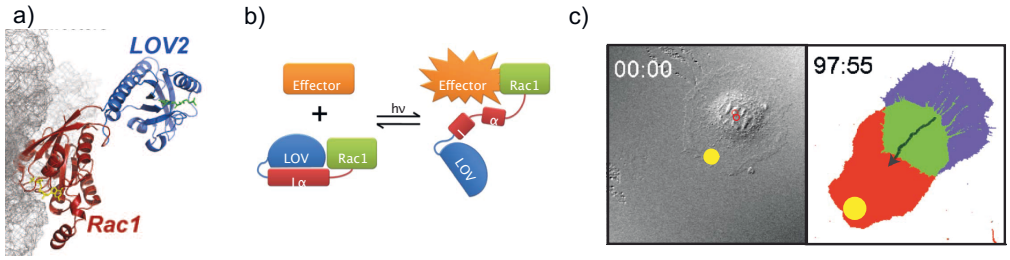

Figure 3.8: Exemplary figure of optogenetic control of Rac1. a) An allosteric photoswitch by incorporation of the LOV2 domain into an exposed loop of the protein RAC1 by the loopology approach. Displayed in blue the LOV2 domain and in red the Rac1. Adapted from Dagliyan et al.[163] b) Sketch of the photo-controlled Rac1 by end-to-end attachment of LOV2 domain to Rac1. c) Blue light-guided cell migration by stimulus-control of the LOV2 caged Rac1. The yellow dot indicates the illumination site; the red area shows where the cell migrates to and the purple area indicated the cell area which is retracted upon migration. Adapted from Wu et al.[164]

Since, many points have to be considered, the successful incorporation of the peptides into the Jα-helix it still a delicate matter. Besides computational estimations about which positions can be or have to be rendered and the knowledge of already published systems, it is still difficult to generate functional mutants from scratch. A library of mutants has to be established and evaluated for their potential in the respective experiments.

Aim and Motivation

In order to circumvent many of the afore-mentioned drawbacks, I decided to utilize optogenetic tools to generate light-switchable surfaces for cell-matrix adhesion, which are facile to produce. Therefore, I chose the green light-decomposable protein CarH to catch and release cell on command of non-toxic green light. To generate a switchable system for light-induced cell-matrix adhesion, I employed the blue light-switchable protein domain LOV2. The reversibility of the latter system guaranties not only the capture of cells and on command release, but also to gain insight into dynamic processes within the cell when it migrates or loses matrix contact.

For addressing natural cell adhesion ligands, like integrins, this thesis is based on incorporation of the RGD motif into the mentioned proteins. Since, the systems are not based on dimerization partners, the need to transfect and render cell lines in advance is avoided. Thereby, the so obtained surfaces can be used to modulate cellular adhesion to all cell lines presenting RGD binding integrins, without further manipulation.

II. Results and Discussion

4. Photo-Cleavable Cell Adhesion

Since light has the advantages to achieve high spatial and temporal control, I designed photo-responsive interphases to precisely control cell-matrix adhesions. To circumvent the drawbacks of current methods including tedious chemical synthesis and the toxicity of UV light cleavable caging groups, I used the green light responsive protein CarH to generate surfaces, which allow tuning cell-matrix adhesion using green light.

4.1 Design Principle of Green Light-Controlled Cell Adhesion Using the CarH Protein

In the first part of this thesis, I employed the light sensing part of the protein CarH (21 kDa) from *T. thermophilus,* build of a four-helix bundle and a Rossmann-fold.[125] Since the DNA binding domain is not involved in tetramer assembly, the protein was truncated and only the light sensing part was used. When bound to its cofactor vitamin B_{12}, CarH forms a tetramer, which is photo-cleaved upon green light illumination. Therefore, CarH is used as a photo-cleavable molecular building block to alter cell adhesion. To allow cells to adhere to CarH functionalized surfaces, the cell adhesion peptide RGD was introduced at different positions close to the C-terminal His-tag of CarH to yield CarH-RGD. Due to the tetrameric protein structure of CarH, the His-tags at two of the C-termini bind to the Ni^{2+}-NTA functionalized PEG surface and the respective RGD motifs are not accessible for integrin binding due to the CarH protein above them. The other two C-termini face the solution and the RGD motifs are thereby accessible to integrin binding (Figure 4.2a). In the dark, integrins recognize the presented RGD motifs on top of the CarH tetramer and mediate cell adhesion. Upon green light illumination, the tetramer disassembles, which consequently leads to the detachment of the cells and the CarH monomers bound to integrin cell receptors (Figure 4.1).

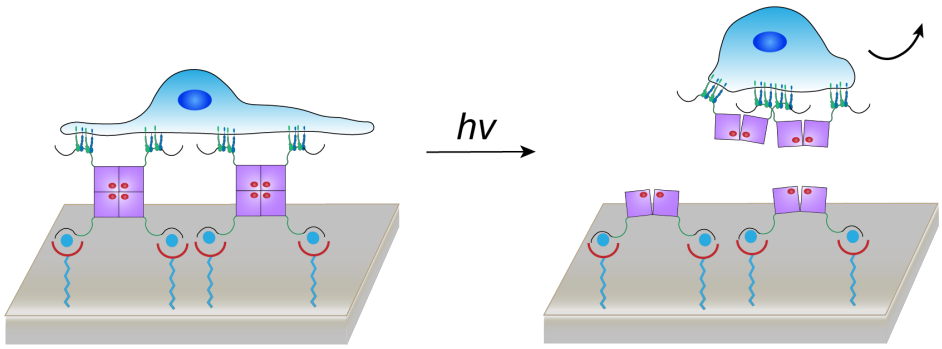

Figure 4.1: Schematic representation of the design principle to control cell-surface adhesion with green light. The CarH tetramer with an RGD sequence is immobilized on a surface through its His-tag on a Ni^{2+}-NTA functionalized PEG coated surface. This allows the cells to adhere to these surfaces in the dark via the interaction of integrins and the incorporated RGD motifs facing the solution. Upon illumination with green light the CarH-RGD tetramer disassembles into dimers resulting in cell detachment. The CarH monomere is displayed in purple, the vitamin B12 in red, the PEG is indicated by the blue line functionalized with a NTA-group displayed in red.

4.2 Incorporation of the RGD Motif in the CarH Monomer

To prevent perturbation of the protein structure (Figure 4.2a) and function by the introduction of the RGD motifs, a site close to the C-terminal His-tag was chosen. One of the RGD motifs was introduced to a position where the protein sequence of CarH already bears the amino acids RG (underlined in the WT, Figure 4.2b), being a predestinated mutation site for RGD incorporation. Alternatively, the RGD motif was directly introduced right before the His-tag, to create a larger distance between the RGD motif from the folded protein core. To increase the surface density of RGD motifs, double and triple RGD mutants were also generated. In addition, the flanking amino acids from cellular fibronectin were introduced in the C-terminus, resulting in the following mutant library (Figure 4.2b).

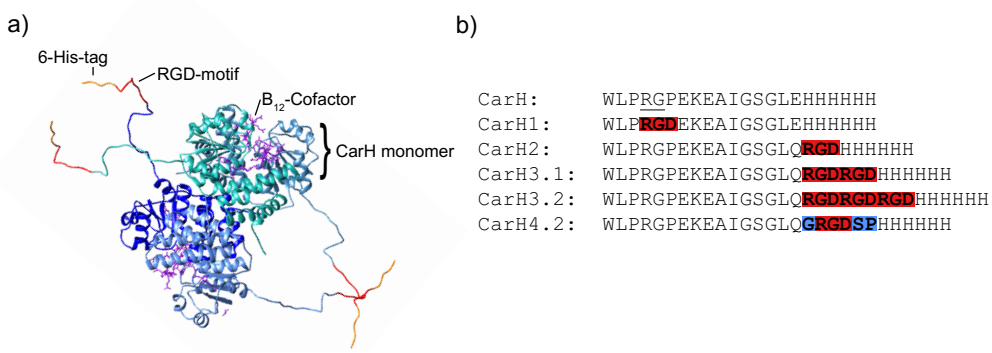

Figure 4.2: CarH protein structure and mutant library. a) CarH tetramer structure. Displayed in blue are the respective protein monomers assembled into the tetramer, the cofactor vitamin B12 is shown in purple, the position of the RGD motif(s) are labeled in red and in yellow the C-terminal His-tags. b) Amino acid sequences of the C-terminal tail of the CarH mutant library, the RGD motif is shaded in red, the flanking amino acids of the RGD motif from cellular FN are shaded in blue.

The protein mutants were generated and purified like described in section 7.1 and section 7.2. The tetramer was formed by incubation with a four-fold excess of vitamin B12 on ice in the dark. For further characterization, the proteins were kept either in dark or under red light illumination to prevent the CarH tetramer from disassembling.

4.3 The Tetrameric CarH proteins Disassembles under Green Light Illumination

The vitamin B12 cofactor in the CarH tetramer and monomer has distinct absorption bands in its UV/Vis spectrum, which can be used to monitor the disassembly process of the tetramer into its monomers. Therefore, a spectrum of the protein tetramer was taken in dark and after different time points with green light illumination. Exemplary the disassembly of CarH3.2 is shown in Figure 4.3a. The arising absorption bands were confirmed by the results of Hardmann et al.[126] The kinetics of the tetramer disassembly shows that an illumination time of 100 s is needed to fully convert the tetramer to the monomers (Figure 4.3b).

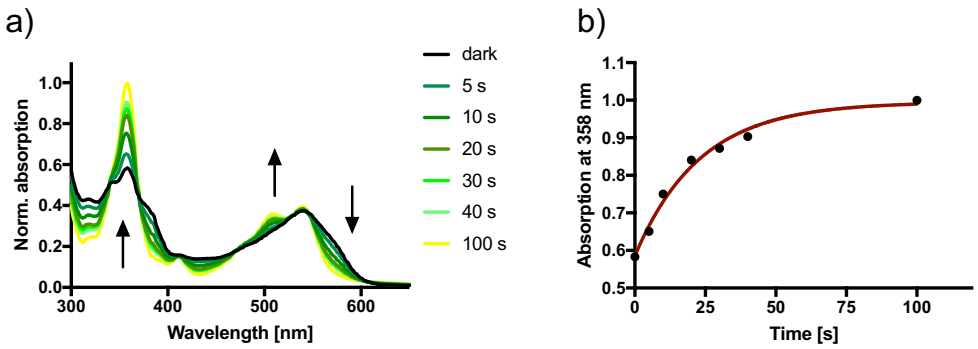

Figure 4.3: Green light induced disassembly of the CarH3.2 tetramer monitored by UV/Vis spectroscopy. a) The black curve presents the dark state, the green curves show the stepwise tetramer disassembly according to the illumination times, the yellow curve shows the absorption spectrum of a fully disassembled tetramer. b) Absorbance at 358 nm plotted over time and fit to a first order kinetic, indicating that an illumination time of 100 s is needed for full conversion.

4.4 CarH-RGD Tetramers can be Recognized by Integrin

After the tetramer formation and disassembly of different CarH-RGD mutants was successfully confirmed by UV/Vis spectroscopy, the orientation of the surface-immobilized proteins as well as their capability to bind integrin was investigated. Therefore, immunofluorescence staining and quartz crystal microbalance with dissipation (QCM-D) was utilized, as described in the following section

4.4.1 The Tetramer Binds to the Surface and Present the RGD Motif to the Solution

To assess the orientation of the proteins on the surface, indirect immunofluorescence staining was performed to visualize the His-tags accessibility of the immobilized CarH-RGD. The protein tetramer of CarH3.2 was immobilized on glass surfaces with a PEG coating and Ni^{2+}-NTA end group as described in section 9.3. While one sample was kept in the dark (dark state), another sample was illuminated with green light for 20 min (lit state). Subsequently, both samples were incubated with anti-His antibodies, which recognizes the accessible His-tags on the surface. Finally, the surfaces were incubated with a secondary antibody which bind to the anti-His antibody and is conjugated to an Alexa 488 fluorophore for detection. To measure the average fluorescence of each surface, the imaging parameters were kept constant and the fluorescence profile of the secondary antibody was measured on a line plot along the x-axis of the single images (Figure 4.4).

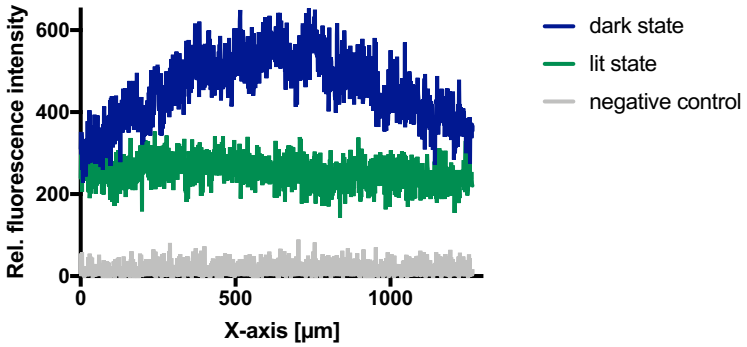

Figure 4.4: Fluorescence signal along a line plot of detected His-tags on surfaces functionalized with CarH3.2 mutant in dark (displayed in blue), illuminated with green light (displayed in green) and on a surface which was not incubated with protein (negative control, displayed in grey), assessed via indirect immunofluorescence staining of the His-tags.

The fluorescence detected on the dark state sample functionalized with CarH3.2 tetramer is higher than on samples not functionalized with protein. This indicates that the protein is successfully immobilized via the His-tags, and that at least two of the His-tags are accessible for antibody binding. The surface illuminated with green light exhibits a decreased fluorescence signal compared to the dark state surfaces, indicating a reduced His-tag density on the surface. The reduced fluorescence intensity after green light illumination shows the disassembly of the tetrameric protein and that the protein is immobilized with two His-tags facing the surface and two His-tags are facing the solution. The lit state surfaces, which are coated with the disassembled protein tetramer, still exhibit a significant higher fluorescence signal than the negative control. This hints at the fact that the His-tags at the surface are accessible for antibody binding. Since antibodies (35 kDa[166]) are smaller in size than the integrin heterodimers (190 kDa[27,167]), the binding of integrins is expected to be sterically more hindered and thus the integrins may not interact with the surface-facing RGD motifs.

4.4.2 Integrin can Recognize the RGD Motif and Bind It

To determine whether integrin can recognize the presented RGD motifs in the CarH, QCM-D measurements were performed. For immobilization of the proteins on the gold crystals, surfaces were coated with thiol-PEG_{azide}, forming a cell-inert SAM on the crystal. NTA-alkyne was clicked with copper catalyzed click reaction to the terminal azide groups and loaded with Ni^{2+}. The crystals were washed and the frequency and dissipation baseline was measured (1 in Figure 4.5). Subsequently, the purified CarH3.2 tetramer washed over the crystals in dark and immobilized by coordination of the C-terminal His-tag with the Ni^{2+}-NTA groups (2), leading to a frequency change of 45 Hz. The dissipation increase is negligible, indicating a tightly bound protein layer. Afterwards, the excess of protein was removed by washing (3) and the buffer system was switched to integrin binding buffer, containing divalent cations (4). 170 nM integrin fragment $\alpha_v\beta_3$ was added to each crystal leading to a frequency change of 10 Hz (5) and thereby showing a binding of the integrin to the RGD motifs. After incubation time of 45 min the crystal was once again washed with integrin binding buffer to remove the unbound integrin fragments. After 10 min washing (6), one chamber was illuminated with green light for the rest of the experiments, in order to disassemble the protein tetramer and thereby also detach

the integrin fragment from the crystal (7) (Figure 4.5a, indicated with the green arrow). This led to an increase in frequency of almost 20 Hz, indicating the disassembly of the tetramer and the attached integrin fragment, which was not observed in the sample permanently kept in dark. After a washing step with integrin binding buffer (8), the resulted monomer or the tetramer, respectively, was detached from the crystal with imidazole containing buffer (9). By recovering the original buffer system through washing with buffer A, the baseline could be restored for both samples (10) (Figure 4.5).

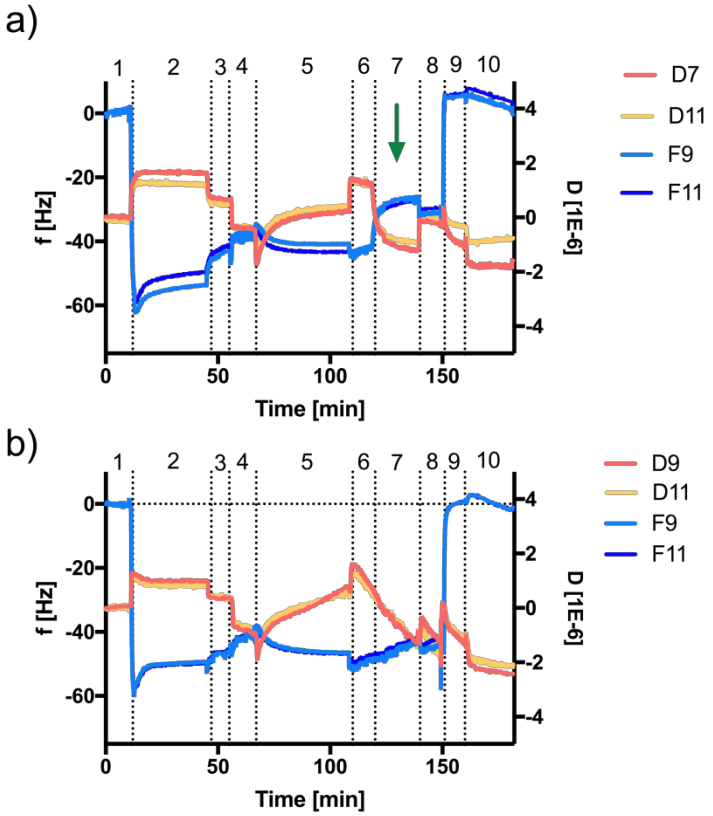

Figure 4.5: QCM-D measurements for the immobilization of CarH3.2 tetramer on PEG_{azide} functionalized gold crystals clicked with NTA-alkyne and subsequent binding of integrin fragment $\alpha_v\beta_3$ to the RGD motifs of the protein. a) Crystals illuminated with green light at t = 120 min, showing a shift in frequency caused by protein decomposition initiated detachment of the protein and the integrin from the crystal. b) Crystals kept in dark for the whole time did not show a frequency shift at t = 120 min indicating no decomposition of the protein. Frequencies overtones 7, 9 and 11 are displayed in blue, the respective dissipation is displayed in red colors. Numbers indicate: (1) buffer baseline, (2) incubation with CarH3.2 tetramer in dark, (3) washing step with buffer, (4) buffer change to integrin binding buffer, (5) incubation with integrin, (6) washing step with integrin binding buffer, (7) switch on green light on a), (8) washing step with integrin binding buffer, (9) washing with imidazole containing buffer, (10) restoration of the original buffer system a baseline recovery.

4.5 Cell Adhesion to CarH-RGD

After observation of integrin binding to the CarH3.2 tetramer in QCM-D measurements, the different CarH-RGD mutants were used in cell adhesion studies. First, the influence of green light of 532 nm on the viability of human breast cancer (MCF7) cells was assessed with a colorimetric metabolic activity assay (Figure 4.6). In the MTT assay performed in five technical repeats, no decreased activity of cells under different intensities of green light as compared to the dark sample, was

observed. Further experiments were, therefore, conducted using a light flux of 12.5 µM/m^{2}s intensity of 532 nm green light, to guarantee complete photo conversion of the protein without induction of cell damage.

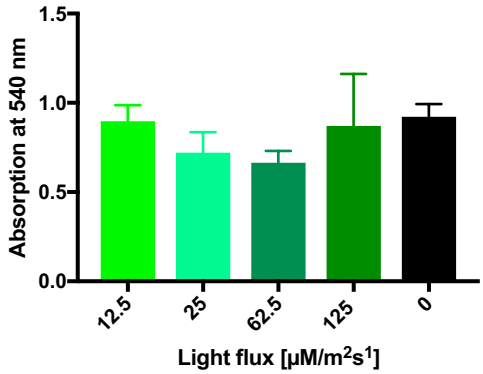

Figure 4.6: The metabolic activity of MCF7 cells under illumination of 532 nm green light was assessed with a colorimetric assay, showing no decreased activity of cell cultures under different light intensities of green light compared to dark.

4.5.1 Cells can Adhere to Dark State CarH3.2 Coated Surfaces but not to the Lit State

To test if the cells adhere differently to CarH-RGD coated surfaces which were kept in the dark and which were exposed to green light, cell adhesion experiments were performed. For this purpose, glass surfaces were functionalized with proteins as described in section 7.3. After immobilization of the protein, the surfaces were washed and 5000 cells/cm^2 were seeded in serum free medium and in dark onto the surfaces. Subsequently, the cells were incubated in dark or under green light for 2 hours, and finally the samples were fixed and stained for the actin skeleton and the nuclei. The number of adherent cells on the respective surfaces was quantified by counting the nuclei in the nucleus staining and the spreading area of the cells was quantified using the actin cytoskeleton staining.

Cells did not adhere to surfaces functionalized with most of the CarH-RGD mutants (Figure A3) in comparison to the passivation control, except for CarH3.2. This indicates that the RGD density on the surfaces is too low for the other mutants as CarH3.2 is the only CarH-RGD mutant with 3 RGD motifs and the other mutants do not provide enough anchor points for cell adhesion. On surfaces functionalized with mutant CarH3.2 cells adhered more cells in comparison to the passivation control if the surface was kept in the dark and the number of adherent cells decreased upon green light illumination. Therefore, the mutant CarH3.2 was further investigated in cell-adhesion experiments.

In order to increase the density of protein on the surface, the tetramer was assembled and subsequently purified with size exclusion chromatography in dark (Figure A1). The adhesion studies were performed as described before, but with the concentrated protein sample. It was found that cells adhere significantly more to surfaces kept in dark as compared to the surfaces illuminated with green light or to the negative control without protein functionalization. As a positive control a surface with cyclic RGD, which is a very strong adhesion ligand was used. Indeed, cells adhered better to cRGD functionalized surfaces than to CarH3.2 surfaces (Figure 4.7a).

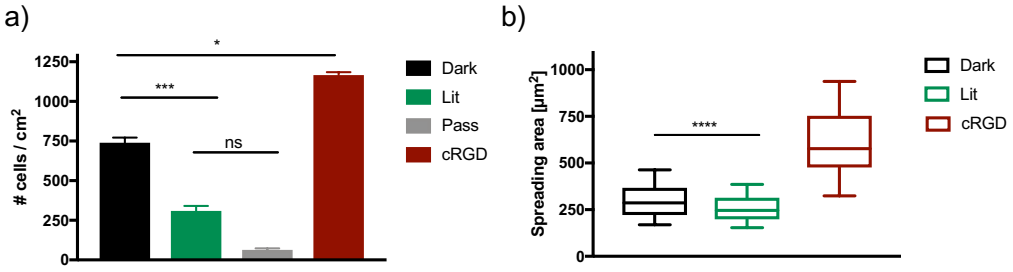

Figure 4.7: Cell-surface adhesion experiments. Cells were incubated for 2 hours in dark or under green light on surfaces functionalized with concentrated CarH3.2 tetramer. a) Number of cells adhering to surfaces in dark or under green light illumination in comparison to the passivation (negative) control and cRGD functionalized surfaces (positive control). Experiments were conducted in triplicates. b) Spreading area of cells attached to surfaces kept in dark or exposed to green light in comparison to cRGD functionalized surfaces. Experiments were conducted in triplicates, n > 220 cells. 10 – 90 % confidence interval is shown. p-values: * < 0.1, ** < 0.01, *** < 0.001, **** < 0.0001.

In addition to the number of cells on the surfaces also the analysis of the spreading area on the respective surfaces showed that cells spread more on surfaces kept in dark than on surfaces illuminated with green light (Figure 4.7b). Not only adhesion points for the initial cell contact of cells with the surface were decreased as indicated by the cell number, but also for successful spreading of the cells. Exemplary pictures of cells adhered to the dark state and the lit state surface in comparison to the cRGD functionalized surface are shown in figure 4.8.

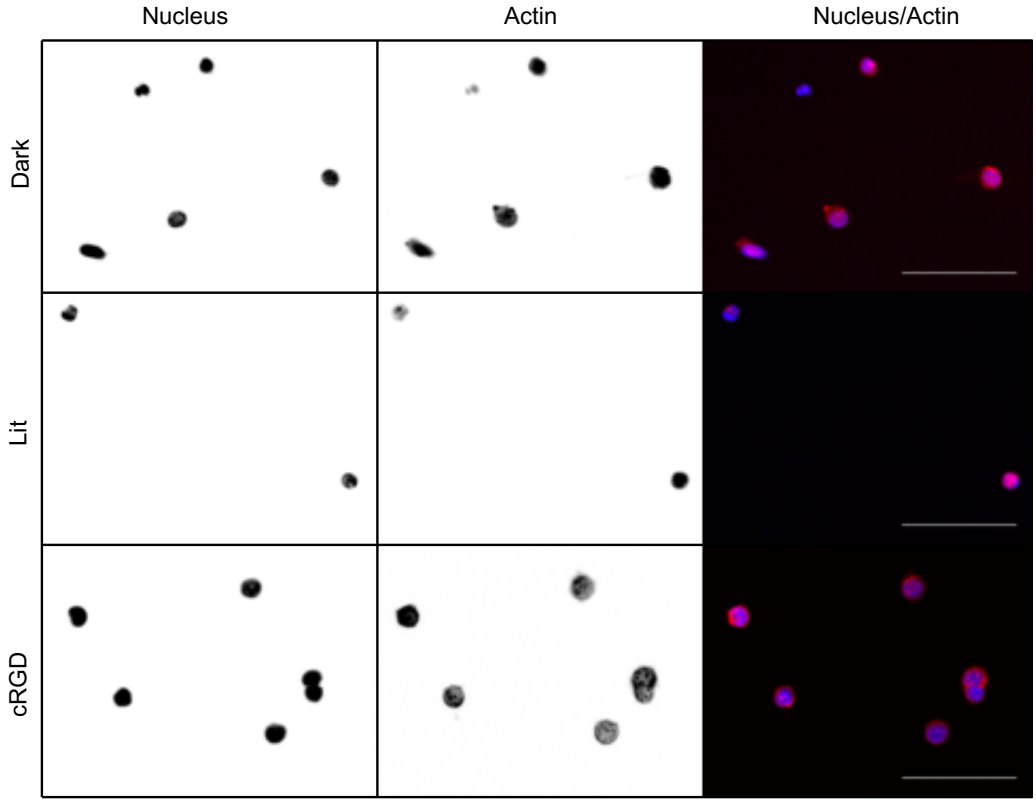

Figure 4.8: Actin and nucleus stain of MCF7 cells either incubated on CarH3.2 functionalized surfaces in dark or under green light illumination, respectively, or on cRGD functionalized surfaces. In the merged channel: actin is displayed in red, nucleus is displayed in blue. Scale bar: 100 µm.

Overall, in this part of the work rational protein design was used to incorporate the adhesion peptide RGD found in many ECM proteins into the green light sensitive protein CarH, which serves as a photo-cleavable linker. The tetramer formation of CarH-RGD proteins and their disassembly under green light could be verified by UV/Vis spectroscopy and with QCM-D. The protein mutant CarH3.2, which includes three RGD motifs, was successfully used to alter cell adhesion in response to light; cells adhered well to CarH3.2 functionalized surfaces in the dark state, but almost no cells adhered after green light illumination. The herein presented CarH-RGD protein is able to mediate switchable cell-matrix adhesion in response to green light. Hence, the CarH protein enlarges the tool box of photo-cleavable cell adhesion from UV-light cleavable nitrobenzenes to the first green light-switchable surfaces for cell adhesion, combining optogenetic approaches with material science.

5. Photo-Switchable Cell Adhesion

The reversibly control of cell adhesion still remains a challenge. In order to establish a system to control cell adhesion reversibly and dynamically, a reversible optogenetic protein was employed. Therefore, the LOV2 domain from *Avena sativa* was chosen. As described before, the LOV2 domain can reversibly switch its conformation under blue light due to a bond formation between the cofactor FMN and an internal cysteine residue, when illuminated with blue light. The bond formation results in the unwinding of the long C-terminal helix, called Jα-helix. This conformational change is reversed in the dark. Hence, this conformational change in protein structure can be employed for photo-switching the effector by incorporating the effector amino acid sequence in the sequence of the Jα-helix.

5.1 Photo-switchable Cell-Matrix Adhesion with LOV2 Mutants

Our design is based on the incorporation of the RGD motif into the LOV2 domain. The cell-binding RGD sequence can interact with a variety of integrins. Using naturally binding ligands facilitates the application of the approach and expands its applicability to a broad range of adherent cell types without the need of manipulating the cells. Furthermore, the motif is very small, increasing the possibility to successfully incorporate the motif into the Jα-helix, thus minimizing potential disturbances of the dark state protein structure.

The RGD motif was incorporated at different positions in the Jα-helix, yielding LOV2-RGD mutants. The proteins were expressed in bacteria and purified. Immobilization of the respective LOV2-RGD protein by complexation of the His-tags via surface-bound NTA groups, led to full coverage of the surface with the protein mutant. The helical conformation of the Jα-helix shields the RGD motif from cell recognition and cell do not adhere to the dark state protein. Upon blue light illumination, leading to unwinding of the terminal helix, the RGD-binding motif is exposed to the cell. Cellular integrins can bind to the RGD motif, recognize it and mediated cell adhesion. Thermal relaxation in the dark leads to refolding of the helix and subsequent caging of the RGD motif (Figure 5.1).

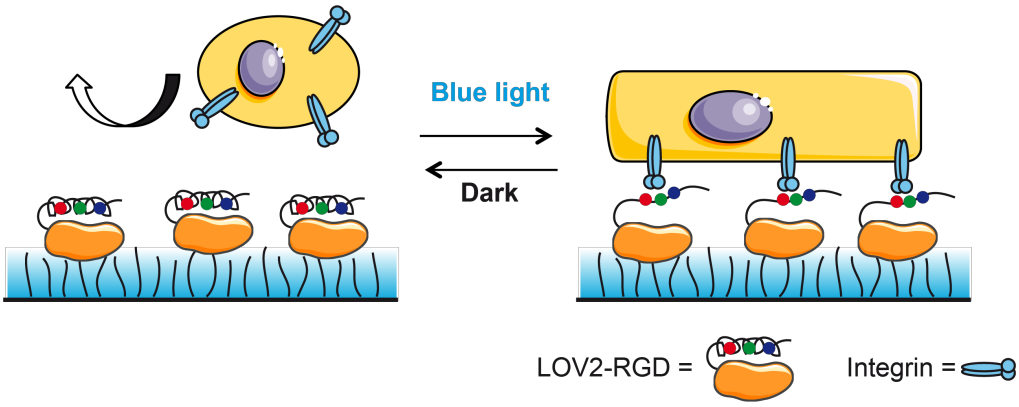

Figure 5.1: Photo-switchable cell-matrix adhesion with LOV2-RGD mutants. The RGD motif is introduced in the Jα-helix of the LOV2 domain and caged by the helical conformation in the dark state. Upon blue light illumination, the helix unravels, exposing the RGD motif to the integrins and thus facilitating cell adhesion. The PEG-layer is indicated by the blue background.

5.2 Incorporation of RGD-motif in the LOV2 Domain Yielding LOV2-RGD

In the design of the protein library five different engineering strategies were followed (Figure 5.2a). To implement the RGD motif, amino acids were chosen exhibiting a similar polarity than RGD. Amino acids mediating the β-sheet docking are preserved as far as possible. These amino acids are underlined in the wild type (WT) sequence of the LOV2 domain (Figure 5.5).

First, the RGD motif was introduced at several different positions in the Jα-helix, leading to nine mutants (Figure 5.2b). The LOV2-RGD mutants are named RGD1 - 8, whereas RGD 1 is located at the beginning of the helix and the numbers increased in direction of the C-terminal of the Jα-helix.

The RGD motif was not only introduced to the end of the Jα-helix but also in the middle and in the beginning, in order to achieve better caging. Most approaches mentioned in literature attached the effector to the end of the Jα-helix[147,148,168-171] since it bears a higher risk to disrupt the protein structure by incorporation of amino acids at the beginning of the helix, but also potentially improved caging.

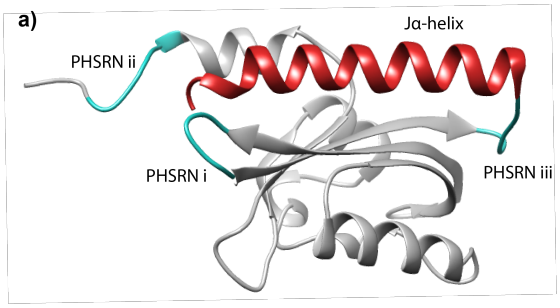

b)

```
                    Jα-helix
LOV2(WT): DAAEREGVMLIKKTAENIDEAAKEL
RGD 1:    DAARGDGVMLIKKTAENIDEAAKEL
RGD 2:    DAAERGDVMLIKKTAENIDEAAKEL
RGD 3:    DAAEREGVMLIRGDAENIDEAAKEL
RGD 4:    DAAEREGVMLIKKRGDNIDEAAKEL
RGD 5:    DAAEREGVMLIKKTAERGDEAAKEL
RGD 6:    DAAEREGVMLIKKTAENIDERGDEL
RGD 7:    DAAEREGVMLIKKTAENIDEAARGD
RGD 7c:   DAAEREGVMLIKKTAENIDEAAGRGDSP
RGD 8:    DAAEREGVMLIKKTAENIDERGD
```

Figure 5.2: a) The structure of the LOV2 domain with the Jα-helix displayed in red, and the PHSRN motifs in turquois. b) Amino acid sequence of the Jα-helix of the WT LOV2 domain and the first generation of mutants. Important amino acids promoting the interaction with the β-sheet are underlined. Amino acids, which can be exchanged to stabilize the helix docking are highlighted in yellow, the positions where the RGD motif was introduced are displayed in red and the context amino acids of the RGD motif in fibronectin are shown in blue.

Second, I implemented stabilizing mutations to increase the dynamic range of the LOV2-RGD mutants. Strickland et al.[172] found several amino acids, which are involved in the docking of the Jα-helix to the β-sheet and therefore stabilizing the dark state. By replacing these amino acids with amino acids allowing better hydrophobic interactions, the dynamic range of the protein mutants could be increased, namely less protein is active in the dark. I followed this approach, by substitution of the original amino acids (indicated in yellow in the WT sequence of LOV2, Figure 5.2b) with alanine.

Third, to increase the local density of the RGD motif on the surface, different RGD-sequence positions of the initial LOV2-RGD set were combined, resulting in LOV2 mutants with double or even triple RGD motifs. The detailed amino acid sequences can be found in the appendix (Figure A11).

Forth, it is known that the PHSRN motif can act synergistically on the binding of integrins to RGD and that the synergistic effect is based on the distance between the PHSRN and the RGD motif.[16,22] Since, the helix has a distance of about 31 Å, the PHSRN motif can be combined with RGD motifs in the helix when localized at the beginning or the end of the Jα-helix. Here, I exchanged original amino acid sequence with the PHSRN motif at positions localized either at the beginning of the Jα-helix (PHSRN iii), in a β-sheet loop close to the end of the Jα-helix (PHSRN i) or at the N-terminus (PHSRN ii). I investigated the effect of distance dependent synergistic influences by combining for example, PHSRNii with the RGD 7 mutant on integrin binding affinity upon helix unfolding. Due to the distance dependency, only specific combinations with the already designed LOV2-RGD mutants were taken (for sequences see appendix, Figure A11).

Last, it is known that the RGD motif is the minimal binding motif for integrin adhesion, but there are several other factors playing a role in integrin-matrix adhesion. The studies of Hautanen et al. showed that the context amino acids of the RGD motif also increases cell adhesion.[173] Therefore, I also implemented the framing amino acids of the RGD motif of cellular fibronectin into the Jα-helix, namely mutant RGD 7c (Figure 5.2b). The incorporation was only realizable at the C-terminal end of the helix since proline is known to destroy α-helix conformations.

To generate the respective protein mutants, I designed the respective primers and inserted the desired mutations with site directed mutagenesis polymerase chain reaction (PCR). The detailed nucleobases rendered by mutagenesis are listed in the appendix.

5.3 Characterization of LOV2-RGD Mutants

As described in the chapter IV (Materials & Methods) LOV2-RGD mutants were expressed, amplified and purified in *E. coli* (NiCO). Before interrogating the effects of the LOV2-RGD mutants in cell adhesion experiments, the proteins were characterized with regard to the switching kinetics. Hence, the dark state recovery after blue light illumination was monitored in UV/Vis spectroscopy. Furthermore, the binding affinity of the LOV2-RGD mutants to the integrin fragment $\alpha_v\beta_3$ was

determined in a competitive fluorescence anisotropy binding assay in order to rank the LOV2-RGD mutants for their ability to bind integrin.

5.3.1 Recovery of Dark State after Illumination

The cofactor FMN has a distinct absorption pattern in its UV/Vis spectrum. If the bond between the cofactor and the core cysteine is formed these absorption bands disappear. Upon thermal dark state recovery, the bond between FMN and the protein breaks and the absorption bands are recovered. Therefore, the UV/Vis spectrum can be used to determine the half-life times and therefore, the kinetic of the cofactor recovery. The protein solution was illuminated for 1 min with blue light, and the dark state recovery of the FMN absorption was monitored starting 1 s after illumination with an interval of 18 s for 5 min, as described in section 9.3.1. The absorption at 450 nm was measured and fit with a one-phase association curve, resulting in a half-life time for the cofactor recovery (Figure 5.3a+b).

The LOV2-RGD mutants were categorized according to the half-life times of dark state recovery. The fast switching mutants exhibit a half-life time under 50 s (Figure 5.3b), the medium switching mutants between 50 s and 70 s (Figure 5.3c) and the slow switching mutants of more than 70 s (Figure 5.3d). Mutants with the RGD motif incorporated at the beginning or the end of the Jα-helix show a similar switching behavior than the WT LOV2 domain, displayed in red. Also, mutants with multiple RGD motifs (at the beginning or end of the helix) show a fast switching. In contrast, mutants with the RGD motif incorporated in the middle of the helix exhibit a decreased switching speed, as well as the double mutants with one of the respective RGD motif positions. Incorporation of the helix stabilizing mutations as well as the PHSRN motifs led to an increased half-life time of the dark state recovery, as shown below (Figure 5.3c-e). However, the reversion times of all LOV2-RGD mutants are in a similar range as the reversion time of the WT LOV2 domain.[174-177]

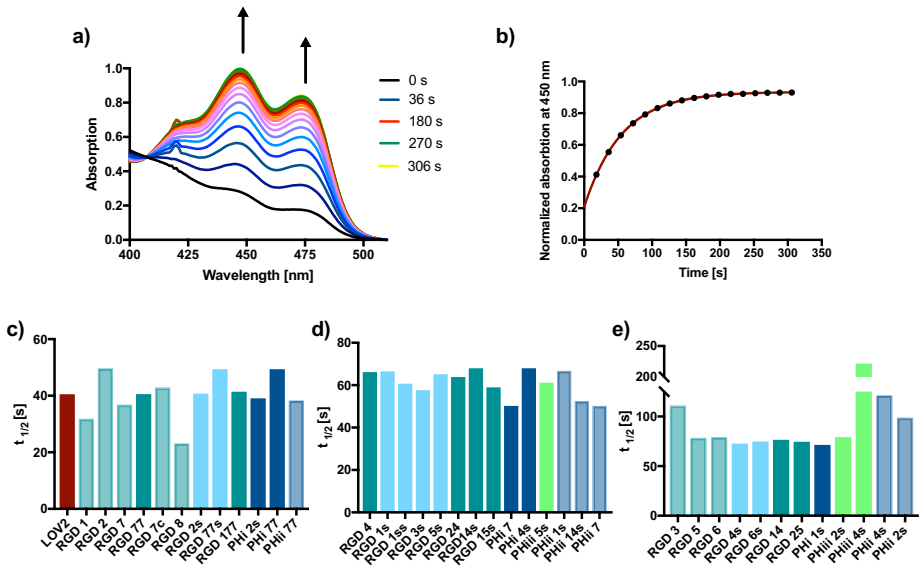

Figure 5.3: Dark state recovery after blue light illumination monitored via the specific absorption bands of FMN. Indicated in red the WT LOV2 domain, the initial mutant set with a single RGD motif is displayed in light turquoise, the set of mutants with multiple RGD motifs are displayed in turquoise and the mutant set with additional stabilizing mutations are displayed in light blue. The combinations with the PHSRN motifs are displayed in dark blue, light green and faint dark blue for PHSRNi, PHSRNiii

and PHSRNii, respectively. a) Exemplary a normalized UV/Vis reversion kinetics of PHii 77 is shown, every 18 s a spectrum was taken. b) Plot of normalized values at 450 nm over time, fit with a first order kinetic. c) Fast switching mutants exhibiting a half-life under 50 s. c) Medium switching mutants exhibiting a half-life of 50 s – 70 s. d) Slow switching mutants, exhibiting a half-life > 70 s.

5.3.2 Determination of the Binding Affinity of LOV2-RGD Mutants to Integrin

In order to select the most promising candidates from the library of LOV2-RGD mutants, the binding affinity of the LOV2-RGD to the integrin fragment $\alpha_v\beta_3$ (MW = 192300 g/mol) was assessed in a competitive fluorescence anisotropy binding assay (Figure 5.4a). As competitor for the mutants, an RGD motif attached to the TAMRA fluorophore (TAMRA-RGD; MW = 960 g/mol) was used in the assay. Addition of LOV2-RGD to the preformed TAMRA-RGD/integrin complex, led to displacement of the fluorophore by LOV2-RGD and thereby to decreased fluorescence anisotropy.

Formation of TAMRA-RGD/integrin Complex

First the amount of integrin $\alpha_v\beta_3$ fragment needed to saturate 20 nM TAMRA-RGD fluorophore was determined by addition of integrin $\alpha_v\beta_3$ fragment to a solution of the fluorophore (Figure 5.4b). Upon addition of integrin fragment $\alpha_v\beta_3$ the anisotropy of TAMRA-RGD increased due to decreased mobility of the fluorophore in the solution. The saturation level was determined at 60 nM $\alpha_v\beta_3$, which was further applied in all competitive binding assays as well as in the control experiments (Figure 5.4 b, indicated by the dashed grey line).

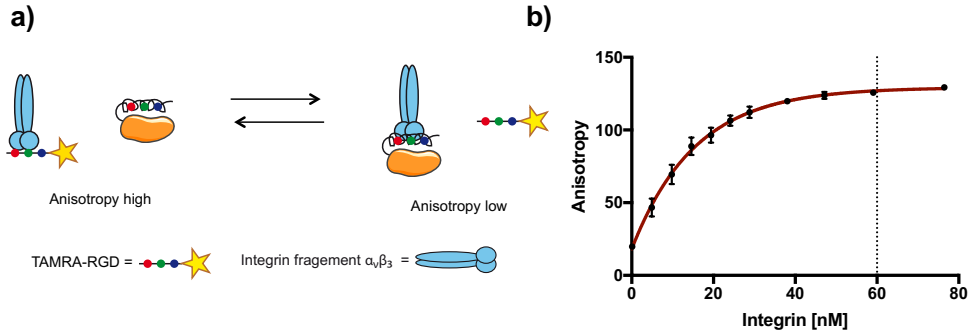

Figure 5.4: a) Sketch of fluorescence anisotropy competitive binding assay, showing high anisotropy upon TAMRA-RGD binding to integrin and low anisotropy when it is replaced from the complex by LOV2-RGD. b) Titration of integrin fragment αvβ3 to TAMRA-RGD, yields in saturation of the fluorophore at 60 nM, indicated by the dashed line. Experiment conducted in triplicates.

To eliminate the possibility of unspecific binding, the formation of the TAMRA-RGD/integrin complex in buffer lacking divalent ions was monitored. No formation of TAMRA-RGD/integrin complex (Figure A13b) could be observed. Moreover, further addition of RGD 7 to this solution did not alter the anisotropy of the fluorophore solution. To assess the specificity of the binding, I performed a competitive binding assay between the WT LOV2 domain and the preformed TAMRA-RGD/integrin complex, showing only a slight decrease in anisotropy upon protein addition (Figure A13c). This indicates specific recognition of the RGD motif by the integrin fragment. The formation of the TAMRA-RGD/integrin complex was completed after 45 min as shown by observation of the complexation kinetics.

Furthermore, the TAMRA-RGD/integrin complex was stable over 300 min, as shown by a constant anisotropy over this time interval (Figure A13a).

Competitive Binding Assay

After determination of the needed integrin concentration to form the initial TAMRA-RGD/integrin complex, competitive binding assays were performed. For this, LOV2-RGD was successively added to the solution of TAMRA-RGD/integrin complex, which was preformed for 45 min. After an equilibration time of 30 min, the anisotropy of the solution was determined in dark and equilibrated in blue light for another 30 min before measurement. The obtained anisotropy curves were fit (Figure 5.5), and the amount of protein to displace 50 % of the integrin from the TAMRA-RGD/integrin complex was calculated (Equation 1-5). Three separate experiments per LOV2-RGD mutant were performed and the mean was calculated.

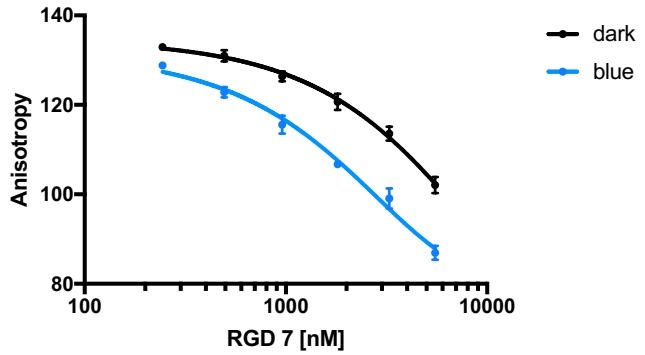

Figure 5.5: Exemplary anisotropy curve of the competitive binding assay of RGD 7. Three independent experiments were performed, SD is displayed. Data points were fit to a Hill equation.

In order to compute the final K_d values, the obtained values from the fit curves have to be adjusted to the competing equilibrium. Therefore, kinetic considerations have to be conducted, as shown below.

Calculation of the Dissociation Constant

The obtained curves were fit with the Hill1 equation using Origin, assuming the starting value of anisotropy as a fixed starting point. From these fits the required concentration of LOV2-RGD mutant needed to replace half of the TAMRA-RGD fluorophore from the complex, was determined. For the first equilibrium between TAMRA-RGD/integrin and free integrin and free fluorophore, equation 1 is set:

$$[\text{TAMRA-RGD/integrin}] \overset{K_{d1}}{\rightleftharpoons} \text{TAMRA-RGD}_{free} + \text{Integrin}_{free}$$

Equation 1:

$$K_{d1} = \frac{[\text{Integrin}_{free}] \cdot [\text{TAMRA-RGD}_{free}]}{[\text{TAMRA-RGD/integrin}]}$$

Equation 1 describes the equilibrium for TAMRA-RGD/integrin and can be solved by the following assumptions: K_{d1} was derived from the curve fit (Figure 5.4b) and determined to be 15.48 nM ± 1.7 nM. In the equilibrium, the concentration of TAMRA-

RGD/integrin was set (emanating from 20 nM fluorophore and 60 nM integrin fragment as starting concentrations) as 20 nM-x, the concentration of free integrin can be set as 40 nM+x, whereas x represents the amount of free fluorophore when the equilibrium is reached. With these values the amount of free fluorophore (TAMRA-RGD_{free}, x) was determined as 5.09 nM and the concentration of TAMRA-RGD/integrin (20 nM - x) at the equilibrium is 14.92 nM.

Upon addition of LOV2-RGD the equilibrium (equation 1) was shifted to a lower concentration of TAMRA-RGD/integrin complex. From the Hill1 fit the amount of protein required for displacing 50 % of the fluorophores from the integrin complex was determined for both conditions in dark and under blue light illumination, respectively. The equilibrium between TAMRA-RGD/integrin, TAMRA-RGD_{free} and $Integrin_{free}$ was now shifted to only half of the concentration of the TAMRA-RGD/integrin complex (7.46 nM), accompanied by an increased concentration of free fluorophores (12.54 nM) and $Integrin_{free}$ (9.21 nM).

To determine K_{d2} of the competing reaction, the equilibrium between LOV2-RGD/integrin and the free components is given with equation 2.

$$\text{LOV2-RGD/integrin} \overset{K_{d2}}{\rightleftharpoons} \text{LOV2-RGD}_{free} + \text{Integrin}_{free}$$

Equation 2:
$$K_{d2} = \frac{[\text{Integrin}_{free}] \cdot [\text{LOV2-RGD}_{free}]}{[\text{LOV2-RGD/integrin}]}$$

Combining equations 1 and 2 allows to assess K_{d2} with equation 3, taking both reactions into account, as shown in the following equilibrium:

$$[\text{Integrin}_{free}] = \frac{K_{d2} \cdot [\text{LOV2-RGD/integrin}]}{[\text{LOV2-RGD}_{free}]} = \frac{K_{d1} \cdot [\text{TAMRA-RGD/integrin}]}{[\text{TAMRA-RGD}_{free}]}$$

Equation 3:
$$K_{d2} = \frac{K_{d1} \cdot [\text{TAMRA-RGD/integrin}] \cdot [\text{LOV2-RGD}_{free}]}{[\text{TAMRA-RGD}_{free}] \cdot [\text{LOV2-RGD/integrin}]}$$

The concentration of LOV2-RGD/integrin can be assessed by assuming that the total amount of integrin equals the sum of all integrins either bound in complexes (with TAMRA-RGD or LOV2-RGD) or as free integrins (equation 4).

Equation 4:
$$\text{Integrin}_{total} = \text{TAMRA-RGD/integrin} + \text{Integrin}_{free} + \text{LOV2-RGD/integrin}$$

With TAMRA-RGD/integrin = 7.46 nM, $Integrin_{total}$ = 60 nM and $Integrin_{free}$ = 9.21 nM, the concentration of LOV2-RGD/integrin complex was calculated to be 43.33 nM. The

concentration of free protein was similarly derived by the assumption shown in equation 5. Thereby, LOV2-RGD$_{total}$ represents the amount of protein required to replace 50 % of the fluorophores from the TAMRA-RGD/integrin complex and was given by Hill1 fit of the original curves.

Equation 5: $$LOV2\text{-}RGD_{total} = LOV2\text{-}RGD_{free} + LOV2\text{-}RGD/integrin$$

With the values for K_{d1} = 15.48 nM, TAMRA-RGD/integrin = 7.46 nM, TAMRA-RGD$_{free}$ = 12.54 nM, LOV2-RGD/integrin = 43.33 nM and the values for LOV2-RGD$_{free}$ extracted from equation 5; equation 4 can be solved for each LOV2-RGD mutant for the dark and lit states, respectively (Figure A14).

Ranking of Mutant Library

After calculation of the K_{d2} values, the protein mutants were ranked due to their capability to bind integrin in the lit state but not in dark. Therefore, the ratio of the $K_{d2,dark}/K_{d2,blue}$ was used as a figure of merit for photoswitchability (Figure A14). The mutants were grouped into four categories. One group comprises the mutants with a $K_{d2,dark}/K_{d2,blue}$ above 1.95 showing also a significant difference between the values in dark and blue (Figure 5.6).

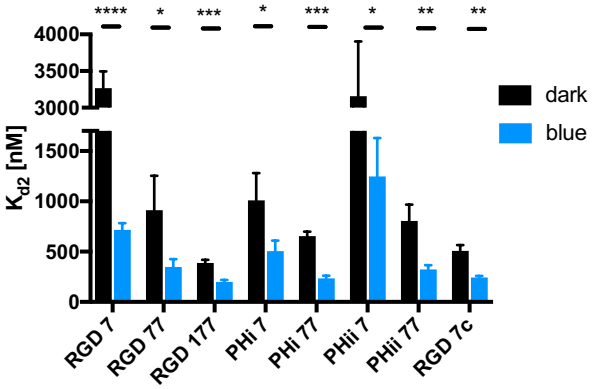

Figure 5.6: K_{d2}-values of the most promising LOV2-RGD mutants showing the highest difference in affinity to integrin between dark and lit state. SD displayed. Experiments were conducted in triplicates.

Only the incorporation of the RGD motif at the beginning and at the end of the Jα-helix led to significant photoswitchablility. The affinity for integrin was almost 4.5-fold higher under blue light than in dark for the RGD 7 mutant with one RGD motif integrated at the end of the helix, and 1.7-fold for the RGD 1 mutant (Figure 5.7a).

The introduction of helix stabilizing mutations did not, or only neglectably led to an increased caging of the RGD in the dark state. For mutant RGD 7 the stabilization led to an even significantly decreased dissociation constant in the dark, meaning enhanced binding in the dark, in comparison to the original mutant.

Combining several RGD motifs in one RGD mutant led to increased binding affinity of the mutant to integrin and therefore to a smaller dissociation constant in dark and under blue light. This could be monitored for all combinations of RGD motifs

independent from the position of the motifs. Nevertheless, some RGD motif positions exhibited a higher binding affinity than others, no matter if they were introduced alone or in combination with other motifs (RGD 1 vs RGD 2, Figure 5.7). The most promising mutants with multiple RGD motifs is RGD 77 with two consecutive RGD motifs at the end of the helix (exhibiting a 2.6-fold increased affinity to integrin under blue light illumination than in dark), and the combination of RGD 7 with RGD 1, yielding RGD 177 with a 1.9-fold affinity increase.

The effect of the incorporation of the PHSRN motif is highly dependent on the position of the RGD motif. Introduction of PHSRNi (PHi) (in the β-sheet loop, close to the end of the Jα-helix (Figure 5.2a), led to an increased binding affinity when combined with RGD motifs at the end of the helix, like PHi 7, PHi 77 and PHi 4s, but not when combined with motifs at the beginning of the helix like PHi 1s and PHi 2s. However, the $K_{d2,dark}/K_{d2,blue}$ ratio was not increased upon PHSRNi introduction. The insertion of PHSRNiii (PHiii) (immediately before the Jα-helix) did only exhibit any increase in the binding affinities or on the $K_{d2,dark}/K_{d2,blue}$ ratio, therefore this set of mutants was discarded and not further taken into account for cell adhesion studies. Incorporation of the PHSRNii (PHii) motif at the N-terminus of the Jα-helix did not result in a significant increase in the binding affinity of the LOV2-RGD mutants, nevertheless a reasonable $K_{d2,dark}/K_{d2,blue}$ ratio is preserved for PHii mutants combined with RGD motifs at the end of the helix (PHii 7, PHii 77). Because the synergistic effect of PHSRN may only be significant when integrins are engaged in FA, these mutants were further tested in cell adhesion experiments.[14]

The incorporation of the surrounding amino acids of the RGD from cellular fibronectin led to a major enhancement in binding affinity of integrin to the RGD 7c mutant in comparison to RGD 7, while a 2-fold increase in integrin affinity under blue light is preserved. Since also other integrin types than $\alpha_v\beta_3$ are involved in cell-matrix adhesion, which are exhibiting different kinetics and binding affinities to cellular FN, the trends found in in vitro studies do not necessarily reproduce the trends in cell-matrix adhesion,[15,20,178-180] and need to be tested in cell adhesion experiments.

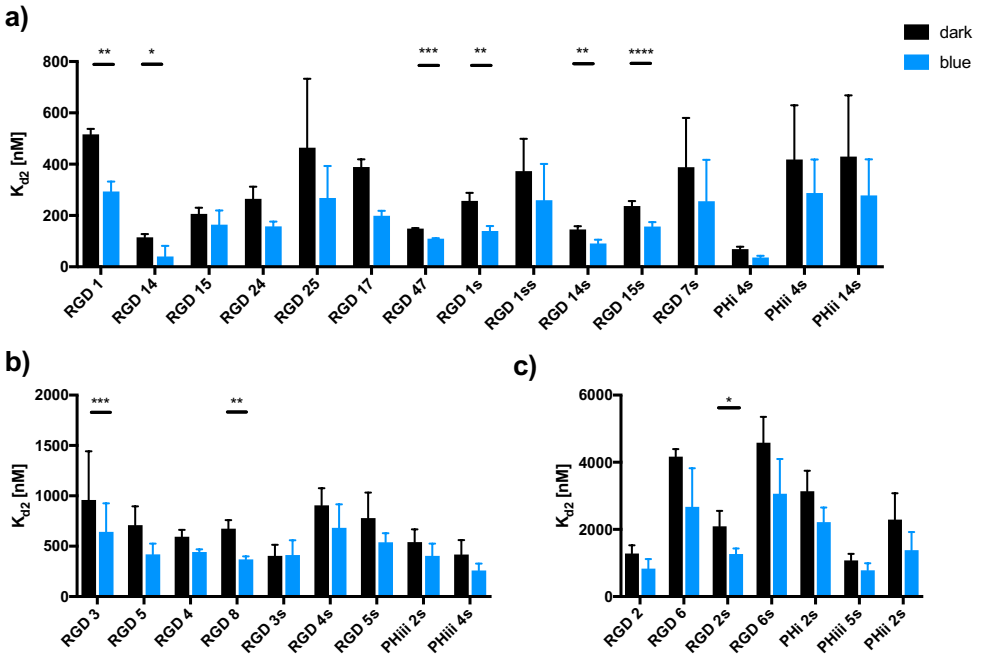

Figure 5.7: K_{d2}-values grouped according to their dark state affinity in a) good binders with a Kd2 < 800 nM, and b) medium binders Kd2 <1000 nM and >800 nM. SD displayed. c) Group of non binders exhibiting a K_{d2}-value above 1000 nM.

Besides the LOV2-RGD mutants exhibiting a $K_{d2,dark}/K_{d2,blue}$ above 1.95 the mutants were sorted regarding their binding affinity in dark. For the group of good binders all mutants exhibiting a dark state binding affinity below 800 nM were chosen. For the group of medium good binders, a limit of the $K_{d2,dark}$ of below 1000 nM was chosen. Some design strategies did not lead to significant binding of integrin. These mutants, exhibited a dark state dissociation constant above 2000 nM and a $K_{d2,dark}/K_{d2,blue}$ ratio < 1.66. These were categorized as "non-binders" and not further used in cell adhesion studies (Figure 5.7c). As a positive control cRGD was used, showing a $K_{d2,dark}$ of 54 nM ± 2.8 nM (Figure A13d).

With our protein design strategies, a library of 40 mutants representing different dynamic range in the affinity to integrin could be obtained. The dynamic range in binding affinity of other LOV2 based systems varies broadly depending on the introduced effector,[150,154] additional mutations[151] in the protein domain and the experimental setup the photo-switch is used in,[181] and need to be adapted or chosen in regard of the dynamic range of the modulated process.

From the 40 mutants of the LOV2-RGD library, eight mutants (Figure 5.6) were selected showing the highest photoswitchability (Figure A14) and further characterized in cell adhesion studies.

5.4 Cell-Matrix Adhesion Studies

In order to assess the ability of the most promising LOV2-RGD mutants derived from the fluorescence anisotropy measurements, the mutants were employed in cell adhesion studies. To determine whether the employed light intensities negatively affect the cell metabolism, a colorimetric metabolic activity assay was performed. Therefore, the cell induced reduction of 3-(4,5-dimethylthiazol-2-yl)-2,5-

dephenyltetrazolium bromide (MTT) dye to a formazan derivative was studied by absorption measurement of the product at 540 nm after 4 hours incubation with the cells. Reduced absorption indicates a reduced metabolic activity and thereby an influence of the employed light on the cells. The metabolic activity of U-2 OS cells was determined in dependence of different light intensities (Figure 5.8).

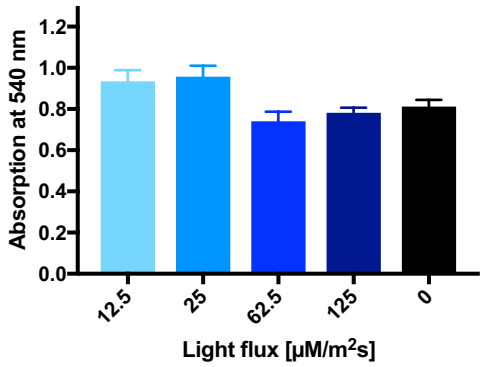

Figure 5.8: Colorimetric metabolic activity assay to determine phototoxic effects of blue light in different intensities on U-2 OS cells. No significant change in the metabolic activity could be observed in all light intensities in compared to samples kept in dark.

The absorption at 540 nm is the same within the error bars under all employed light intensities and in dark (Figure 5.8). This concludes that light of the wavelength of 471 nm does not have phototoxic effects on the metabolic activity of the cells. In order to employ enough intensity to sufficiently reach the switching equilibrium of the LOV2-RGD mutants, light of 471 nm at an intensity of 12.5 µM/m^{2}s was used for all further cell adhesion studies. Higher intensities may not affect the metabolism of U-2 OS cells, but since the system should be employable to less robust cell types,[182] or primary cells,[183] t higher intensities are avoided.[184]

5.4.1 Cells can Adhere to Surfaces Modified with LOV2-RGD Mutants

Before investigating the ability of LOV2-RGD mutants to reversibly switch cell-surface adhesion, the ability to mediate cell adhesion was assessed. Therefore, glass surfaces were coated with a self-assembled monolayer (SAM) of PEG_{azide} and further functionalized with copper mediated click-reaction with NTA-alkyne. The NTA groups were charged with Ni^{2+} and the respective protein mutant was subsequently immobilized. 5000 cells/cm^2 were seeded in serum free medium onto the protein functionalized surfaces and incubated in dark or under 12.5 µM/m^{2}s blue light illumination for 2 hours. After fixation, the actin network was stained with phalloidin-Tritc to observe whether cell spreading has occurred and the nucleus with dapi, which allowed to assess the number of adherent cells on 1 cm^2 (Figure 5.9). Non-adherent cells were washed away during the staining process.

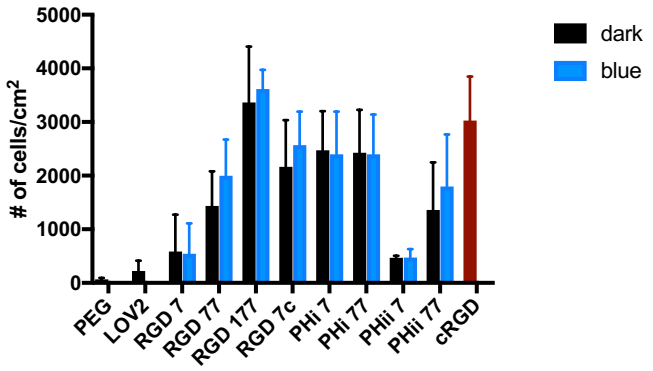

Figure 5.9: Number of adherent cells on surfaces coated with the respective LOV2-RGD mutants in dark or under 12.5 µM/m^{2}s blue light illumination. Surfaces coated with LOV2 as well as the PEG passivated surface (PEG) served as negative controls, whereas surfaces coated with cRGD were taken as positive control. No difference in the cell number between the lit state and the dark state could be found, but trends found in the fluorescence anisotropy experiments could be confirmed. Multiple RGD motifs increased the integrin binding capability of the surfaces compared to surfaces with single mutants. Also the incorporation of the context amino acids found in cFN led to increased cell adhesion. Experiments were conducted in triplicates and the error bars represent the SD.

The LOV2-RGD mutants are able to mediate cell adhesion to different degrees. The trends found in the fluorescence anisotropy characterization could be reproduced. Mutants showing only low binding to the integrin fragments in the fluorescence anisotropy measurements, exhibited a higher dissociation constant (K_{d2}) and also less cells could adhere to the respectively modified surfaces. The trend of increased affinity to integrin by introduction of multiple RGD motifs was also confirmed in the cell adhesion study. A single RGD motif was not enough to mediate proper cell adhesion. The number of cells on surfaces functionalized with RGD 77 was higher than on surfaces with RGD 7 and RGD 177 showed the highest number of adherent cells. Almost as many cells adhered to surfaces coated with RGD 177 than to the positive control cRGD. As negative controls PEG covered surface itself or functionalized with the WT LOV2 was utilized, showing almost no adherent cells (Figure 5.9). Only few cells could attach to surfaces functionalized with the LOV2 domain; however, no spreading occurred, indicating that the adhesion mediated by the LOV2-RGD mutants is specific recognition of the RGD motif by the cellular integrins. The six-fold increase in affinity to integrin for RGD 7 received from the anisotropy fluorescence experiments could not be reproduced in cell adhesion experiments. The caging of the RGD motif in solution was more efficient than if cells adhere actively to the LOV2-RGD 7 protein. As afore mentioned also other families of integrin are involved in cell-matrix adhesion and contribute to the binding of to the RGD motif. Integrins like $\alpha_5\beta_1$ are binding exclusively FN and exhibit different dynamics and affinities to the RGD-motif, which cannot be compared to the in vitro studies with isolated $\alpha_v\beta_3$.[185]

The incorporation of the PHSRN motifs had a significant effect on cell adhesion and the response to blue light. When RGD 7 was combined with PHi or PHii, cells adhered more efficiently to these surfaces than to surfaces with mutants without the synergy peptide. Additionally, the cells spread better under blue light than in dark, and in comparison to RGD 7. The improved spreading under blue light was according to the initial design. In dark the PHSRN motifs are spatially close to the RGD 7 motif (< 5 Å),

whereas under blue light the helix unwound and the optimal distance between the PHSRN motif and the RGD motif was achieved. The PHSRN motifs (PHi, PHii) are in close proximity to each other but exhibit different effects when combined with RGD 7. However, the combination of the PHi motif (in the loop of the β-sheet, Figure 5.2a) with the RGD 7 at the end of the helix resulted in increased cell numbers on the respective surfaces, the combination with the PHii motif (which is located at the N-terminus, so in close proximity to the PHi motif) did not improve cell adhesion compared to the RGD 7 mutant. Similar effects can be observed with the combinations of the respective PHSRN motifs and the RGD 77 mutants. The combinations of the particular PHSRN motifs and the mutant RGD 1s did not lead to higher cell numbers on the respective surfaces (Figure A15).

The introduction of the amino acid context of RGD found in cellular fibronectin led to an increase in the number of adherent cells in comparison the RGD 7, confirming trends already found in literature.[173] Since integrin mediated cell-matrix adhesion is a complex process, many other aspects can influence cell-matrix adhesion. Not only other integrins are involved in adhesion to the RGD motif and the PHSRN motif, the cells can also apply force, which activates and strengthens the integrins bonds.[186] By the application of force it is also conceivable that the cells will model the synthetic FN, LOV2-RGD.[187,188]

Not only the number of adherent cells is an aspect in cell-matrix adhesion, but also the adhesion area of the spread cells. Proper cell adhesion leads to cell spreading, which is a prerequisite for cell performance. If the cell can find enough adhesion points, it will spread and explore the given environment. If the cells cannot sufficiently establish cell-matrix contacts, they retain their spherical shape with only little contact to the surface. Upon spreading the cell flattens to a fried-egg morphology and form FA. The actin staining was used to evaluate the spreading area of the cells on the different LOV2-RGD mutants. The adhesion area of 70 cells was determined, and the distribution of the spreading area on the respective surfaces was analyzed and displayed in a frequency plot. Figure 5.10 depicts examples of the spreading area of cells interacting with surfaces functionalized with RGD 177 in dark and under blue light illumination, respectively. As a positive control cells on surfaces covered with cRGD are shown.

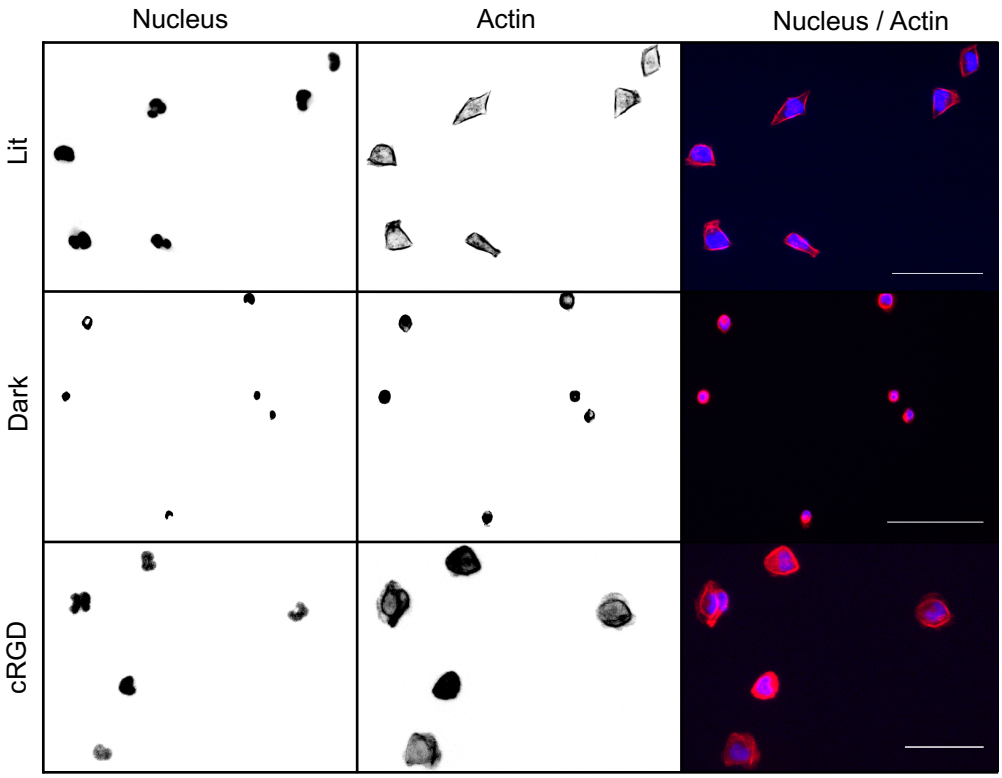

Figure 5.10: Exemplary images of cells adhered to surfaces coated with RGD 177 either incubated in the dark or under blue light illumination. Cells on cRGD functionalized surfaces are shown as a positive control. In the merged image, actin is displayed in red and the nucleus is displayed in blue. Scale bar 100 µm.

The frequency analysis (Figure 5.11a) of the distribution of the spreading area on RGD 177 surfaces, showed a shift to larger areas on blue light illuminated samples compared to cells grown in the dark. Cells adhered to the lit state surfaces exhibited two different fractions, one fraction with spreading areas around 200 µm^2, similar to the dark state, and a second fraction with a broader distribution peaking around 320 µm^2. It can be assumed that the first fraction are cells, which found only few adhesion spots to attach to the surface, but not enough for sufficient spreading, similar to the dark state surfaces. Whereas the second fraction of cells were able to form enough adhesion contacts to effectively spread (Figure A16).

Figure 5.11b depicts the spreading areas as box plots determined on surfaces kept in dark or under blue light illumination for each mutant, respectively. As afore mentioned, the median spreading area on several LOV2-RGD mutants exhibited differences between samples kept in dark or under blue light illumination. The most promising candidates were RGD 77, RGD 177, RGD 7c, PHi 7 and PHii 7, since they exhibited a significant difference between the spreading area of cells on dark samples compared to lit samples. The mutants RGD 177 and PHi 7 show a difference of about 60 µm^2 difference in the median spreading area, indicating a stronger adhesion under blue light. PHii 7 only exhibit a difference of about 40 µm^2, showing a decreased adhesion within the timescales compared to the aforementioned protein mutants under blue light illumination. Interestingly RGD 7c showed a higher spreading area on the dark state samples. As aforementioned, cRGD exhibits a higher affinity to

integrin than the natural ligand, which is attributed to the relative orientation of the amino acids to each other in the cyclic orientation.[78] Suggesting that in the dark state RGD 7c exhibits a helical conformation of the GRGDSP motif, it may be a preferred conformation for integrin adhesion in the dark (pseudo cyclic) than in the lit, disordered, state, which favors the adhesion of integrin.

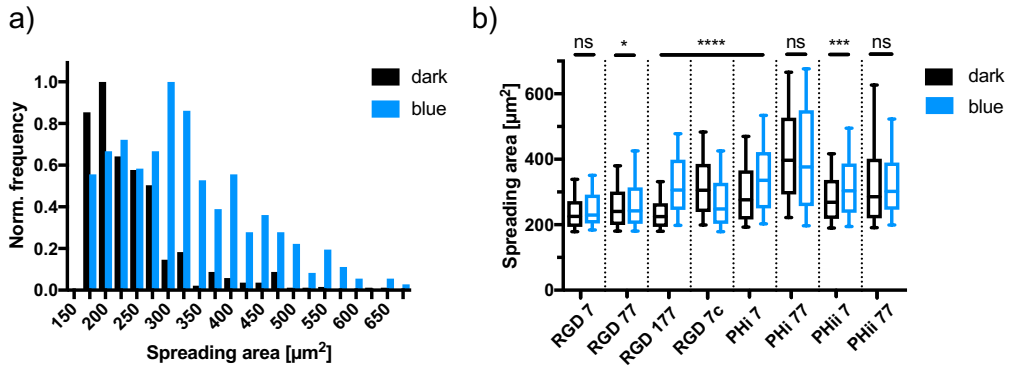

Figure 5.11: Spreading area analysis of cells incubated on surfaces functionalized with the respective protein mutant, in dark or under blue light illumination. a) Frequency plot of cells spread on LOV2-RGD 177 functionalized surfaces in dark (black) or in lit state, showing two populations in the lit state (blue). The spreading area of the first population peaks at 200 µm^2 , whereas the spreading area of the second population peaks at 320 µm^2 b) Spreading area of cells incubated on the respective surfaces in the dark or under blue light illumination. Experiments were conducted in triplicates, cell number analyzed: n > 500, 10 - 90 % confidence interval is shown.

5.4.2 Formation of Focal Adhesions in Dependence of LOV2-RGD Mutants

In order to investigate the formation of focal adhesions on the different surfaces, FA proteins were visualized by immunofluorescence. To visualize the formation of FAs, vinculin was targeted as it is recruited at an early time point of the focal adhesion. To verify the tension-mediated maturation of the focal adhesion, the late time point FA protein zyxin was chosen. Zyxin is recruited to actin stress fibers with increasing forces applied from the cell to the surface.[38,189] In the magnification of the FAs, it can be observed that zyxin is recruited to the tip of the FA, whereas vinculin is present in the complete FA. Mature FA can be found on surfaces coated with the respective protein mutants independently of the state (light or dark) of the respective protein mutants (Figure 5.12). Differences in shape and polarization of the cells (Figure 5.12) are caused by the selection of images and do not show any trend based on the respective protein mutant or illumination state.

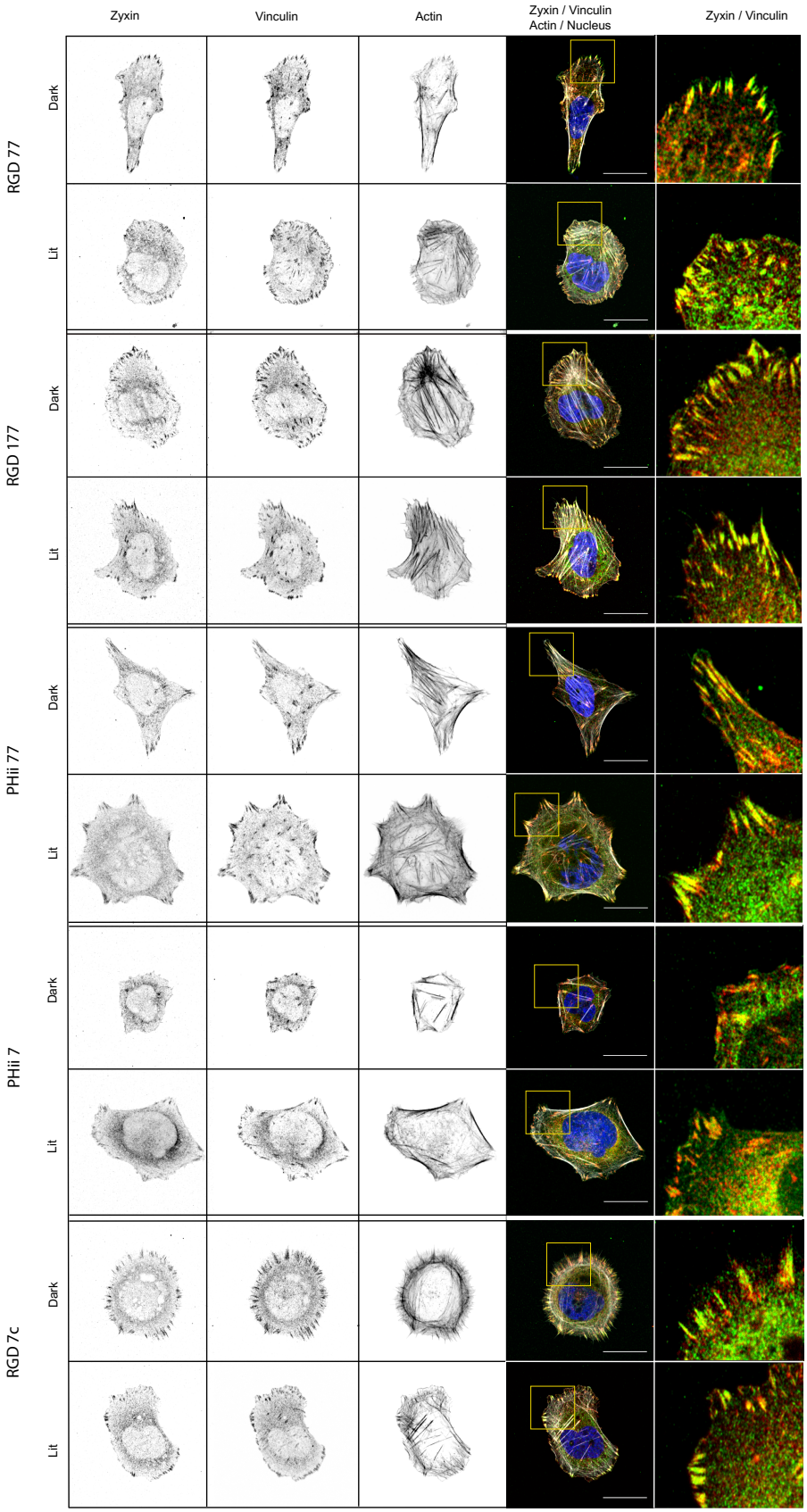

Figure 5.12: Immunofluorescence of focal adhesion proteins in cells, cultured on the different indicated surfaces. In the merged image, zyxin is displayed in green, vinculin is displayed in red, actin is displayed in grey and the nucleus is displayed in blue. No difference in the formation of focal adhesions between the dark and the lit state could be observed. Scale bar 20 µm, panel length: 20 µm.

In cell adhesion experiments five mutants were found, which mediated proper cell adhesion and changes cell adhesion in response to blue light. These mutants cover a range of adhesiveness and switchability. The most promising designs were RGD 177, PHi 7, PHii 7, RGD 77 and RGD 7c. After the capability of the LOV2-RGD mutants to mediate different degrees of cell adhesion depending on the protein state was assessed in cell adhesion experiments, the reversibility of these systems needed to be verified.

5.4.3 Reversible Switching of Cell Adhesion

To determine the reversibility of cell adhesion on surfaces functionalized with the LOV2-RGD mutant, cells were seeded on surfaces functionalized with the respective protein mutant. To compare the change in the spreading area upon switching the protein surface to the less adhesive, dark state, surfaces were either kept under blue light illumination for 3 h, kept in dark for 3 h or were switched from the illuminated state to the dark state after two hours.

Subsequently, the spreading area based on the actin staining was analyzed. Cell adhesion could only be switched effectively on surfaces functionalized with the mutants RGD 77 and PHii 7 (Figure 5.13).

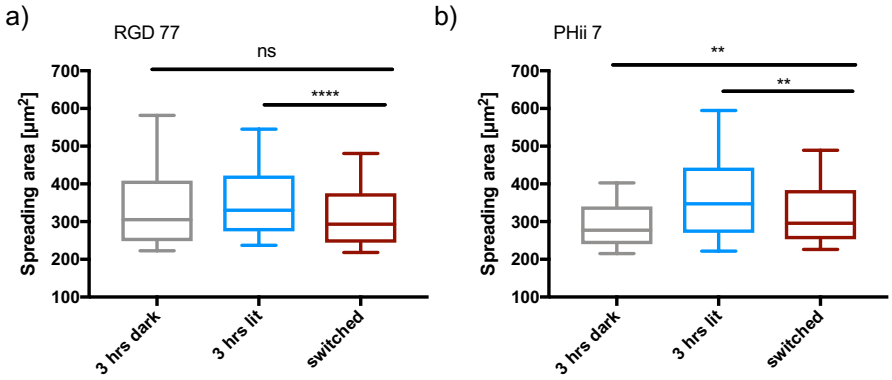

Figure 5.13: Reversion of the spreading area of cells cultured for 3 h on the respective protein surfaces in either dark (grey box), lit (blue box) or switched to dark after 2 h blue light illumination (red box). The experiments were conducted in three technical repeats, cell number analyzed: n > 140. 10 % - 90 % confidence interval is shown.

The surfaces functionalized with RGD 77 were successfully switched resulting in a decreased spreading area of 310 µm^2 (Figure 5.14a). Since the cells on surfaces kept in the lit state exhibited a spreading area of 360 µm^2, the spreading area decreased about 14 % when the illumination was stopped. The spreading area of cells on surfaces kept in dark do not differ from the spreading area on the switched sample, indicating a full reversion to the dark state within one hour. Similar results were obtained for PHii 7 (Figure 5.13b). However, the average spreading area did not completely but partially switch back to areas obtained in the dark state. This indicates a different adhesion kinetic on surfaces functionalized with PHii 7, which was expected since the PHSRN motif is an additional adhesion motif and will positively render the mode of integrin adhesion to the RGD motif.

Noticeable is also the variance of the average spreading area on both samples. Cells on surfaces coated with RGD 77 have a distribution of about 150 µm^2 (25 % - 75 %

confidence interval), independent of the illumination state. Cells on surfaces coated with PHii 7 have a variance in the dark of about 100 μm^2 but almost double on lit state surfaces. This indicates that the cells start to spread more on illuminated samples. Cells on reversed surfaces exhibit a variance of about 120 μm^2, showing a partial reversion in the spreading areas when illumination is stopped. For the other mutants, no reversion could be observed (Figure A17). Cell adhesion was reversible on surfaces where cells adhered but spread less (RHD 77 and PHii 7) in comparison to surfaces where cells adhered and spread extensively (RGD 177, PHi 7, RGD 7c). Potentially, this is caused by strong binding of integrin to the RGD which prevents the refolding of the Jα-helix in the dark and thereby reversion. Thus, LOV2-RGD mutants exhibiting a weaker binding to RGD can undergo reversible conformational changes when the integrin dissociates from the Jα-helix.

To verify the reduced average spreading area on samples kept in dark, cell-surface interactions of living cells were monitored during the dark state induced detachment process using the (interference reflection microscopy) IRM setup. In the IRM setup the proximity of the sample to the surface is assessed, allowing an estimation of the spreading area of each cell. Additionally it is noninvasively, can be used without pre staining of the cells and was used at longer wavelength (632 nm) to avoid unintentional activation of the LOV2-RGD mutants.

U-2 OS cells were seeded on protein functionalized surfaces and incubated in serum free medium under blue light illumination for two hours to allow adequate cell-matrix adhesion. Afterwards the surfaces were transferred to the microscope and further monitored in the IRM mode in either dark or under blue light illumination for three additional hours. The experiments were conducted in duplicates, averaging the spreading area of at least 70 cells per condition and error was displayed as SEM.

Integrin mediated cell-matrix adhesion could be reversibly switched for both mutants in dark. When the cells were subsequently incubated in dark, the average spreading area decreased on both LOV2-RGD mutants. Cells cultured on surfaces coated with RGD 77 showed a decrease in spreading area to 86 % but cells cultured under blue light on the respective surfaces increased in spreading area to 110 % exhibiting a difference in spreading area of 24 % (Figure 5.14a). Since the intial average spreading area on samples which were monitored in dark in IRM was bigger compared to the samples monitored in IRM under blue light, the total average spreading area after three hours in the respective lit state, does not show the reversion as the normalized average spreading area (Figure 5.14a). Note that also in the live cell reversiblity experiments, the variance of the average spreading area on surfaces coated with RGD 77 is constant, confirming the observation of the previous reversibility experiments.

The spreading area of cells adherent to surfaces coated with PHii 7 in dark, decreased to 86 %. In comparison, cells cultured on the same surfaces under blue light illumination increased their average spreading area to 136 %. This results in a 50 % difference in the spreading area of cells between the dark and lit state of LOV2-RGD coated surfaces (Figure 5.14b). The average spreading area of cells on lit state surfaces is 208 μm^2, whereas cells on surfaces kept in dark only, exhibit a average spreading

area of 81 µm^2. In Figure 5.14c a cell monitored via IRM in dark on a PHii 7 coated surface for three hours is shown exemplarly.

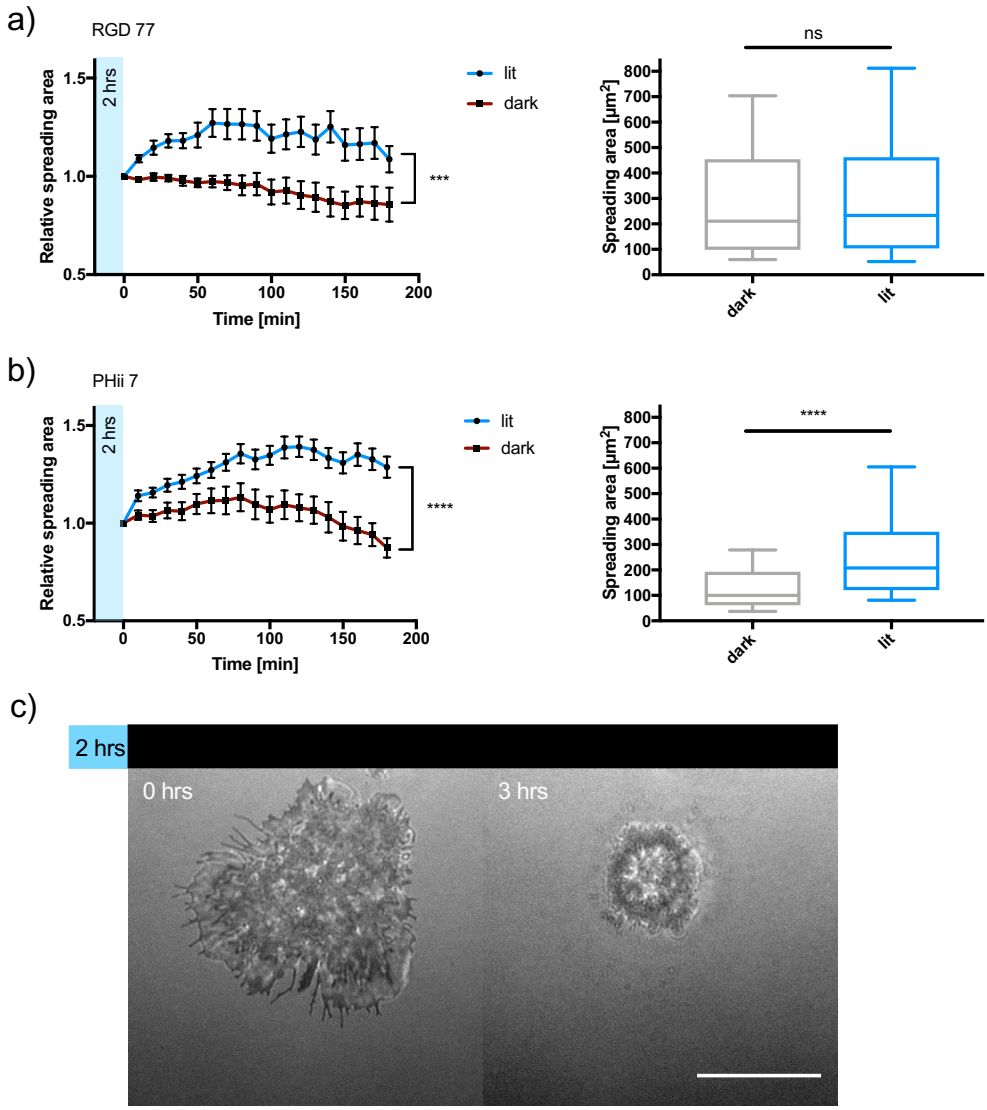

Figure 5.14: Live cell experiments with cells cultured on surfaces functionalized with RGD 77 or PHii 7. First column: Reversion of normalized spreading area of cells on surfaces kept in dark or as a positive control under blue light illumination, after 2 hours blue light preincubation. n = 70 cells, two independent experiments, SEM displayed. Second column: Plot of the not normalized final spreading area between the dark and lit state, 10 – 90 % percentile displayed. a) on surfaces with RGD 77, b) on surfaces with PHii 7. c) Retracting cells on a PHii 7 functionalized surface kept in dark in IRM over the time scale of 3 hours. Scale bar: 15 µm.

Cell-matrix adhesion is not a linear process but can be grouped into three phases. If cells are added to an adhesive surface, they first sedimentate on the surface, forming initial electrostatic interactions. In the second phase initial integrin contacts and nascent FA are formed, strengthening the contact to the underlying substrate and giving the cell a flattened shape. In the third phase, the FA mature, the cells reach the full spreading and the intracellular actin network is formed (e.g. formation of stress fibres). In this phase the cell is able to apply forces to the surface remodel the ECM, polarize and migrate.[190,191] Since RGD 77 and PHii 7 present different adhesion motifs, it is hypothesized that the cells also exhibit different adhesion kinetics on the

respective surfaces, which consequently alters the speed the cells enter into the repsective adhesion phases.

These changes in cell adhesion area have high impact on cell behaviour, since already small changes can lead to altered gene expression[100] or even stem cell differentiation into different cell lines.[107]

Notably, the reversion of cell adhesion is relatively slow and not completed even after three hours, in contrast to the half-life times of the protein recovery itself (Figure 5.3). This can be ascripted to the tight binding of integrin to the RGD motif. If integrin is docked to RGD the binding most probably outperforms the switching of the protein, making the integrin recycling and focal adhesion turnover the rate limiting step.[41] Additionally, the cells apply forces on the proteins, which possible impede the refolding of the Jα-helix. To further characterize if the integrin binding alters the switching dynamics of the proteins itself, a reversibility assay with fluorescence anisotropy was performed.

5.5 In Vitro Characterization of Reversible Integrin Binding of LOV2-RGD Mutants

In oder to monitor the switching of the protein in vitro, I performed an anisotropy assay to see if the binding of LOV2-RGD mutants to TAMRA-RGD can be reversed. After formation of TAMRA-RGD/integrin complex, the protein concentration yielded from the initial titration (see chapter 5.3.2) was added to the solution and incubated for 90 min. Subsequently the solution was illuminated with blue light for 15 min and the anisotropy was measured, followed by a 30 min relaxation time in dark prior to an additional measurement. The reversion monitored in fluorescence anisotropy of the lit state LOV2-RGD/integrin complex to the equilibrium in dark was already achieved after several minutes as shown in the kinetic estimations (Figure 5.15 a) for RGD 77 and b) PHii 7, respectively). For PHii 7, the reversion time was 10 min, as indicated with the dashed line (Figure 5.15b).

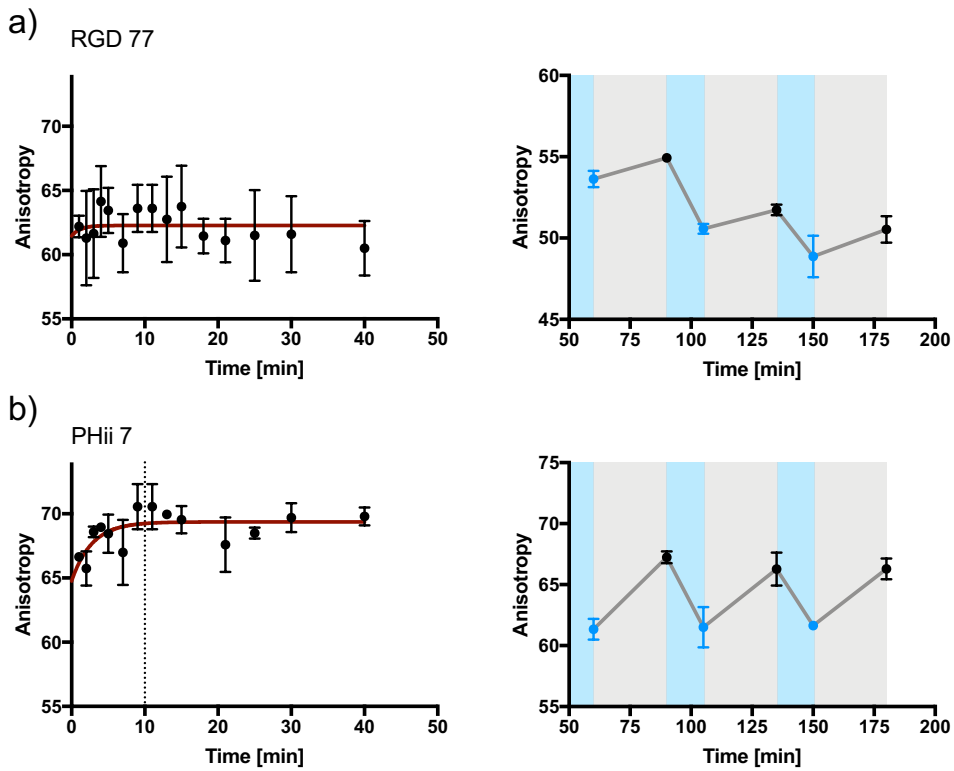

Figure 5.15: In vitro reversibility assessed with competitive fluorescence anisotropy binding assay. First column: Dark reversion kinetics. Second column: reversible switching for three times after an initial incubation time of 60 min under blue light illumination. a) For mutant RGD 77 and b) for mutant PHii 7, showing a switching kinetic of 10 min. Experiments conducted in quadruplicates, SD displayed.

The general trend of decreasing anisotropy values for RGD 77 (Figure 5.15a) is possibly due to incomplete complex formation but will be further investigated. Nevertheless, a reversion for both mutants from the less binding (dark) state to the improved binding (lit) state, triggered by illumination can be observed. The difference in the anisotropy was smaller for RGD 77, indicating a less complete caging of the RGD motifs in dark, as already observed in cell adhesion experiments (Figure 5.9). For PHii 7 the switching was more significant (Figure 5.15b).

With the herein presented approach of rationally designing a mutant library and selection of the suitable mutants with the combination of *in vitro* and *in cellulo* experiments, two LOV2-RGD mutants were chosen to reversibly switch cell adhesion with blue light.

III. Conclusion and Outlook

6. Substrates for Photo-Cleavable Cell-Surface Adhesion

Adhesion of cells to the ECM is an important factor in many cellular processes, like wound healing and embryogenesis and is tightly regulated in time and space. Therefore, the development of platforms that can effectively control cell adhesion to manipulate these processes are of great interest. Light is often preferred to dynamically regulate the ability of substrates to mediate cell-matrix adhesions, since light is the only stimulus providing both a high spatial and temporal resolution, predestining it for the application in tissue engineering. Additionally, light allows to tune interactions by changing illumination time or frequency, can be employed in a dynamic manner and different processes can be addressed with different wavelengths. Light-regulated substrates for cell-matrix adhesions often employ UV-light, bearing the risk of phototoxicity by generation of reactive oxygen species. Therefore, systems responding to light of longer wavelength need to be engineered. The combination of optogenetic building blocks responding to longer wavelengths and tissue engineering creates a feasible tool for studying cell-surface interactions using visible light. In this work, I effectively combined optogenetic proteins with material science to control cell adhesion with green light based on CarH, a green light-cleavable protein derived from *T. thermophilus*. The here employed protein CarH, originally functions as a gene repressor, which assembles upon interaction with the cofactor vitamin B12 into a tetramer, and is disassembled upon green light illumination (λ = 523 nm). I successfully modified the protein monomer sequence by introducing the RGD motif at four different positions, as well as its surrounding amino acids in cellular fibronectin. Since the RGD motif is a versatile ligand for many integrins, the system can be employed for a variety of different cell types, without the need of invasive manipulations of the cells. The protein can be recombinantly expressed in *E. coli* in large amounts, preventing tedious and costly preparations of chemically synthesized building blocks. The protein expression was quantified with SDS PAGE and the protein tetramer assembly upon cofactor addition was visualized by indirect immunofluorescence. I showed by UV/Vis spectroscopy that the monomer assembles into the respective tetramer and disassembles upon green light illumination. The tetramer could be immobilized on NTA-coated surfaces via the His-tags as confirmed with QCM-D experiments. By incubation of integrin $\alpha_v\beta_3$ on the tetramer coated QCM-D crystals, the frequency shifted, indicating a successful binding of integrin to the RGD motif of CarH. Upon green light illumination, the tetramer disassembled and the integrin/protein complex successfully detached from the crystal. In samples kept in dark, the frequency did not shift, indicating that the tetramer was stable in the dark.

After the CarH-mutants were successfully generated and characterized on their ability to attach to surfaces as well as to bind integrin, the most promising candidate was further tested in cell adhesion experiments. I showed that in the dark, when the protein is a tetramer, the protein-coated surfaces mediate cell adhesion. After green

light illumination, the CarH tetramer disassembled and the number of adherent cells decreased. Approximately 2.5-fold more cells adhered to surfaces kept in dark compared to the illuminated sample. Moreover, the median spreading area determined on the dark samples was 13 % larger than on the illuminated samples, confirming the trend of improved cell adhesion and spreading to substrates functionalized with the tetrameric form of the protein.

In this thesis, I engineered a surface, which is switchable with green light from an adhesive dark state to a less adhesive lit state. I characterized the protein characteristics with QCM-D, UV/Vis spectroscopy and indirect immunofluorescence staining. In cell-adhesion experiments I showed that cells can adhere to the dark state but not to the lit, decomposed state of the protein. With this system, I demonstrated for the first time that cells can be effectively captured and released by utilizing green light as a stimulus for direct manipulation of ligand presentation.

Drawbacks of this systems are that the CarH is sensitive to very little intensities of ambient light. Therefore, the experiments need to be performed exclusively under red light or in the dark, which is not so convenient for the experimental setup.

7. Substrates for Reversible Cell-Surface Adhesion

One of the remaining challenges in controlling cell-matrix adhesions is to control them reversibly. In order to generate a reversibly switchable surface for cell-matrix adhesion, I designed a protein library based on the blue light-switchable LOV2 domain. Therefore, I successfully incorporated the RGD and the synergy peptide PHSRN from cellular fibronectin in various positions within the LOV2 domain. The LOV2 protein domain is a blue light photoreceptor that undergoes a huge conformational change upon blue light illumination, resulting in the unfolding of an C-terminal helix. Thereby, amino acid sequences hidden within the helix, are exposed. The RGD and the PHSRN motif were chosen because they are versatile ligands of many integrins and can be employed to trigger adhesion in a variety of cell lines. The PHSRN motif has a synergistic effect on the affinity of integrin to the RGD motif, which is depending on the distance between both motifs. In cellular fibronectin, the motifs are 35 Å apart, which is matching the length of the LOV2 domain (31 Å). Since LOV2 undergoes a conformational change, the distance increase was used to enhance the binding affinity of integrin to the RGD motif in the unfolded state of the protein. In dark, the LOV2 domain thermally relaxes within minutes into the dark state and refolds its helix, such that the RGD motif is hidden again. Therefore, the designed proteins allow a blue light induced reversible RGD exposure.

A library of 40 LOV2-RGD mutants was successfully designed, expressed and purified in high yields. To assess the mutants' affinity to integrin in dark and under blue light illumination, I established an *in vitro* fluorescence anisotropy assay. For this, I determined the binding affinity of integrin $\alpha_v\beta_3$ to a TAMRA labeled RGD and performed a competitive binding assay with the mutant library to quantify K_d values.

The library of LOV2-RGD mutants was ranked based on the change in K_d under blue light compared to the dark and on the ability to bind integrin. I showed that the increase in the number of RGD motifs in a mutant and the incorporation of the context amino acids of the RGD motif as found in cellular fibronectin led to a smaller dissociation constant. However, only little change in K_d could be seen upon the insertion of the PHSRN motif or stabilizing amino acids. The protein mutants showing the highest $K_{d2,dark}/K_{d2,blue}$ ratio were selected for cell adhesion studies.

In cell adhesion experiments, the number of adherent cells on surfaces coated with the respective LOV2 mutant was assessed in the dark and under blue light. While the number of cell on the surfaces did not change for surfaces kept in dark or illuminated with blue light, the cell spreading area significantly changed. The spreading area on samples illuminated with blue light was larger than on samples kept in dark for almost all protein mutants. Trends in the cell number on the respective surfaces resembled the trends already obtained from the fluorescence anisotropy measurements, thus validating the experimental setup *in cellulo*. To assess if the cells could form FA, the FA proteins vinculin and zyxin were detected by indirect immunofluorescence staining in a reduced mutant library. I showed that cells can form mature focal adhesions on surfaces with the respective protein mutants in dark and also under blue light illumination. To further characterize the reversibility of the system, I performed switchable cell adhesion experiments. By comparing the median spreading area on surfaces switched from the lit to the dark state, and samples constantly kept in dark or light, I could demonstrate that only cells adhering to surfaces functionalized with PHii 7 or RGD 77 showed photo-induced reversion in the spreading area. In order to avoid unwanted photo-activation of the protein, I used IRM at longer wavelengths to label free monitor changes in cell-surface interactions. I could show that the spreading area decreased when the samples were monitored in dark, but increased when the surfaces were kept under blue light. Since the timescale for cell detachment is long in comparison with the protein switching (which occurs within minutes), I concluded that the rate limiting step is not the switching of the protein, but the turn-over of the integrins, which mediate the cell adhesion.

Herein, I designed and developed a reversible blue light switchable system which can be utilized to switch cell-matrix adhesion by adressing the natural adhesion proteins, integrins. The blue light did not show any photo-toxic effects on the cells and potentially toxic wavelengths as UV-light were avoided. Additionally, the building block is recombinantly expressed, not cell-toxic and facile to purify in high amounts. Since the LOV2 domain is intrinsically reversibly switchable, surfaces coated with the introduced mutants dynamically modulate cell-matrix adhesion.

To further impove the here presented systems, either the optogenetic proteins themselves can be improved, or the presentation of the proteins to the cells can be modulated. For the LOV2-RGD mutants, the dynamic range of the two mutants employed in cell experiments was only small and could be further improved by insertion of specific mutations. As already described in the introduction, the dynamic range of the oLID system for example was improved from an initially 8-fold difference between the illumination states to a 59-fold difference for iLID/Micro.[150] This was

achieved by an integrated approach of computational design, phage display and high-throughput binding assays. During this process, Guntas et al. considered 743 mutations and 49 positions closely located to the Jα-helix, to identify several single mutations, which led to this enormous increase in binding affinity. Following a similar approach for my optogenetic setup could lead to a larger dynamic range of the respective LOV2-RGD mutants, and therefore, to a higher significance in cell behavior on the lit state surfaces in comparison to the dark state surfaces. Regarding the CarH-RGD mutant, the accessibility of the RGD motif needs to be enhanced, to improve cell spreading. This can be achieved by incorporation of a linker between the RGD motifs and the protein core. Further, additional binding motifs like the PHSRN motif can be inserted to gain a higher ligand density on the surfaces.

For LOV2-RGD controlled cell-matrix adhesion, not only the ligand presentation of the RGD motif itself is a factor, also ligand density on the surface plays an important role for cell adhesion. In this work the surfaces had always been functionalized with 100 % protein, thus the RGD density was only determined by the the number and accessibility of the incorporated RGD motif.[15,192] Since the LOV2 domain has a diameter of 3 nm, the surfaces present sufficient adhesion motifs for cell spreading. If the ligand density is shifted to hight distances, thus providing enough anchoring points for cells in the illuminated state, reversion to the dark state could switch the surface "off" and prevent cell adhesion. Altering the ligand density can be achieved by changing the amount of functionalizable groups immobilized on the surface. Here, I demonstrate preliminary data of a proof of principle experiments, where surfaces were modified with different percentages of clickable PEG_{azide}, leading to a lower LOV2-RGD mutant coverage. The number of cells adhering to surfaces of different RGD 177 densities in the dark was analyzed (Figure 5.16). Reducing the ligand density from the previously shown 100 % coverage to 35 %, (dashed line in Figure 5.16) at the inflection point, modulated the light-driven effect of ligand accessibility. The inflection point of the graph varies for each LOV2-RGD mutant, which is further characterized in ongoing studies.

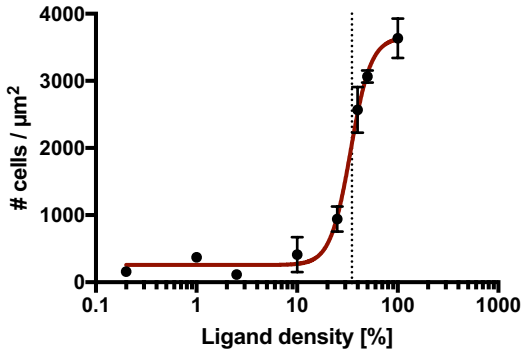

Figure 5.16: Characterization of the influence of LOV2 mutant density on cell number. Shown are surfaces functionalized with RGD 177 in dark, featuring the point of inflection at 35 % surface coverage, as an optimized protein density for this RGD mutant.

However, the here presented reversible switchable system can already be applied to investigate cellular processes, like the formation and turnover of FA in a time controlled manner. Since the system is applicable within the time scale of cell-matrix

adhesion and biological processes dependent on cell-matrix adhesion such as directed migration or stem cell differentiation can be investigated in a dynamic manner with high spatiotemporal resolution, which was not possible with the previous systems.

The green-light switchable system can be used to capture and release cells with the speed of light and could be further used to investigate cellular responses to sudden loss of ECM contact or to investigate reorganization of the actin cytoskeleton upon partial disassembly of the adhesion sites.

IV. Materials and Methods

8. Materials

8.1 Chemicals and Reagents

25 % (*v/v)* Ammonia	Merck, Darmstadt, Germany
4',6-diamidino-2-phenylindole, DAPI	Merck, Darmstadt, Germany
Agarose	Carl Roth, Karlsruhe, Germany
Agarose for DNA	Serva, Heidelberg, Germany
Alkyne-EG_6GRGDSP	Peptide Specialty Laboratories GmbH, Heidelberg, Germany
Ampicillin	Gold Biotechnology, Inc.®, St. Louis, MO, USA
Ascorbic acid	Merck, Darmstadt, Germany
Bovine serum albumin, BSA	Merck, Darmstadt, Germany
Conc. hydrochloric acid	Merck, Darmstadt, Germany
Conc. sulphuric acid	Merck, Darmstadt, Germany
Copper sulfate, $CuSO_4$	Merck, Darmstadt, Germany
Cyanobocalamin, Cbl (B12)	Merck, Darmstadt, Germany
Cyclic Arg-Gly-Asp-alkyne, cRGD-alkyne	Biotrend, Köln, Germany
Deoxynucleotide triphosphates, dNTP	Agilent Technologies, Santa Clara, CA, USA
Digestion buffer 10x	Agilent Technologies, Santa Clara, CA, USA
Dimethylsulfoxid, DMSO	Merck, Darmstadt, Germany
Dithiothreitol, DTT	Merck, Darmstadt, Germany
DNA Loading Dye 6x	Biolabs®Inc., Ipswich, MA, USA
Dpn1	Biolabs®Inc., Ipswich, MA, USA
Duebecco's Modified Eagle Medium, DMEM	Thermo Fisher Scientific, Carlsbad, CA, USA
Ethanol	Carl Roth, Karlsruhe, Germany
Ethylacetate	Merck, Darmstadt, Germany
Ethylendiaminetetraacetat, EDTA	Merck, Darmstadt, Germany
Fetal bovine serum, FBS	Merck, Darmstadt, Germany
Hydrogenperoxide	AppliChem GmbH, Darmstadt, Germany
Imidazole	Merck, Darmstadt, Germany
Integrin fragment $\alpha_v\beta_3$	R&D Systems, Minneapolis, Minnesota, USA
Isopropyl β-D-1-thiogalactopyranoside, IPTG	Gold Biotechnology, Inc.®, St. Louis, MO, USA
L-Glutamine	Thermo Fisher Scientific, Carlsbad, CA, USA
Lysogeny Broth, LB powder (Luria/Bertani)	Carl Roth, Karlsruhe, Germany
Magnesium chloride	Merck, Darmstadt, Germany
Manganese (II) chloride	Grüssing GmbH, Filsum, Germany

Methanol	Carl Roth, Karlsruhe, Germany
MOPS 20x buffer	Thermo Fisher, Carlsbad, CA, USA
Nickel (II) chloride	Merck, Darmstadt, Germany
Nitrilotriaceticacid-alkyne, NTA-alkyne	Synthesized in this lab
Paraformaldehyde, PFA	Riedel de Haen, Hannover, Germany
Penicillin/Streptomycin, PenStrep	Thermo Fisher, Scientific Carlsbad, CA, USA
Phalloidin TRITC	Merck, Darmstadt, Germany
Phenylmethanesulfonylfluoride, PMSF	Merck, Darmstadt, Germany
Phosphate buffered saline, PBS	Merck, Darmstadt, Germany
Polyethyleneglycoazide, PEG_{azide}	IRIS Biotech, Marktredwitz, Germany
Polyethyleneglycol, PEG_{2000}	RAPP Polymere, Tübingen, Germany
Q5 DNA Polymerase	NEB, Ipswich, Massachusetts, USA
Quick load ladder	Biolabs®Inc., Ipswich, MA, USA
SERVA DNA Stain G	Serva Electrophoresis, Heidelberg, Germany
Sharp Pre-stained prot-standard, Intermer Typ XC13	Thermo Fisher Scientific, Carlsbad, CA, USA
Sodium chloride	Merck, Darmstadt, Germany
Sodium dodecyl sulfate, SDS	Carl Roth, Karlsruhe, Germany
Sodium hydrogenphosphate	Merck, Darmstadt, Germany
Stempro® Accutase	Thermo Fisher Scientific, Carlsbad, CA, USA
Toluene	Merck, Darmstadt, Germany
Triethylamine	Merck, Darmstadt, Germany
Tris	Carl Roth, Karlsruhe, Germany
Triton X-100	Merck, Darmstadt, Germany

Deionized water was used in all experiments. The water was purified by a MilliQ® Integral water treatment plant (Merck, Darmstadt, Germany) or ELGA Labwater (Veolia Water Technologies, Celle, Germany). If an experiment is executed in normal water it will be indicated in the text.

8.2 Antibodies

Epitope	Isotope	Conjugation	Cat. number	Distributor
Vinculin	Mouse, IgG		V9131	Merck
Zyxin	Rabbit, IgG		Z4751	Merck
Mouse-IgG	Donkey	Alexa647	A-31571	Thermo Fisher Scientific
Rabbit-IgG	Goat	Alexa488	A-11034	Thermo Fisher Scientific
6x His-tag	Rabbit		Ab9108	Abcam

8.3 Kits

For purification of plasmids the QIAprep Spin Miniprep Kit (Qiagen, Venlo, Netherlands) was used. For site-directet mutagenesis the QuikChange II Site-Directed Mutagenesisi Kit (Agilent Technologies, Santa Clara, CA, USA) was used.

8.4 Cell Lines and Bacteria Strains

U-2 OS (human osteosarcoma cells, ATCC) and MCF 7 (human adenocarcinoma cells, ATCC) were used for cell adhesion studies. Electro competent *E. coli* (DH5α), were used for plasmid amplification. The proteins were expressed in chemo competent *E. coli* strain BL21DE* and NiCO, and purified as described in chapter 7.2. Generation of electro and chemo competent *E. coli* is described in chapter 7.1.1.

8.5 Buffers and Media

8.5.1 LB Medium for *E. coli* Culture

For cultivating *E.* coli, LB powder (Luria/Miller) 20 g/L was autoclaved. LB Agar plates were produced from autoclaved LB Agar (7.5 g Agar, 10 g LB medium per 500 mL) and selective antibiotics were added prior plate pouring.

8.5.2 Mammalian Cell Culture Media

Growth medium for cell-lines	DMEM with: 4.5 g/L *D-Glucose,* 1 mM *Sodium pyruvate, Phenol Red* *Supplements:* 4 mM L-Glutamine, 10 % *v/v* FBS, 1 % *v/v* Pen Strep
Adhesion study medium	DMEM with: 4.5 g/L *D-Glucose,* 1 mM *Sodium pyruvate, Phenol Red* *Supplements:* 4 mM L-Glutamine, 1 % *v/v* Pen Strep

8.5.3 Buffers

Buffer A	300 mM NaCl, 50 mM TRIS pH 7.4
Integrin Binding Buffer	150 mM NaCl, 50 mM TRIS pH 7.4, 2 mM $MgCl_2$, 1 mM $MnCl_2$
Elution Buffer	300 mM NaCl, 50 mM TRIS pH 7.4, 250 mM imidazole
TAE Buffer	40 mM Tris pH 8.5, 20 mM Acetic acid, 1 mM EDTA
Coomassie Staining	0.1 % (*w/v*) Coomassie brilliant blue, 50 % (*v/v*) Methanol, 10 % (*v/v*) Glacial acetic acid, 40 % (*v/v*) water
Destain Buffer	10 % (*v/v*) Acetic acid, 50 % (*v/v*) Ethanol

8.6 Disposables

Cell culture flask 25 cm^2	Greiner Cellstar®, Sigma Aldrich, Germany
Cell culture flask 75 cm^2	Greiner Cellstar®, Sigma Aldrich; Germany
Coverslips, 20x20 mm, standard thickness # 1	Roth, Germany
Object slide	Roth, Germany
Multiwell culture plates	Greiner bio one, USA
Stericup sterile filter device, 0.22 µm	Rotilabo®, Roth, Germany

9. Methods

9.1 Synthesis of Protein Mutants

9.1.1 Cloning

i) Plasmids and Primer

The LOV2-ipaA plasmid was kindly provided by Brian Kuhlman (Addgene plasmid # 40236). The CarH plasmid was kindly provided by Fei Sun.

Table 2: Specification of original plasmids.

Plasmid name	Vector and Coding Gene	Selection Marker
LOV2-ipaA	pET21b-LOV2-ipaA	Ampicillin
CarH	pET22b-CarH	Ampicillin

The LOV2-ipaA sequence was mutated to create LOV2 protein. Derivatives were produced by insertion of point mutations. All sequences, and templates are listed in the appendix. The primers were customized synthesized by Eurofins®. The standard protocol described in the QuikChange II Site-Directed Mutagenesis Kit was used for introducing point mutations. Plasmids were isolated using the QIAprep Spin Miniprep Kit.

ii) Insertion of point mutations

For the polymerase chain reaction (PCR) the following reagents were gently mixed by pipetting:

- 0.2 µL forward primer (10 µM in water)
- 0.2 µL reverse primer (10 µM in water)
- 1.5 µL 10x reaction buffer (Buffer of PFU Polymerase)
- 0.2 µL template plasmid (100 µg/µL in water)
- 7.5 µL water
- 0.2 µL deoxynucleotide triphosphates, dNTPmix

After addition of 0.2 µL Q5 polymerase, the PCR tube was transferred immediately to the PCR machine (DNA engine, Peltier thermal cycler T-100, BioRAD, USA). 18 PCR cycles were performed, each consisting of the following three phases after an initial melting at 97 °C for 3 min:

- 97 °C for 30 s
- annealing temperature for 30 s
- 72 °C for 0.5 min/kDa

The annealing temperature was varied between 65 °C - 75 °C depending on the primers. After a final elongation time of 5 min at 72 °C, 0.2 µL of DpnI (10 units/µL) were added and the solution was incubated at 37 °C for 1 h. After completion of the DpnI digestion, the PCR reaction was incubated on ice to stop the enzymatic activity. 1.0 µL PCR product was mixed with 5 µL 5x DNA loading dye and separated via agarosegel electrophoresis (0.8 % *w/v* Agarose in TAE buffer and 12 µL SERVA DNA Stain G with a Quick load ladder as marker to confirm the PCR reaction product.

iii) Transformation in Electro Competent E. coli

48 µL pre-chilled electro competent *E. coli* (10^6 cells/150 µL in glycerol) were transferred into a pre-chilled 1.5 mL tube, and 2 µL of the plasmid (100 ng/µL) was added on ice. The solution was gently mixed 2-3 times and transferred in a pre-chilled electroporator cuvette (1 mm distance from Sigma Aldrich). The *E. coli* were pulsed (GenePulser Xcell™, BioRAD, USA, voltage 1800 V, capacity 25 µF, resistance 200 Ω) and 450 µL pre-heated (37 °C) LB medium was immediately added afterwards. The bacteria solution was transferred into a 1.5 mL tube and incubated at 37 °C and 240 rpm for 1 h. Subsequently the bacteria solution was plated on ampicillin agar plates and incubated at 37 °C overnight. For plasmid amplification, colonies were picked from each plate and transferred to separate 15 mL falcon tubes each containing 10 mL LB medium with 100 µg/mL ampicillin. The cultures were grown at 230 rpm and 37 °C, overnight.

iv) Plasmid Purification

The plasmid purification was done with the QiAprep®Spin Miniprep Kit (Qiagen, Germany). The bacteria from the overnight cultures were spun down in a table-top centrifuge at 6000 rpm and RT for 10 min (Rotina 380R, Hettich Zentrifugen). The supernatant was discarded, and the bacteria pellet was resuspended in 250 µL P1 buffer and transferred into a 1.5 mL eppendorf tube. 250 µL P2 lysis buffer was added and the solutions were gently mixed by inverting the vial 5 times. After 2 min incubation time, 350 µL N3 neutralization buffer was added and mixed by inverting the vial several times. Subsequently the precipitant was spun down in a table-top microcentrifuge at 13000 rpm and RT for 10 min (Centrifuge 5418, Eppendorf, Germany).

The DNA containing supernatant was applied on a QIAprep® spin column and centrifuged at 13000 rpm and RT for 1 min. The flow-through was discarded, and the column was washed with 750 µL PE buffer. Then the column was transferred to a fresh 1.5 mL tube, and 40 µL elution buffer was applied and incubated on the column for 2 min before centrifuging at 13000 rpm and RT for 1 min. The concentration of the flow through was determined with NanoDrop (ND-1000 V3, peQLab Biotech GmbH, USA) and sent in in a concentration of 100 ng/µl for sequencing (seqlab®, Germany).

v) Preparation of Chemo Competent E. coli

100 mL LB medium was inoculated with Bl21DE* from the glycerol stock and incubated at 240 rpm and 37 °C till an optical density of 4.2. The optical density at 600 nm of the bacterial culture was determined with an UV-Vis spectrometer (Lambda25, PerkinElmer, Germany). The culture was cooled on ice for 10 min, divided into two fractions and spun down at 4 °C at 6000 rpm for 10 min (Avanti® J-26 XP, Beckman Coulter, USA, rotor: JA 10). After removal of the supernatant the pellets were separately resuspended in 30 mL ice cold buffer (80 mM $MgCl_2$, 20 mM $CaCl_2$) and the pellet was recovered by a second centrifugation step with the settings mentioned before. Hereafter the bacteria were resuspended and recovered for a second time as described before and finally each pellet was resuspended in 2 mL ice cold 0.1 M $CaCl_2$ solution. To each solution 70 µL DMSO was added, mixed and incubated on ice for 15 min. Finally, another 70 µL DMSO was added to each solution. The so derived solution was aliquoted, freeze dried immediately on dry ice and stored at -80 °C till further use.

vi) Preparation of Electro Competent E. coli

1 L LB medium was inoculated with DH5α from the glycerol stock and incubated at 240 rpm and 37 °C till an optical density of 0.4. The culture was harvested by spinning down at 4 °C at 6000 rpm for 10 min (Avanti® J-26 XP, Beckman Coulter, USA, rotor: JA 10). After removal of the supernatant the pellet was resuspended in 450 mL ice cold deionized water and the pellet was recovered by a second centrifugation step with the settings mentioned before. Hereafter the bacteria were resuspended and recovered for a second time as described before and finally the pellet was resuspended in 40 mL ice cold 10 % *v/v* glycerol and recovered by centrifugation. After removal of the supernatant the pellet was resuspended in 3 mL ice cold 10 % *v/v* glycerol, freeze dried immediately on dry ice and stored at -80 °C till further use.

9.2 Protein Expression

9.2.1 Transformation of Chemo Competent *E. coli*

50 µL chemo competent *E. coli* BL21DE* or NiCO (10^6 cells/150 µL) were mixed with 0.5 µL purified plasmid (100 ng/µL) and incubated on ice for 20 min. The transformation was performed by heat shock at 42 °C for 1 min (Thermomixer comfort, Eppendorf, Germany). Thereafter, the bacteria were cooled down on ice for 2 min before adding 750 µL LB medium and incubating at 37 °C at 230 rpm for 1 h. Finally, the bacteria solution was plated on a selective ampicillin LB-agar plate and incubated at 37 °C overnight.

9.2.2 Protein Expression

One colony from the selective BL21DE* or NiCO agar plate was picked and transferred into a 15 mL falcon tube containing 10 mL LB medium with 100 µg/mL ampicillin. The bacteria solution was incubated at 230 rpm and 37 °C overnight. The 10 mL overnight culture was transferred into 1 L LB medium with 100 µg/mL ampicillin and incubated at 37 °C for 3 h. At an optical density of 0.80 – 1.0, the temperature of the incubator

was reduced to 16 °C for 15 min and afterwards 500 µL isopropyl β-D-1-thiogalactopyranoside (IPTG, 1 M) solution (final concentration 0.5 µM) was added to the bacteria solution to induce expression of the His-tagged protein of interest. The IPTG-induced bacteria were incubated at 230 rpm and 16 °C overnight.

9.2.3 Protein Purification

The overnight bacteria cultures that express the protein of interest were spun down at 4 °C at 6000 rpm for 10 min (Avanti® J-26 XP, Beckman Coulter, USA, rotor: JA 10). The supernatant was discarded and the bacteria pellet was transferred to a pre-chilled 50 mL falcon. The bacteria pellet was resuspended in 20 mL buffer A with 1 mM phenylmethylsulfonylfluoride (PMSF, 100 mM in methanol) and 1 mM dithiothreitol (DTT, 1 M in water). Thereafter, the bacteria were ruptured by sonication (OMNI sonic ruptor 400, OMNI international, USA; Settings: 40 % pulse, 50 % frequency, 10 min). The obtained lysate was transferred to a pre-chilled centrifuge tube and spun down at 4 °C and 12000 rpm for 30 min (Avanti® J-26 XP, Beckman Coulter, USA, rotor: JA 25.5).

The supernatant was filtered through a 0.45 µm cellulose filter. The obtained protein solution was purified over a Ni^{2+}-NTA column (Ni-NTA, Superflow cartridge, Qiagen) in the Äkta HPLC system. Before, the column was equilibrated with 25 mL buffer (300 mM NaCl, 50 mM Tris pH 7.4, 30 mM imidazole). The protein was loaded over a superloop (50 ml, GE Healthcare, USA), washed with 10 mL loading buffer and eluted with a gradient from 50 % - 100 % elution buffer over 15 mL, applying a flow of 1 mL/min.

The purified protein was dialysed against buffer A to remove the imidazole (Dialysis membrane, SpectraPor®, MWCO = 10 kDa) overnight exchanging the buffer two times. The protein concentration for LOV2RGD mutants was determined absorption measurement at 473 nm (after 5 min relaxation time in dark) assuming an extinction coefficient of 9200*1/Mcm.[97]

The CarH tetramer complex was assembled upon addition of a four-fold molar excess of vitamin B12 to the monomer solution in the dark and incubation at 4 °C overnight. The obtained tetramer was further purified utilizing a size exclusion column (Quiagen, HiLoad 16/600, Superdex 200 pg) with buffer A as fluid phase. The retention time of the tetramer was 75 min, as shown in the appendix.

9.2.4 SDS-PAGE

The protein (LOV2RGD mutants and CarH monomeres) purity was assessed by SDS-PAGE (4-12 % Bis-TRIS; Thermo Fisher Scientific). For that purpose, 4 µg protein was mixed with 4x loading dye and denatured at 97 °C for 10 min. For the SDS-PAGE 20 µL pre-mixed solution per condition was used. The gel was run in MOPS buffer at 200 V, 160 A for 40 or 50 min. The gel was stained with coomassie brilliant blue staining solution (0.025 g/L in glacial acetic acid/methanol/water 10/45/45 ml) for 5 min and heating to the boiling point and afterwards destained in destain buffer while shaking at RT, overnight. The images of the SDS-Pages can be found in the appendix.

9.3 Characterization of Mutants

9.3.1 Kinetic Studies

To measure the recovery of the specific absorption of the flavin mononucleotide after excitation, the LOV2RGD mutant sample was illuminated with blue light (470 nm) for 1 min. A spectrum was recorded every 18 s with a UV-Vis spectro-photometer to observe the recovery of the flavin mononucleotide starting 1s after the illumination. Representatively for the spectra of all examined mutants, the spectrum of PHii 77 is shown in section 5.3.1. To obtain the half-live of the dark state recovery, the absorption maximum at 450 nm is plotted over time and fitted to a first order kinetics.

The CarH tetramer were stepwise illuminated with a green LED (515 nm – 520 nm) to monitor the successive disassembly of the tetramer. The spectrum was recorded with a plate reader (Tecan infinite M200, Tecan, Männedorf, Switzerland) using an integration time of 5 – 10 s, up to a final illumination time of 1 min.

9.3.2 QCM-D Measurements

The gold QCM-D crystals (E4, Q-sense, Sweden), were activated with UV-ozone (UVO cleaner, Model NO342-220, Jelight Company Inc, USA) for 10 min. Each surface was coated with 50 µL of a solution containing 32.4 µM HS-$(CH)_{11}$-EG_6-N_3 (Prochimia, Sopot, Poland) and 20 µM HS-$(CH)_{11}$-EG_3-OH (Prochmia, Sopot, Poland) diluted in buffer A on parafilm at RT for 1 h. The azide groups were clicked with NTA-alkyne according to the protocol described in 7.3.2. Afterwards, the crystals were washed twice with buffer A, once with 50 mM EDTA (pH 7.4), once with buffer A and dried under a stream of nitrogen. All measurements were performed at 25 °C with a pump speed of 0.2 mL/min. The QCM-D measurements were performed in dark following the protocol stated below. For monitoring the binding of integrin to the protein coated surfaces, the integrin fragment $\alpha_v\beta_3$ (R&D Systems, MN, USA), 100 µg/ml) was used.

QCM-D protocol:

1) 10 min buffer A
2) 30 min CarH3.2 tetramer (400 µL)
3) 10 min buffer A
4) 10 min integrin binding buffer
5) 300 µL integrin fragment (16.6 µg/ml)
6) 10 min integrin binding buffer
7) 20 min green light illumination in one chamber, the other kept in dark, constant washing with integrin binding buffer in both chambers
8) 10 min buffer A
9) 10 min elution buffer
10) 10 min buffer A

After the measurements, the crystals and the chambers were cleaned with 2 % (*v/v)* SDS in water for 10 min, followed by incubation with deionized water for 10 min and

drying under a nitrogen stream. The crystals were further cleaned via UV-ozone for 10 min and incubated in basic ammonia hydrogen peroxide containing a (*v/v/v*) ration of water/ammonia (25 %)/hydrogen peroxide of 5/1/1 at 75 °C for another 10 min. Subsequently the crystals were washed several times with water and dried under a stream of nitrogen before further usage.

9.3.3 Competitive Fluorescence Binding Assay

The competitive fluorescence binding assay was performed at a Clario Star plate reader (BMG Labtech, Ortenberg, Germany), which was kindly provided from Prof. Dr. Mayer at ZMBH (Zentrum für Molekulare Biologie, University Heidelberg, Germany). The experiments were measured in a black 384 well plate (Corning, flat bottom, black, Ref 3820) with a LP5966 dichroic filter with an excitation maximum at 540 nm (bandwidth 20 nm) and emission maximum at 590 nm (bandwidth 20 nm). The assay is based on the effect that fluorophores excited with linear polarized light will emit also polarized light. By determining the anisotropy value, which is the ratio of the parallel and vertical perpendicular light (equation 1), the rotational freedom of the fluorophore is displayed. A free fluorophore sustains the exited polarization in its fluorescence to a lower extent than a bound fluorophore and therefore exhibiting a lower anisotropy value.

Equation 1:

$$A = \frac{I\parallel - G*I\perp}{I\parallel + 2G*I\perp}$$

A = anisotropy, I_{II} = intensity of parallel polarized light, $I_{\perp}$ = intensity of perpendicular polarized light and G = grating factor

The grating factor is an instrument dependent correction factor and that determines the detectors sensitivity for the respective polarization direction. To design an assay based on fluorescence anisotropy, a small fluorophore should bind to a comparable big binding partner. In our case, we designed the fluorophore based on TAMRA conjugated with a RGD sequence (MW: 960 g/mol) as displayed in Figure 4, which is bound by the integrin heterodimer $\alpha_v\beta_3$ (MW:191300 g/mol).

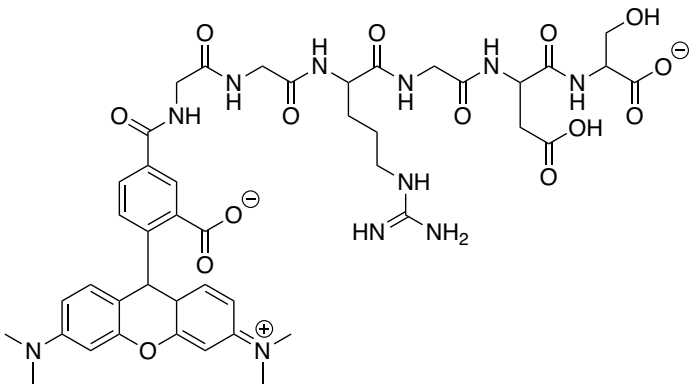

Figure 9.1: Structure of TAMRA-RGD fluorophore.

Since the integrin has 10-fold the mass as the TAMRA-RGD conjugate, it is suitable for fluorescence anisotropy measurements. TAMRA has an excitation wavelength of 543 nm and an emission of 576 nm.

For determination of the K_{d1} of integrin a titration of TAMRA-RGD (200 nM in deionized water) with integrin fragment (100 µg/ml, $\alpha_v\beta_3$ (R&D Systems, MN, USA),) was performed at RT. An incubation time of 30 min was needed to reach the equilibrium after each addition step. Therefore, the components were always incubated for this complex formation time. The complex was found to be stable over a time of more than 330 min.

The competitive binding assay was performed in triplicates. Therefore, the initial complex of 20 nM fluorophore and 60 nM integrin fragment was preformed in dark at RT for 45 min. Afterwards, increasing concentrations of LOV2RGD solution (stock, 10 µM) were added to the initial solution. After each step the solution was incubated in dark for 30 min, measured and equilibrated under blue light illumination for additional 30 min (5.35 mW/cm^2) before measuring the lit state. The following pipetting scheme was applied:

Table 3: Volume of LOV2-RGD mutant solution added to the preformed TAMRARGD/integrin complex and the obtained concentration.

Volume protein solution [µL] (stock c =10 µM)	Final concentration [nM]
0.75	244
0.75	476
1.5	909
3	1666
6	2857
12	4444

The obtained curves were fitted with the Hill1 equation in Origin (OriginLab, Northamton, Massachusetts, USA), assuming the first data point of the pure TAMRA-RGD/integrin complex as a fixed starting point. From the fits the concentration of LOV2RGD mutants can be determined that are required to replace half of the TAMRA-RGD fluorophore in the TAMRA-RGD/integrin complex. With the obtained concentration for LOV2RGD the K_{d2} value of the competing equilibrium can be calculated as described in 5.3.2.

As a control the ion dependency of the integrin binding was tested by using buffer A instead of integrin binding buffer in the titration assay. The specificity of the binding was determined by using the unmodified LOV2 domain as a competitor, and as a positive control cRGD (circular-RGD-alkyne, Biotrend, Köln, Germany) instead of the LOV2-RGD mutant was used as a ligand. The respective spectra are listed in the appendix.

The reversibility of the LOV2-RGD mutant binding to TAMRA-RGD was tested for PHii 7 and RGD 77. Therefore, the concentration of LOV2-RGD mutant required to replace half of the fluorophore from the TAMRA-RGD/integrin complex was added to the solution of the preformed TAMRA-RGD/integrin complex and incubated for initial 45 min. After 15 min blue light illumination, the anisotropy of the lit state was measured. The solution was always relaxed for 30 min in the dark or for 15 min under blue light illumination before recording of the next data point. The switching was monitored for 3 cycles.

9.4 Surface Functionalization

9.4.1 Surface PEGylation

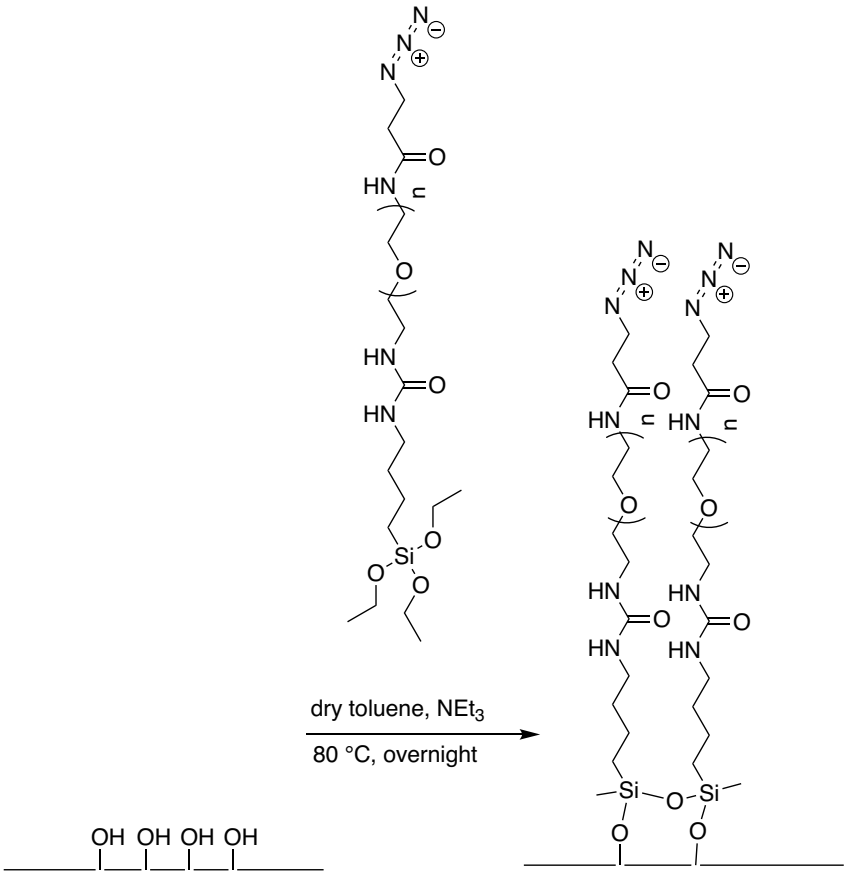

Figure 9.2: Surface functionalization and passivation with polyethylene glycols (PEGs).

For the surface preparation, 20x20 mm^2 glasscoverslips were cleaned with peroxymonosulphuric acid (H_2SO_5) (formed by 3:1 sulphuric acid (H_2SO_4) and hydrogen peroxide (H_2O_2)) for 1 h. After removal of the acid by washing three times with water, the surfaces were dried with a stream of nitrogen. In a flask 12 mg silane-PEG_{azide} (MW: 3245 g/mol; Rapp Polymere, Tübingen, Germany) were dissolved in 35 mL dry toluene ($0.98*10^{-11}$ mM) and 10 µL triethylamine (final concentration 25 µM) under nitrogen atmosphere. The cleaned surfaces were placed into the PEG-containing solution under nitrogen atmosphere and kept at 78 °C overnight. Afterwards, the surfaces were first sonicated in ethyl acetate and then in ethanol for 5 min each. Finally, the surfaces were dried under a stream of nitrogen before further modification.

Surfaces were coated with different densities to study the effect of ligand distribution on cell adhesion. Therefore, the silane-PEG_{azide} was mixed in different molar ratios with silane-$PEG_{methoxy}$ (MW: ~2000 g/mol; Rapp Polymere, Tübingen, Germany).

Table 4: Used concentrations and masses of the respective silanePEGs to yield different surface densities of clickable $silanePEG_{azide}$.

Ligand density [%]	$silanePEG_{azide}$ [mg]	$silanePEG_{methoxy}$ [mg]
0.2	0.0032	4.8
1	0.0157	7.35
2.5	0.0394	4.3
10	0.1575	4.39
25	0.3938	3.01
40	0.63	2.03
50	0.7875	1.45
100	15	-

Following functionalization, the surfaces were further modified with NTA-alkyne like described in chapter 7.3.2 and incubated with LOV2RGD 77. According to 7.4.2 U-2 OS cells were seeded onto the surfaces. After 2 hours, the medium was removed and cells were fixed with 1 mL of 4 % *(w/v)* paraformaldehyde (PFA) solution in PBS per well at RT for 20 min. Surfaces were mounted in mowiol supplements with 0.75 µL/mL DAPI to stain the nuclei. Immunofluorescence imaging was carried out as described in 7.4.7 followed by image analysis with imageJ (see section 7.4.9).

9.4.2 Click Reaction on PEGazide Functionalized Surfaces

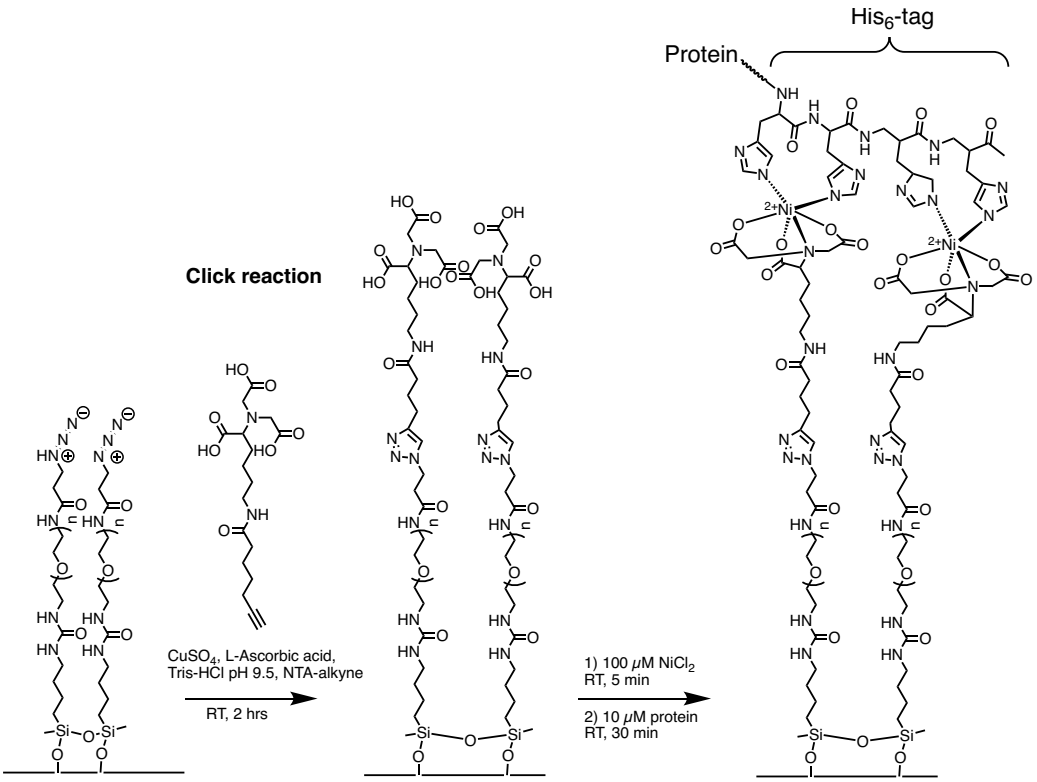

Figure 9.3: Click reaction for PEGazide functionalization.

The passivated surfaces were incubated in a humid chamber at RT in 100 µL reaction solution each for 2 h. The reaction solution for NTA-functionalization contains: 100 µM Tris pH 9.5, 100 µM ascorbic acid, 150 µM NTA-alkyne, 1 mM $CuSO_4$ in water. The reaction solution for cRGD functionalized surfaces contains: 100 µM Tris pH 9.5, 100 µM ascorbic acid, 150 µM cRGD-alkyne (100 mM, BioTrend, Köln, Germany), 1 mM $CuSO_4$ in water.

The NTA functionalized surfaces were washed twice with buffer A, once with 50 mM EDTA pH 7.4 in water and once with buffer A. Afterwards the surfaces were incubated with 100 mL 0.1 M $NiCl_2$ solution each at RT for 5 min. The surfaces were washed once with buffer A and stored in buffer till further modification. The cRGD functionalized surfaces were washed with water and dried in a stream of nitrogen.

To coat the surfaces with protein, they were incubated with 100 µL protein solution (10 µM in buffer A) at RT for 30 min.

9.4.3 Determination of Protein Immobilization

The amount of CarH tetramer immobilized on the surfaces was assessed with detection of the Histag with antibodies. Therefore, two surface were washed with 1 % BSA solution in PBS at RT in dark for 20 min. One surface was illuminated for 10 min with green light, washed once with with 1 % BSA solution in PBS for 5 min while the other was kept in dark. Both surfaces were fixed with 4 % *w/v* PFA in water at RT for 20 min and washed with 1 % BSA solution in PBS for 5 min in dark. As a negative control a pegylated surface without protein was taken, blocked with 1 % BSA solution

in PBS at RT in dark for 20 min and fixated and washed like described above. The respective surfaces were incubated with 100 µL each with 1 % BSA, 1/300 anti-His rabbit IgG (Ab9108, Abcam) at RT in dark for 30 min. The surfaces were washed with 1 % BSA in PBS solution three times for 5 min each. The surfaces were incubated with 100 µL each with 1 % BSA in PBS and 1/500 Alexa488 goat anti-rabbit IgG (A-11034, Thermo Fisher Scientific) and phalloidin-TRITC (2 µg/mL) at RT in dark for 2.5 h. The surfaces were washed twice with PBS and mounted with 20 µL mowiol containing 0.75 µg/mL DAPI upside down on a glass slide.

9.5 Cell Experiments

9.5.1 Cell Culture

For adhesion studies with LOV2RGD mutants, U-2 OS (ATCC, USA) human osteosarcoma cells, an adherent epithelial cell line expressing several different integrin heterodimers were used. For adhesion studies with CarH mutants, MCF-7 (ATCC, USA) human adenocarcinoma cells, also an adherent epithelial cell line, expressing several heterodimer integrins. In addition to cell-matrix contacts they also establish tight cell-cell contacts and form an epithelium. All cells were kept in growth medium (see section 6.4.2) at 37 °C, 5 % CO_2 saturation in a humified atmosphere. Cells were subcultured every 2-3 days by detaching them with StemPro Accutase (Thermo Fisher Scientific, USA) and splitting them 1:5 in fresh growth medium. For adhesion experiments cell were seeded in serum free medium.

9.5.2 Cell Seeding

The NTA functionalized surfaces were each incubated with 100 µL of a 10 µM protein solution in buffer (300 mM sodium chloride, 50 mM TRIS pH 7.4) upside down on parafilm at 25 °C for 30 min. After incubation with the respective proteins, surfaces were washed with PBS buffer. Meanwhile cells were detached with 1 mL StemPro accutase at 37 °C for 5 min. The detached cells were resuspended and counted with a Neubauer Haemocytometer (2500 mm^2, Laboroptik, Germany). 5000 cells/cm^2 were seeded into each well in 2 mL serum free medium. Cells were either incubated under the irradiation of blue or green light (*flora*LED^s, PLANT CLIMATICS, Germany, light intensity: 25 µmol/m^2s, blue light: 471 nm / or green light: 532 nm) or in the dark (at 37 °C and 5 % CO_2 for 2 h).

9.5.3 Indirect Immunofluorescence of Focal Adhesion Proteins

After 2 hours, the medium was removed and cells were fixed with 4 % *(w/v)* PFA solution in PBS at RT for 20 min. Subsequently, the fixing solution was removed, and each surface was washed twice with PBS buffer, treated with 1 mL 0.1 % *(v/v)* Triton X-100 in PBS buffer at RT for 5 min and washed with PBS buffer again. The surfaces were blocked with 1 mL 1 % BSA *(w/v)* in PBS at RT for 30 min. The respective surfaces were incubated with 100 µL of anti-vinculin mouse IgG (1 µg/mL in BSA in PBS) (V5255, SigmaAldrich) and anti-zyxin rabbit IgG (1 µg/mL in BSA in PBS) (Z4751, SigmaAldrich) at RT for 30 min. The surfaces were washed with 1 % *(w/v)* BSA in PBS three times for 5 min each. The surfaces were incubated with 100 µL Alexa647 donkey anti-mouse IgG (1 µg/mL in BSA in PBS) (A-31571, Thermo Fisher Scientific), Alexa488

goat anti-rabbit IgG (A-11034, Thermo Fisher Scientific) and phalloidin-TRITC (2 µg/mL) at RT in dark for 1 h. The surfaces were washed once with 1 % BSA in PBS and once with PBS and mounted with 20 µL mowiol containing 0.75 µg/mL DAPI upside down on a glass slide.

9.5.4 Staining and Mounting

In order to stain the cytoskeleton, each surface was fixed like afore mentioned, and subsequently incubated with 100 µL phalloidin-TRITC (2 µg/mL) in PBS buffer solution upside down on parafilm at RT for 30 min. Thereafter, each surface was washed twice with PBS buffer and mounted with 20 µL Mowiol containing DAPI (0.75 µg/mL) on a glass slide. After a polymerization time of 16 h the samples were imaged by fluorescence microscopy.

9.5.5 Determination of Adhesion Area in Live Cell Experiments

Surfaces were functionalized with PEG_{azide}, NTA-alkyne and protein as described in section 7.3.2. The surfaces were glued into a homebuild incubation chamber. In brief, a 1.13 cm^2 hole was cut into the bottom of a 35 mm diameter plastic petridish. The aforementioned surfaces were mounted with an addition-curing duplication silicone (Picodent Twinsil, Picodent, Wippenfürth, Germany) to cover the opening in the incubation chamber. The surfaces were washed once with PBS. Cells were seeded as described above in 2 mL serum free medium and incubated at 37 °C under illumination of 25 $\mu mol*m^{-2}s^{-1}$ blue light for 2 h. The change in the adhesion area was monitored with a DeltaVision Elite microscope system. The positions to be monitored were manually chosen under constant illumination (approximately 30 min). Afterwards, the cells were monitored with a 63x/1.4NA oil objective at 37 °C and 5 % CO_2 under either blue light illumination (0.77 mW/cm^2) or in dark for 3 h using interference reflection microscopy (IRM). As an excitation wavelength 632 nm with a bandwidth of 20 nm was chosen and an image was taken every 10 min.

9.5.6 Metabolic Activity Test

The influence of light on the metabolic activity of cells was determined with the 3-(4,5-Dimethylthiozol-2-yl)-2,5-diphenaltetrazolium bromide (MTT) assay. Therefore, cells (U-2 OS for blue light, and MCF7 for green light) were seeded in a density of 50 000 cells/0.3 cm^2 in a 96 well plate in 100 µL complete growth medium. The cells were incubated at 37 °C exposed to the respective wavelength and light intensity for 2 h. The control was kept meanwhile in the dark. Afterwards 75 µL medium per well were removed and 10 µL MTT (saturated solution in PBS) was added. The cells were incubated at 37 °C in dark for 4 h. 50 µL DMSO per well was added and incubated at RT in dark for 10 min. The absorption at 540 nm was measured with a Tecan plate reader.

9.5.7 Determination of Cell Number and Adhesion Area

The cell number was determined by staining the nuclei with DAPI and cell area was derived via staining the cytoskeleton with phalloidin-TRITC. Therefore, wide field fluorescence images (Leica DM6000B, 10x, QAS filter set) of a stitched mosaic surface (12 mm^2) were taken with the respective DAPI and TRITC filters.

9.5.8 Microscopy Settings

Fluorescence Upright Widefield System

Type: Leica DM6000B

Used objectives: HCX PL Apo 10x/0.4 NA phase contrast

Light source: HBO

Camera: DFC 365FX

Software: Leica LAS

Epifluorescence filter setups: QAS, filter

Fluorescence Inverted Widefield System

Type: Delta Vision (GE healthcare, UK) based on Olympus IX inverted microscope (Olympus, Japan)

Used objective: 60x/ 1.4 NA PlanApo oil (Olympus, Japan)

Light source: HBO

Incubator: homebuild

Camera: Coolsnap HQ, Roper Scientific, USA

Software: SoftWorx – version 6.5.2

Epifluorescence filter setup: Alexa filter wheel, filter 632 nm/22 nm, IRM mode

Confocal Laser Scanning Microscope

Type: Zeiss, LSM 880

Used objective 63x/1.4 NA oil (Zeiss)

Laser: UV diode: 405 nm
Argon: 488 nm
DPSS 561: 561 nm
HeNe: 633 nm

Incubator: PM 2000 RBT (PeCon, Germany) + CO_2-module

Detector: PMTs

Software: Zen – version 2.1 SP3

Inverted Phase Contrast Microscope

Type: Leica DMi1

Used objectives:10x

Light source: HBO

Camera: DFC 365FX

9.5.9 Image Analysis

Images were analysed using Fiji open source software (Version: 2.0.0-rc-59/1.15n). The threshold of the images was corrected manually and a binary image was generated. The cell number was calculated by using the plugin: "Analyse particles", considering particles between 50 μm^2 and 50 000 μm^2. The spreading area of the cells on the respective surfaces was determined by picking at least 10 single images ($1.2*10^{-3}$ μm^2) and using Ilastik open source software (GNU General Public License) program to analyse the actin staining. Ilastik was trained to classify objects in three groups: single cells, overlapping cells and cell cut off from the picture edge. The pixels, which were taken into account as contributing to the spreading area were selected manually with one set of images and applied to all images analysed. Fitting and plotting of curves were done in OriginPro 2017G (OriginLab, Northampton, Massachusetts, USA) or Prism7.0d (GraphPad, San Diego, California, USA).

9.5.10 Statistical Tests

One way Anova test was employed for cell numbers in cell adhesion studies with CarH. The student t-test was employed for the statistical analysis of K_{d2}-values and cell numbers for LOV2RGD mutants. Mann-Whitney test was employed to assess the significance of the spreading area analysis in the cell adhesion experiments, in the static reversibility experiments as well as in the live cell reversibility experiments. In Box-plots the 10 - 90 % confidence interval is displayed. The box in box plots show the 25 % - 75 % confidence interval. p-values: * < 0.1, ** < 0.01, *** < 0.001, **** < 0.0001.

9.6 Synthesis of NTA-Alkyne

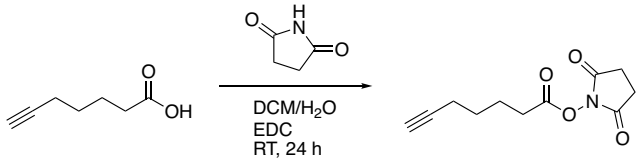

Synthesis protocol: 1 eq. 6-heptynoic acid (1.5 mmol, 0.2 ml) was dissolved in 100 eq. anhydrous dichloromethane. 2.5 eq. of N-Hydroxysuccinimide (NHS, 4.5 mmol, 698 mg) and 1.5 eq. 1-ethyl-3-(3-dimethylaminopropyl)-carbodiimide (EDC, 2.25 mmol, 349.3 mg) were added to the reaction solution. The solution was stirred under N_2 atmosphere at RT overnight. The reaction was quenched upon the addition of 100 ml saturated $NaHCO_3$ solution. The aqueous solution was extracted twice with 50 ml diethylether. The combined organic phases were washed with 100 ml brine and 100 ml water and dried with $MgSO_4$. The filtered organic phase was removed under low pressure. Compound 1 was obtained as yellow crystals and used without further purification.

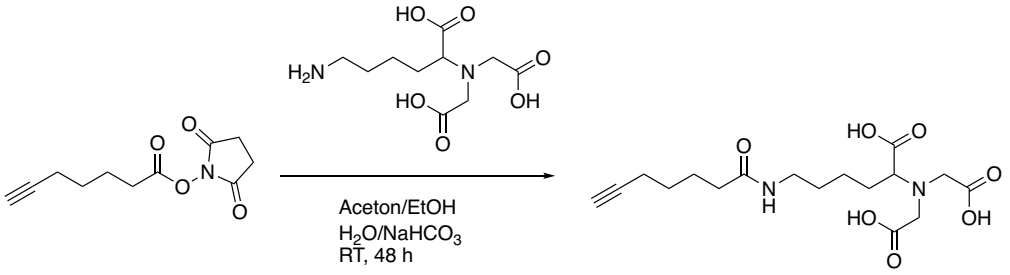

4 eq. $NaHCO_3$ (12 mmol, 1008.12 mg) was dissolved in 15 ml water and 1.2 eq Nα- Nα-biscarboxylysine hydrate (3.6 mmol, 943.6 mg) was added. The solution was slowly added to a solution of 1eq. compound 1 (3 mmol, 621.3 mg) in 3 ml acetone and 30 ml ethanol. The reaction was stirred at RT for 48 h. The solvent was partially removed and 5 ml 0.25 M $NaHCO_3$ solution was added. The precipitate was removed by filtration. The remaining solution was acidified with conc. HCl to pH 3 and the product was lyophilized. The yielded white chrystals were further purified by column chromatography. The eluent was ethanol/ethylacetate 3:1, which was exchanged to pure ethanol later on. The solvent was removed, yielding 0.676 mmol (250 mg). The nuclear magnetic resonance (NMR) spectrum was taken in D_2O and a HR-ESI^- was measured.

δ ppm (660 MHz): 3.76 – 3.74, m, 2*CH_2, CH; 317-3.18, d, *J = 5.4*, CH_2; 2.31, s, CH; 2.25 – 2.16, m, 2*CH_2; 1.89-180, d, *J = 56.76*, 2*CH_2; 1.67-1.48, dquint, $^1J = 7.56$, $^2J = 109.38$, 2 CH_2; 1.55, m, CH_2.

HR-ESI^-: m/z calculated $C_{17}H_{25}N_2O_7^-$ for $[M-H]^-$: 369.17, found: 369.1671

V. Appendix

Content of Appendix

Photo-Cleavable Cell Adhesion

Photo-Switchable Cell Adhesion

Photo-Cleavable Cell Adhesion

```
1     ATG GGC GAG CTC CCA GAA GAT CTG GGC ACC GGC CTG CTG GAA
43    GCA CTG CTG CGC GGT GAT CTG GCG GGC GCC GAA GCT CTG TTT
85    CGT CGT GGC CTG CGT TTC TGG GGC CCG GAA GGC GTT CTG GAG
127   CAC CTG CTG CTG CCG GTG CTG CGT GAA GTG GGC GAA GCT TGG
169   CAC CGT GGT GAA ATC GGC GTT GCA GAA GAA CAC CTG GCG AGC
211   ACC TTC CTG CGC GCG CGT CTG CAG GAG CTG CTG GAC CTG GCA
253   GGT TTC CCG CCG GGT CCG CCG GTC CTG GTG ACT ACG CCG CCG
295   GGC GAA CGC CAC GAA ATC GGT GCG ATG CTG GCG GCG TAC CAT
337   CTG CGT CGT AAG GGC GTC CCG GCG CTG TAT CTG GGC CCG GAT
379   ACT CCG CTG CCG GAC CTG CGT GCA CTG GCG CGC CGC CTG GGT
421   GCA GGC GCG GTC GTG CTG TCT GCT GTT CTG AGC GAA CCG CTG
463   CGT GCT CTG CCT GAC GGT GCC CTG AAA GAT CTG GCA CCG CGT
505   GTT TTC CTG GGC GGC CAG GGC GCA GGC CCG GAA GAG GCA CGC
547   CGT CTG GGT GCC GAA TAC ATG GAA GAC CTG AAA GGC CTG GCT
589   GAA GCG CTG TGG CTG CCG CGC GGT CCG GAA AAA GAA GCA ATC
631   GGA TCC GGT CTC GAG CAT CAT CAT CAT CAT CAT CAT
```

Figure A1: Nucleobase sequence WT CarH without DNA binding sequence.

```
1     MGELPEDLGT GLLEALLRGD LAGAEALFRR GLRFWGPEGV LEHLLLPVLR
51    EVGEAWHRGE IGVAEEHLAS TFLRARLQEL LDLAGFPPGP PVLVTTPPGE
101   RHEIGAMLAA YHLRRKGVPA LYLGPDTPLP DLRALARRLG AGAVVLSAVL
151   SEPLRALPDG ALKDLAPRVF LGGQGAGPEE ARRLGAEYME DLKGLAEALW
201   LPRGPEKEAI GSGLEHHHHH H*
```

Figure A2: Amino acid sequence WT CarH without DNA binding sequence, top codon indicated with a star.

CarH	LPRGPEKEAIGSGLEHHHHHH*
CarH1	LP**RGD**EKEAIGSGLEHHHHHH*
CarH2	LPRGPEKEAIGSGLQ**RGD**HHHHHH*
CarH3.1	PRGPEKEAIGSGLQ**RGDRGD**HHHHHH*
CarH3.2	PRGPEKEAIGSGLQ**RGDRGDRGD**HHHHHH*
CarH4.2	PRGPEKEAIGSGLQ**GRGDSP**HHHHH*

Figure A3: Amino acid sequences of CarH-RGD library. Introduced amino acids in bold, stop codon indicated with a star.

Name	Mutation
CarH1	604 CCG → GAC
CarH2	643 GAG → CAG insertion of CGC GGG GAC
CarH3.1	643 GAG → CAG double insertion of CGC GGG GAC
CarH3.2	643 GAG → CAG triple insertion of CGC GGG GAC
CarH4.2	643 GAG → CAG insertion of GGC CGC GGG GAC TCG CCG

Figure A4: Mutation table of rendered or introduced nucleobases to yield CarH-RGD.

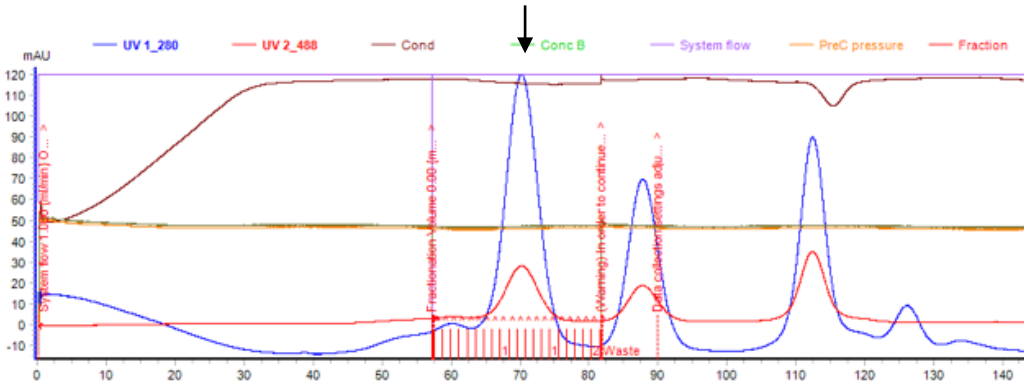

Figure A5: Chromatogram of the elute after size exclusion column. Blue curve: elute monitored at 280 nm, red curve: elute monitored at 488 nm. Tetramer is eluted with a retention time of 70 min, indicated with the arrow, second peak is the CarH3.2 monomer, third peak is the cofactor vitamin B12.

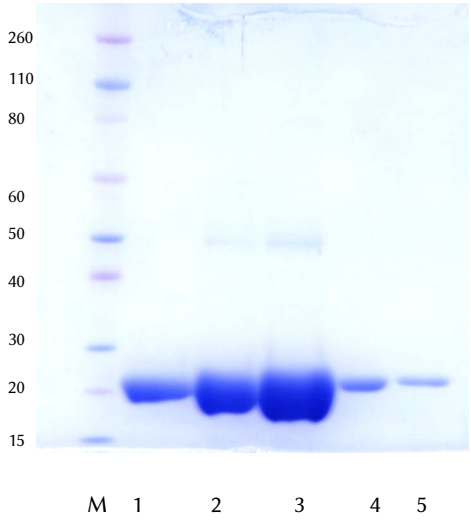

Name	Number
CarH1	1
CarH2	2
CarH3.1	3
CarH3.2	4
CarH4.2	5

Figure A6: SDS-PAGE gel of CarH-RGD mutants. Expected MW is 21 kDa. M indicates the marker with the expected bands in kDa on the left of each gel, the labels and the assigned proteins are shown in the table.

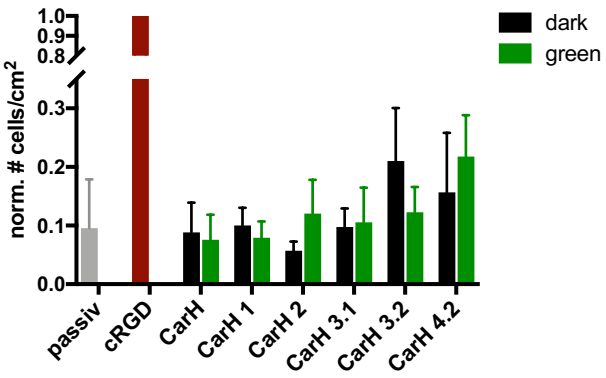

Figure A7: Adhesion experiments of MCF7 cells to surfaces functionalized with the respective CarH-RGD tetramer. Cells were incubated for 2 h in dark or under green light illumination (25 µM/m^{2}s). Cell number normalized on the cell number adhered to surfaces covered with cRGD. As a passivation control a PEG-coated surfaces was used.

Photo-Switchable Cell Adhesion

```
1      ATG CAT CAT CAT CAT CAT CAT GGC AGC CTG GCG ACC ACC CTG
43     GAA CGT ATT GAA AAG AAC TTT GTG ATT ACC GAT CCG CGT CTG
85     CCG GAT AAC CCG ATT ATT TTT GCG AGC GAT AGC TTT CTG CAG
127    CTG ACC GAA TAT AGC CGT GAA GAA ATT CTG GGC CGT AAC TGC
169    CGT TTT CTG CAG GGC CCG GAA ACC GAT CGT GCG ACC GTG CGT
211    AAA ATT CGT GAT GCG ATT GAT AAC CAG ACC GAA GTG ACC GTG
253    CAG CTG ATT AAC TAT ACC AAA AGC GGC AAA AAA TTT TGG AAC
295    CTG TTT CAT CTG CAG CCG ATG CGT GAT CAG AAA GGC GAT GTG
337    CAG TAT TTT ATT GGC GTG CAG CTG GAT GGT ACC GAA CAT GTG
379    CGT GAT GCG GCG GAA CGT GAA GGT GTG ATG CTG ATC AAG AAA
421    ACC GCG GAA AAC ATT GAT GAA GCG GCG AAA GAA CTG TAA
```

Figure A8: Nucleobase sequence WT LOV2.

```
  1    HHHHHHGSLA TTLERIEKNF VITDPRLPDN PIIFASDSFL QLTEYSREEI
 51    LGRNCRFLQG PETDRATVRK IRDAIDNQTE VTVQLINYTK SGKKFWNLFH
101    LQPMRDQKGD VQYFIGVQLD GTEHVRDAAE REGVMLIKKT AENIDEAAKE
151    L*
```

Figure A9: Amino acid sequence of WT LOV2, Jα-helix indicated in red.

Name	Mutation
RGD 1	391 GAA CGT GAA → AGA GGT GAT
RGD 2	394 CGT GAA GGC → CGT GGT GAC
RGD 3	415 AAG AAA ACC→ AGA GGT GAC
RGD 4	421 ACC GCG GAA→ AGA GGT GAT
RGD 5	430 AAC ATT GAT → CGC GGT GAT
RGD 6	442 GCG GCG AAA → AGA GGT GAT
RGD 7	448 AAA GAA CTG → CGT GGT GAT
RGD 7c	448 AAA GAA CTG → GGC CGT GGT GAT and insertion of GAT TCG CCT
RGD 8	442 GCG GCG AAA → AGA GGT GAT depletion of the rest
G → A	400 GGT → GCG
I → A	412 ATC → GCG
N → E	430 AAC → GAG
PHSRNi	319 GAT CAG AAA GGC GAT→ CCT CAC AGT CGC AAT
PHSRNiii	367 ACC GAA CAT GTG CGT→ CCC CAT TCT CGG AAT
PHSRNii	22 Insertion of GGC GGC AGC CCG CAT TCG AGG AAC

Figure A10: Inserted or substituted nucleobases to yield the respective LOV2-RGD mutants. The rest of the LOV2 sequence is preserved.

```
LOV2:              DAAEREGVMLIKKTAENIDEAAKEL
RGD 1:             DAARGDGVMLIKKTAENIDEAAKEL
RGD 2:             DAAERGDVMLIKKTAENIDEAAKEL
RGD 3:             DAAEREGVMLIRGDAENIDEAAKEL
RGD 4:             DAAEREGVMLIKKRGDNIDEAAKEL
RGD 5:             DAAEREGVMLIKKTAERGDEAAKEL
RGD 6:             DAAEREAVMLIKKTAENIDERGDEL
RGD 77:            DAAEREGVMLIKKTAENIDEAARGDRGD
RGD 7:             DAAEREGVMLIKKTAENIDEAARGD
RGD 7c:            DAAEREGVMLIKKTAENIDEAAGRGDSP
RGD 8:             DAAEREGVMLIKKTAENIDRGD
RGD 14:            DAARGDGVMLIKKRGDNIDEAAKEL
RGD 24:            DAAERGDVMLIKKRGDNIDEAAKEL
RGD 15:            DAARGDGVMLIKKTAERGDEAAKEL
RGD 25:            DAAERGDVMLIKKTAERGDEAAKEL
RGD 17:            DAARGDGVMLIKKTAENIDEAARGDRGD
RGD 47:            DAAEREGVMLIKKRGDNIDEAARGDRGD
RGD 1s:            DAARGDAVMLAKKTAENIDEAAKEL
RGD 14s:           DAARGDAVMLAKKRGDNIDEAAKEL
RGD 15s:           DAARGDAVMLAKKTAERGDEAAKEL
RGD 1ss:           DAARGDAVMLAKKTAEEIDEAAKEL
RGD 2s:            DAAERGDVMLAKKTAENIDEAAKEL
RGD 3s:            DAAEREAVMLARGDAENIDEAAKEL
RGD 4s:            DAAEREAVMLAKKRGDNIDEAAKEL
RGD 5s:            DAAEREAVMLAKKTAERGDEAAKEL
RGD 6s:            DAAEREAVMLAKKTAENIDERGDEL
RGD 7s:            DAAEREAVMLAKKTAENIDEAARGDRGD
PHSRNi RGD 1s:     PHSRN_DAARGDAVMLAKKTAEAIDEAAKEL
PHSRNi RGD 2s:     PHSRN_DAAERGDVMLAKKTAENIDEAAKEL
PHSRNi RGD 4s:     PHSRN_DAAEREAVMLAKKRGDNIDEAAKEL
PHSRNi RGD 7:      PHSRN_DAAEREGVMLIKKTAENIDEAARGD
PHSRNi RGD 77:     PHSRN_DAAEREGVMLIKKTAENIDEAARGDRGD
PHSRNiii RGD 2s:   PHSRNDAAERGDVMLAKKTAENIDEAAKEL
PHSRNiii RGD 4s:   PHSRNDAAEREAVMLAKKRGDNIDEAAKEL
PHSRNiii RGD 5s:   PHSRNDAAEREAVMLAKKTAERGDEAAKEL
PHSRNii RGD 2s:    HHHHHHPHSRN … DAAERGDVMLAKKTAENIDEAAKEL
PHSRNii RGD 4s:    HHHHHHPHSRN … DAAEREAVMLAKKRGDNIDEAAKEL
PHSRNii RGD 1s:    HHHHHHPHSRN … DAARGDAVMLAKKTAENIDEAAKEL
PHSRNii RGD 7:     HHHHHHPHSRN … DAAEREGVMLIKKTAENIDEAARGD
PHSRNii RGD 77:    HHHHHHPHSRN … DAAEREGVMLIKKTAENIDEAARGDRGD
```

Figure A11: Amino acid sequences of LOV2-RGD library. Introduced RGD motifs in red, His-tag displayed in yellow, stabilizing amino acids in blue.

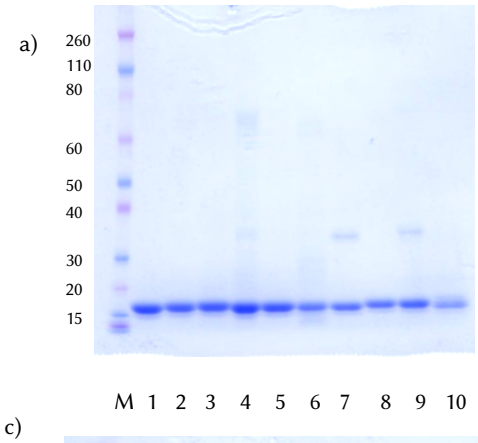

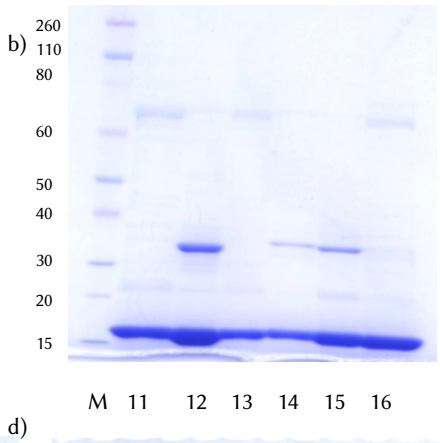

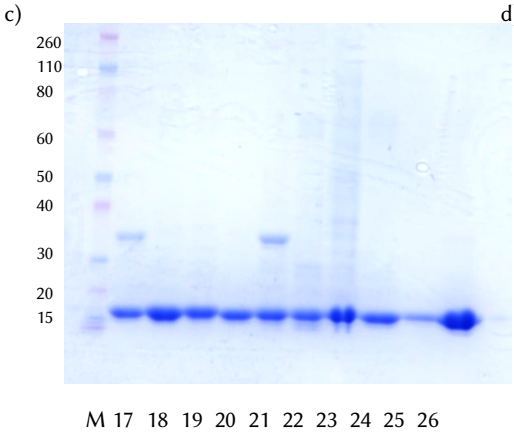

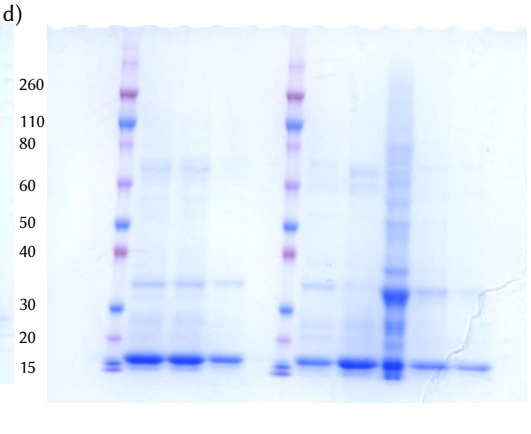

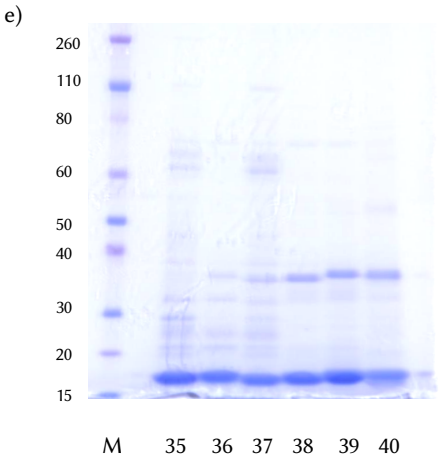

Name	Number
RGD 1	1
RGD 2	2
RGD 3	3
RGD 4	4
RGD 5	5
RGD 6	6
RGD 77	7
RGD 7	8
RGD 7c	9
RGD 8	10
RGD 14	11
RGD 24	12
RGD 15	13
RGD 25	14
RGD 177	15
RGD 477	16
RGD 1s	17
RGD 14s	18
RGD 15s	19
RGD 2s	20

Name	Number
RGD 3s	21
RGD 4s	22
RGD 5s	23
RGD 6s	24
RGD 7s	25
RGD 1GIN	26
PHi 1s	27
PHi 2s	28
PHi 4s	29
PHi 7	30
PHi 77	31
PHiii 2s	32
PHiii 4s	33
PHiii 5s	34
PHii 2s	35
PHii 4s	36
PHii 1s	37
PHii 7	38
PHii 77	39
PHii 14s	40

Figure A12: SDS-PAGE gel from LOV2-RGD mutants. Expected MW is 17 kDa. M indicates the marker with the expected bands in kDa on the left of each gel, the labels and the assigned proteins are shown in the table. On gel a) single mutants, on gel b) mutants with multiple RGD-motifs, c) mutants with stabilizing mutations, d) Mutants with PHSRN motif iii and i, and e) mutants with PHSRNii motif.

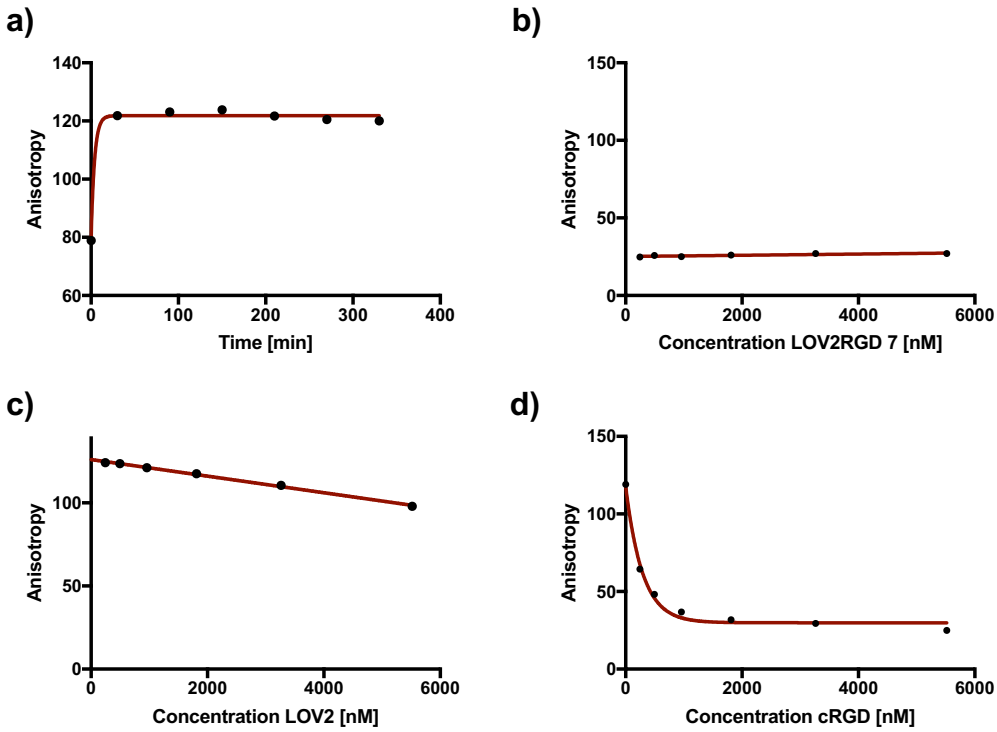

Figure A13: Control experiments of competitive fluorescence binding assay. a) The TAMRARGD/integrin complex was stable over time. b) No complex formation occurs with buffer without divalent ions even when protein concentration is increased. c) Low binding occurs when the WT LOV2 without RGD binding motif was added to the preformed TAMRARGD/integrin complex. d) As a positive control cRGD was used showing a K_{d2} of 54 nM ± 3 nM.

Mutant	$K_{d2,dark}$	error	$K_{d2,blue}$	error	$K_{d2,dark}/K_{d2,blue}$	Significance
RGD 7	3266	230	717	67	4.56	****
RGD 14	115	13	40	41	2.85	*
PHi 77	654	45	235	26	2.78	***
RGD 77	912	343	347	78	2.63	*
PHii 7	3157	747	1248	382	2.53	*
PHii 77	805	162	323	43	2.49	**
RGD 7c	508	58	244	14	2.09	**
PHi 7	1009	273	506	104	1.99	*
RGD 177	389	30	199	20	1.95	***
PHi 4s	69	9	36	7	1.91	**
PHii 1s	1467	423	783	315	1.87	ns
RGD 1s	257	32	140	19	1.83	**
RGD 8	673	86	369	30	1.83	**
RGD 1	517	21	294	38	1.76	***
RGD 25	465	268	268	125	1.73	ns
RGD 5	710	186	419	108	1.70	ns
RGD 24	265	48	158	19	1.68	*
PHi 1s	1709	410	1024	263	1.67	ns
PHii 2s	2293	783	1381	541	1.66	ns
RGD 2s	2093	462	1267	168	1.65	*
RGD 14s	145	13	91	15	1.60	**
PHiii 4s	417	145	260	68	1.60	ns
RGD 6	4169	226	2671	1152	1.56	ns
PHii 14s	430	239	278	141	1.55	ns
RGD 2	1285	243	832	287	1.54	ns
RGD 7s	388	192	255	161	1.52	ns
RGD 15s	237	19	157	17	1.51	**
RGD 6s	4584	766	3064	1032	1.50	ns
RGD 3	959	484	642	284	1.49	ns
RGD 5s	780	252	539	90	1.45	ns
PHii 4s	418	212	288	131	1.45	ns
RGD 1ss	373	126	260	141	1.43	ns
PHi 2s	3136	609	2216	438	1.42	ns
PHiii 5s	1076	196	783	211	1.37	ns
RGD 477	149	2	110	2	1.36	****
RGD 4	594	70	442	26	1.34	*
PHiii 2s	541	127	403	122	1.34	ns
RGD 4s	906	169	682	233	1.33	ns
RGD 15	206	24	164	56	1.26	ns
RGD 3s	404	111	413	147	0.98	ns
cRGD	54	3				

Figure A14: K_{d2}-values in dark and under blue light illumination, calculated as described in section 5.3.2 from the competitive fluorescence anisotropy assay. Values in [nM]. Student t-test was used as statistical test. P-values are defined in section 9.5.10.

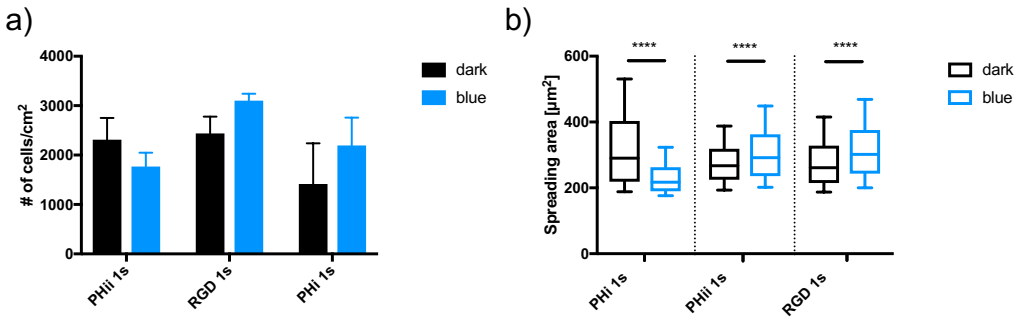

Figure A15: Cell adhesion studies of mutants combined with LOV2RGD 1s. a) Analysis of the cell number on the respective surfaces in dark or under 25 µM/ms blue light illumination. Experiments were conducted in triplicates. b) Analysis of the spreading area. Experiments were conducted in triplicates, cell number analyzed: n > 500, 10 - 90 % confidence interval is shown.

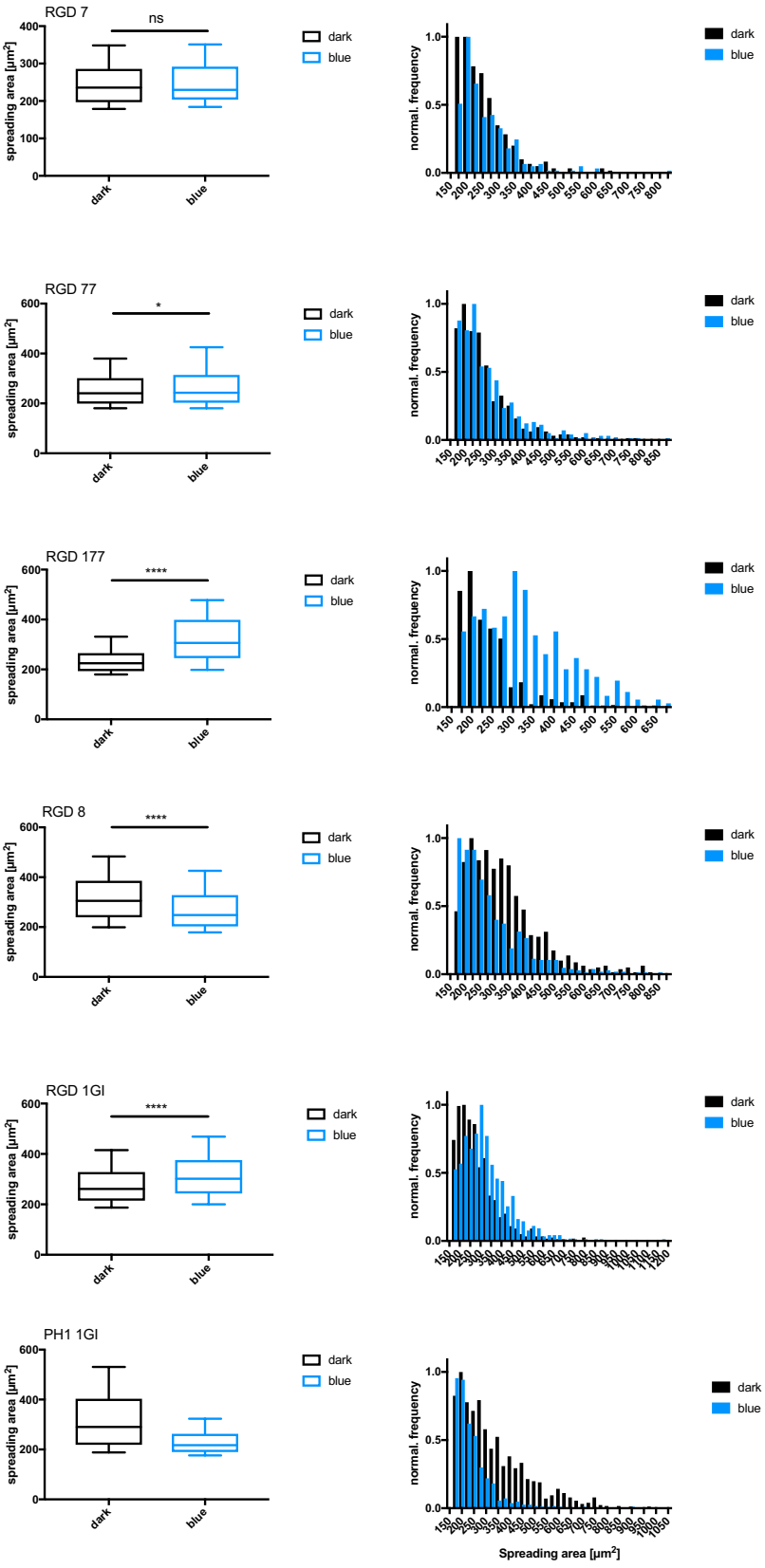
RGD 7
ns
RGD 77
*
RGD 177
****
RGD 8
****
RGD 1GI
****
PH1 1GI
spreading area [µm²]
normal. frequency
dark
blue
Spreading area [µm²]

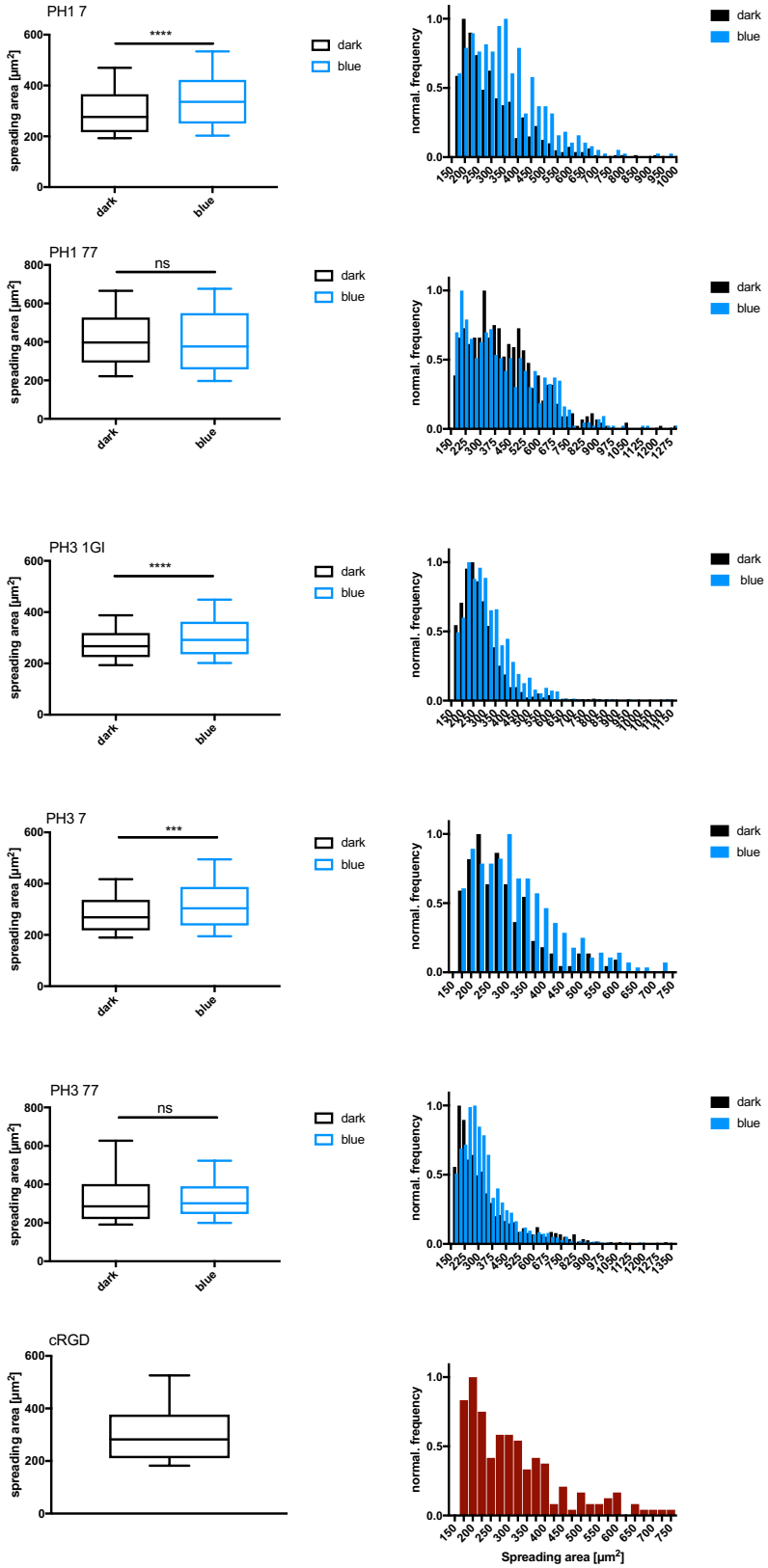

Figure A16: Analysis of the spreading area of the respective LOV2-RGD mutants on the left and the respective analysis of the normalized frequency on the right.

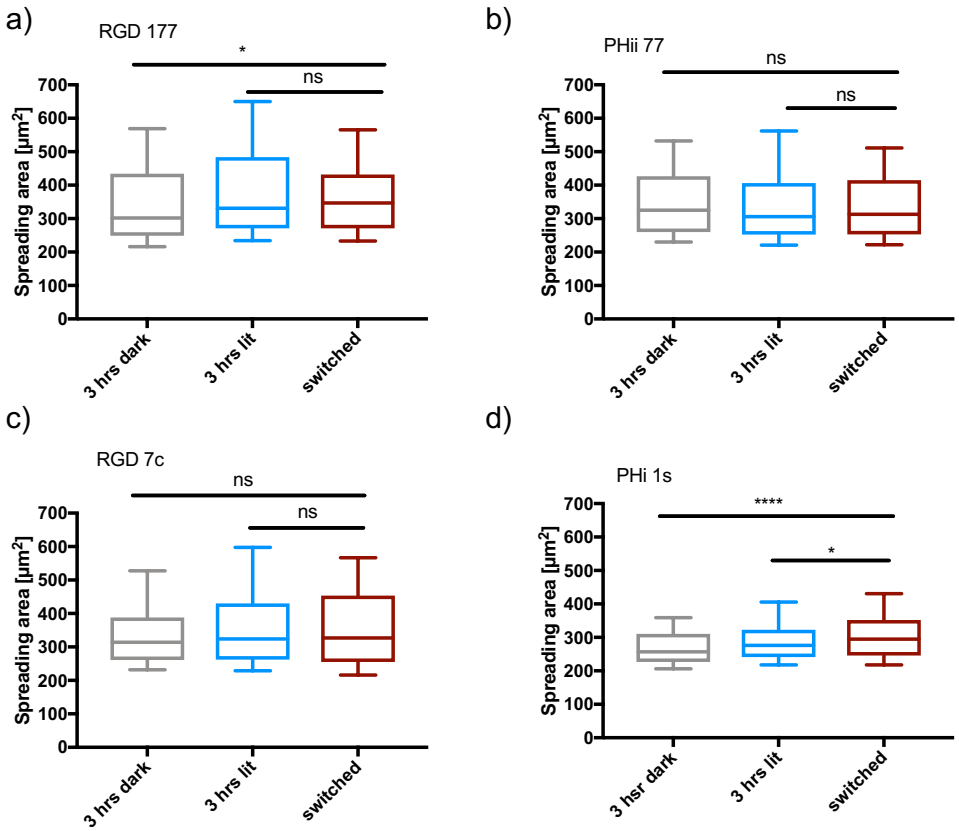

Figure A17: Reversibility of the spreading area of LOV2RGD mutants. Surfaces switched after 2 hours under blue light to dark for 1 additional hour, compared to surfaces kept always in the dark or under blue light illumination. The respective protein mutants do not show a reversion in the spreading area on the switched surfaces.

Bibliography

(1) Mouw, J. K.; Ou, G.; Weaver, V. M. *Nat Rev Mol Cell Biol* 2014, *15* (12), 771.
(2) Charras, G.; Sahai, E. *Nat Rev Mol Cell Biol* 2014, *15* (12), 813.
(3) Hamidi, H.; Ivaska, J. *Nat Rev Mol Cell Biol* 2014, *15* (12), 771.
(4) García, A. J.; Vega, M. D.; Boettiger, D. *Mol. Biol. Cell* 1999, *10* (3), 785.
(5) Paoli, P.; Giannoni, E.; Chiarugi, P. *BBAMCR* 2013, *1833* (12), 3481.
(6) Humphries, J. D.; Byron, A.; Humphries, M. J. *J. Cell Sci.* 2006, *119* (Pt 19), 3901.
(7) Wierzbicka-Patynowski, I. *J. Cell Sci.* 2003, *116* (16), 3269.
(8) Smith, M. L.; Gourdon, D.; Little, W. C.; Kubow, K. E.; Eguiluz, R. A.; Luna-Morris, S.; Vogel, V. *PLoS Biol* 2007, *5* (10), e268.
(9) Pankov, R. *J. Cell Sci.* 2002, *115* (20), 3861.
(10) Geiger, B.; Bershadsky, A. D.; Pankov, R.; Yamada, K. *Nat Rev Mol Cell Biol* 2001, 793.
(11) Custódio, C. A.; Reis, R. L.; Mano, J. F. *Adv. Healthcare Mater.* 2014, *3* (6), 797.
(12) Hersel, U.; Dahmen, C.; Kessler, H. *Biomaterials* 2003, *24* (24), 4385.
(13) Singh, P.; Carraher, C.; Schwarzbauer, J. E. *Annu. Rev. Cell Dev. Biol.* 2010, *26* (1), 397.
(14) Feng, Y.; Mrksich, M. *Biochem.* 2004, *43* (50), 15811.
(15) Schenk, F. C.; Boehm, H.; Spatz, J. P.; Wegner, S. V. *Langmuir* 2014, *30* (23), 6897.
(16) Ochsenhirt, S.; Kokkoli, E.; McCarthy, J.; Tirrell, M. *Biomaterials* 2006, *27* (20), 3863.
(17) Kao, W. J.; Lee, D.; Schense, J. C.; Hubbell, J. A. *J. Biomed. Mater. Res.* 2001, 79.
(18) Bowditch, R. D.; Hariharan, M.; Tominna, E. F.; Smith, J. W.; Yamada, K. M.; Getzoff, E. D.; Ginsberg, M. H. *J. Biol. Chem.* 1994, *269* (14), 10856.
(19) Brown, A. C.; Dysart, M. M.; Clarke, K. C.; Stabenfeldt, S. E.; Barker, T. H. *J. Biol. Chem.* 2015, *290* (42), 25534.
(20) Ebara, M.; Yamato, M.; Aoyagi, T.; Kikuchi, A.; Sakai, K.; Okano, T. *Adv. Mater.* 2008, *20* (16), 3034.
(21) Leahy, D.; Aukhil, I.; Erickson, H. *Cell* 1996, No. 84, 155.
(22) Grant, R.; Spitzfaden, C.; Altroff, H.; Campbell, I. D.; Mardon, H. J. *J. Biol. Chem.* 1997, *272 (10)* (7), 6159.
(23) Mouw, J. K.; Ou, G.; Weaver, V. M. *Nat Rev Mol Cell Biol* 2014, *15* (12), 771.
(24) Kreiner, M.; Chillakuri, C. R.; Pereira, P.; Fairhead, M.; Li, Z.; Mardon, H. J.; Holt, S. A.; van der Walle, C. F. *Soft Matter* 2009, *5* (20), 3954.
(25) Shattil, S. J.; Kim, C.; Ginsberg, M. H. *Nat Cell Biol* 2010, *11* (4), 1.
(26) Takagi, J.; Petre, B.; Walz, T.; Springer, T. *Cell* 2002, *110*, 599.
(27) Campbell, I. D.; Humphries, M. J. *Cold Spring Harb Perspect Biol* 2011, *3* (3), a004994.
(28) Zhang, K.; Chen, J. *Cell Adh Migr* 2012, *6* (1), 20.
(29) Humphries, M. J. *Curr. Opin. Cell Biol.* 1996, *8* (5), 632.
(30) Geiger, B.; Spatz, J. P.; Bershadsky, A. D. *Nat Rev Mol Cell Biol* 2009, *10* (1), 21.
(31) Zaidel-Bar, R. *J. Cell Sci.* 2003, *116* (22), 4605.
(32) Moreno-Layseca, P.; Streuli, C. H. *Matrix Biol.* 2014, *34* (C), 144.
(33) Vicente-Manzanares, M. *J. Cell Sci.* 2005, *118* (21), 4917.
(34) Seetharaman, S.; Etienne-Manneville, S. *Biol. Cell* 2018, *110* (3), 49.
(35) Elosegui-Artola, A.; Oria, R.; Chen, Y.; Kosmalska, A.; Pérez-González, C.; Castro, N.; Zhu, C.; Trepat, X.; Roca-Cusachs, P. *Nat Cell Biol* 2016, *18* (5), 540.
(36) Morse, E. M.; Brahme, N. N.; Calderwood, D. A. *Biochem.* 2014, *53* (5), 810.
(37) Iwamoto, D. V.; Calderwood, D. A. *Curr. Opin. Cell Biol.* 2015, *36*, 41.
(38) Hirata, H.; Tatsumi, H.; Sokabe, M. *Commun Integr Biol* 2008, *1* (2), 192.
(39) De Franceschi, N.; Hamidi, H.; Alanko, J.; Sahgal, P.; Ivaska, J. *J. Cell Sci.* 2015, *128* (5), 839.
(40) Margadant, C.; Monsuur, H. N.; Norman, J. C.; Sonnenberg, A. *Curr. Opin. Cell Biol.* 2011, *23* (5), 607.
(41) Bridgewater, R. E.; Norman, J. C.; Caswell, P. T. *J. Cell Sci.* 2012, *125* (16), 3695.
(42) Iwamoto, D. V.; Calderwood, D. A. *Curr. Opin. Cell Biol.* 2015, *36* (C), 41.
(43) Gilmore, A. P. *Cell Death Differ* 2005, *12*, 1473.
(44) Winograd-Katz, S. E.; Fässler, R.; Geiger, B.; Legate, K. R. *Nat Rev Mol Cell Biol* 2014, *15* (4), 273.
(45) Ley, K.; Rivera-Nieves, J.; Sandborn, W. J.; Shattil, S. *Nat Rev Drug Discov* 2016, *15* (3), 173.
(46) Mas-Moruno, C.; Rechenmacher, F.; Kessler, H. *Anticancer Agents Med Chem* 2010, *10* (10), 753.
(47) Vining, K. H.; Scherba, J. C.; Bever, A. M.; Alexander, M. R.; Celiz, A. D.; Mooney, D. J. *Adv. Mater.* 2017, *30* (4), 1704486.
(48) Hallmann, R.; Zhang, X.; Di Russo, J.; Li, L.; Song, J.; Hannocks, M.-J.; Sorokin, L. *Curr. Opin. Cell Biol.* 2015, *36*, 54.
(49) Maquart, F. X.; Monboisse, J. C. *Pathol Biol* 2014, *62* (2), 91.

(50) Koivisto, L.; Heino, J.; Häkkinen, L.; Larjava, H. *Adv Wound Care* 2014, *3* (12), 762.
(51) Shaw, T. J.; Martin, P. *J. Cell Sci.* 2009, *122* (Pt 18), 3209.
(52) Huang, J.; Gräter, S. V.; Corbellini, F.; Rinck, S.; Bock, E.; Kemkemer, R.; Kessler, H.; Ding, J.; Spatz, J. P. *Nano Lett.* 2009, *9* (3), 1111.
(53) Cavalcanti Adam, E. A.; Aydin, D.; Hirschfeld Warneken, V. C.; Spatz, J. P. *HFSP Journal* 2010, *2* (5), 276.
(54) Cavalcanti Adam, E. A.; Volberg, T.; Micoulet, A.; Kessler, H.; Geiger, B.; Spatz, J. P. *Biophysj* 2007, *92* (8), 2964.
(55) Mrksich, M. *Chem. Soc. Rev.* 2000, *29* (4), 267.
(56) Robertus, J.; Browne, W. R.; Feringa, B. L. *Chem. Soc. Rev.* 2010, *39* (1), 354.
(57) Satav, T.; Huskens, J.; Jonkheijm, P. *Small* 2015, *11* (39), 5184.
(58) Gooding, J. J.; Parker, S. G.; Lu, Y.; Gaus, K. *Langmuir* 2014, *30* (12), 3290.
(59) Koçer, G.; Jonkheijm, P. *Adv. Healthcare Mater.* 2018, *7* (14), 1701192.
(60) Tibbitt, M. W.; Rodell, C. B.; Burdick, J. A.; Anseth, K. S. *Proceedings of the National Academy of Sciences* 2015, *112* (47), 14444.
(61) Kim, J.; Hayward, R. C. *Trends Biotechnol.* 2012, *30* (8), 426.
(62) Ng, C. C. A.; Magenau, A.; Ngalim, S. H.; Ciampi, S.; Chockalingham, M.; Harper, J. B.; Gaus, K.; Gooding, J. J. *Angew. Chem. Int. Ed.* 2012, *51* (31), 7706.
(63) Zeng, H.; Zhang, Y.; Nakajima, H.; Uchiyama, K. *Sens Actuator B Chem* 2017, *251*, 334.
(64) Hou, J.; Cui, L.; Chen, R.; Xu, X.; Chen, J.; Yin, L.; Liu, J.; Shi, Q.; Yin, J. *Macromol. Rapid Commun.* 2018, *39* (6), 1700572.
(65) Wischerhoff, E.; Uhlig, K.; Lankenau, A.; Börner, H. G.; Laschewsky, A.; Duschl, C.; Lutz, J. F. *Angew. Chem. Int. Ed.* 2008, *47* (30), 5666.
(66) Liu, H.; Li, Y.; Sun, K.; Fan, J.; Zhang, P.; Meng, J.; Wang, S.; Jiang, L. *J. Am. Chem. Soc.* 2013, *135* (20), 7603.
(67) Pan, G.; Guo, B.; Ma, Y.; Cui, W.; He, F.; Li, B.; Yang, H.; Shea, K. J. *J. Am. Chem. Soc.* 2014, *136* (17), 6203.
(68) van Dongen, S. F. M.; Maiuri, P.; Marie, E.; Tribet, C.; Piel, M. *Adv. Mater.* 2013, *25* (12), 1687.
(69) Andrews, R. N.; Co, C. C.; Ho, C.-C. *Curr. Opin. Chem. Eng.* 2016, *11*, 28.
(70) Bugga, P.; Mrksich, M. *Curr. Opin. Colloid Interface Sci.* 2018, *38*, 80.
(71) Cui, J.; Miguel, V. S.; del Campo, A. *Macromol. Rapid Commun.* 2012, *34* (4), 310.
(72) Kaneko, S.; Nakayama, H.; Yoshino, Y.; Fushimi, D.; Yamaguchi, K.; Horiike, Y.; Nakanishi, J. *Phys. Chem. Chem. Phys.* 2011, *13* (9), 4051.
(73) Kaneko, S.; Yamaguchi, K.; Nakanishi, J. *Langmuir* 2012, *29* (24), 7300.
(74) Andrews, R. N.; Mun, K.-S.; Scott, C.; Ho, C.-C.; Co, C. C. *J. Mater. Chem. B* 2013, *1* (42), 5773.
(75) Nakanishi, J.; Nakayama, H.; Yamaguchi, K.; García, A. J.; Horiike, Y. *Sci Technol Adv Mater* 2011, *12* (4), 044608.
(76) Rolli, C. G.; Nakayama, H.; Yamaguchi, K.; Spatz, J. P.; Kemkemer, R.; Nakanishi, J. *Biomaterials* 2012, *33* (8), 2409.
(77) Aumailley, M.; Gurrath, M.; Müller, G.; Calvete, J.; Timpl, R.; Kessler, H. *FEBS* 1991, *291* (1), 50.
(78) Gurrath, M.; Müller, G.; Kessler, H.; Aumailley, M.; Timpl, R. *Eur. J. Biochem.* 1992, *210* (3), 911.
(79) Petersen, S.; Alonso, J. M.; Specht, A.; Duodu, P.; Goeldner, M.; del Campo, A. *Angew. Chem. Int. Ed.* 2008, *47* (17), 3192.
(80) Wirkner, M.; Weis, S.; San Miguel, V.; Álvarez, M.; Gropeanu, R. A.; Salierno, M.; Sartoris, A.; Unger, R. E.; Kirkpatrick, C. J.; del Campo, A. *ChemBioChem* 2011, *12* (17), 2623.
(81) Salierno, M. J.; García, A. J.; del Campo, A. *Adv. Funct. Mater.* 2013, *23* (48), 5974.
(82) Weis, S.; Lee, T. T.; del Campo, A.; García, A. J. *Acta Biomater.* 2013, *9* (9), 8059.
(83) Han, K.; Yin, W.-N.; Fan, J.-X.; Cao, F.-Y.; Zhang, X.-Z. *ACS Appl. Mater. Interfaces* 2015, *7* (42), 23679.
(84) Nair, R. V.; Farrukh, A.; del Campo, A. *ChemBioChem* 2018, *19* (12), 1280.
(85) Farrukh, A.; Fan, W.; Zhao, S.; Salierno, M.; Paez, J. I.; del Campo, A. *ChemBioChem* 2018, *19* (12), 1271.
(86) Lee, T. T.; Garcia, J. R.; Paez, J. I.; Singh, A.; Phelps, E. A.; Weis, S.; Shafiq, Z.; Shekaran, A.; del Campo, A.; García, A. J. *Nat Mater* 2014, *14* (3), 352.
(87) Ohmuro-Matsuyama, Y.; Tatsu, Y. *Angew. Chem. Int. Ed.* 2008, *47* (39), 7527.
(88) Muraoka, T.; Koh, C.-Y.; Cui, H.; Stupp, S. I. *Angew. Chem. Int. Ed.* 2009, *48* (32), 5946.
(89) Kloxin, A.; Kasko, A.; Salinas, C.; Ansetz, K. *Science* 2009, *324* (5923), 59.
(90) Wirkner, M.; Alonso, J. M.; Maus, V.; Salierno, M.; Lee, T. T.; García, A. J.; del Campo, A. *Adv. Mater.* 2011, *23* (34), 3907.
(91) Ariyasu, S.; Hanaya, K.; Watanabe, E.; Suzuki, T.; Horie, K.; Hayase, M.; Abe, R.; Aoki, S. *Langmuir* 2012, *28* (36), 13118.
(92) Shin, D.-S.; Hyun Seo, J.; Sutcliffe, J. L.; Revzin, A. *Chem. Commun.* 2011, *47* (43), 11942.

(93) Klán, P.; Šolomek, T.; Bochet, C. G.; Blanc, A.; Givens, R.; Rubina, M.; Popik, V.; Kostikov, A.; Wirz, J. *Chem. Rev.* 2012, *113* (1), 119.
(94) Kadem, L. F.; Holz, M.; Suana, K. G.; Li, Q.; Lamprecht, C.; Herges, R.; Selhuber-Unkel, C. *Adv. Mater.* 2015, *28* (9), 1799.
(95) Ren, T.; Ni, Y.; Du, W.; Yu, S.; Mao, Z.; Gao, C. *Adv. Mater. Interfaces* 2016, *4* (1), 1500865.
(96) Bullock, D. J. W.; Cumper, C. W. N.; Vogel, A. I. *J. Chem. Soc.* 1965, 5316.
(97) Auernheimer, J.; Dahmen, C.; Hersel, U.; Bausch, A.; Kessler, H. *J. Am. Chem. Soc.* 2005, *127* (46), 16107.
(98) Liu, D.; Xie, Y.; Shao, H.; Jiang, X. *Angew. Chem. Int. Ed.* 2009, *48* (24), 4406.
(99) Vaselli, E.; Fedele, C.; Cavalli, S.; Netti, P. A. *ChemPlusChem* 2015, *80* (10), 1547.
(100) Kadem, L. F.; Suana, K. G.; Holz, M.; Wang, W.; Westerhaus, H.; Herges, R.; Selhuber-Unkel, C. *Angew. Chem.* 2016, *129* (1), 231.
(101) Zhang, J.; Ma, W.; He, X.-P.; Tian, H. *ACS Appl. Mater. Interfaces* 2017, *9* (10), 8498.
(102) Gong, Y.-H.; Li, C.; Yang, J.; Wang, H.-Y.; Zhuo, R.-X.; Zhang, X.-Z. *Macromolecules* 2011, *44* (19), 7499.
(103) Wiemann, M.; Niebuhr, R.; Juan, A.; Cavatorta, E.; Ravoo, B. J.; Jonkheijm, P. *Chem. Eur. J.* 2017, *24* (4), 813.
(104) Bian, Q.; Wang, W.; Wang, S.; Wang, G. *ACS Appl. Mater. Interfaces* 2016, *8* (40), 27360.
(105) Shi, P.; Ju, E.; Wang, J.; Yan, Z.; Ren, J.; Qu, X. *Mater. Today* 2017, *20* (1), 16.
(106) Li, W.; Wang, J.; Ren, J.; Qu, X. *J. Am. Chem. Soc.* 2014, *136* (6), 2248.
(107) Yan, Z.; Qin, H.; Ren, J.; Qu, X. *Angew. Chem. Int. Ed.* 2018, *57* (35), 11182.
(108) Li, W.; Chen, Z.; Zhou, L.; Li, Z.; Ren, J.; Qu, X. *J. Am. Chem. Soc.* 2015, *137* (25), 8199.
(109) Giner-Casares, J. J.; Henriksen-Lacey, M.; García, I.; Liz-Marzán, L. M. *Angew. Chem.* 2015, *128* (3), 986.
(110) Gao, X.; Li, Q.; Wang, F.; Liu, X.; Liu, D. *Langmuir* 2018, *34* (28), 8145.
(111) Li, W.; Wang, J.; Ren, J.; Qu, X. *Angew. Chem. Int. Ed.* 2013, *52* (26), 6726.
(112) Cui, H.; Zhang, P.; Wang, W.; Li, G.; Hao, Y.; Wang, L.; Wang, S. *Nano Res.* 2017, *10* (4), 1345.
(113) Wang, X.; Yao, C.; Weng, W.; Cheng, K.; Wang, Q. *ACS Appl. Mater. Interfaces* 2017, *9* (34), 28250.
(114) Ming, Z.; Hua, X.; Xue, Y.; Lin, Q.; Bao, C.; Zhu, L. *Colloids Surf B Biointerfaces* 2018, *169*, 41.
(115) Vining, K. H.; Mooney, D. J. *Nat Rev Mol Cell Biol* 2017, *18* (12), 728.
(116) Yüz, S. G.; Ricken, J.; Wegner, S. V. *Adv. Sci.* 2018, *5* (8), 1800446.
(117) Lyu, S.; Fang, J.; Duan, T.; Fu, L.; Liu, J.; Li, H. *Chem. Commun.* 2017, *53* (100), 13375.
(118) Wang, R.; Yang, Z.; Luo, J.; Hsing, I.-M.; Sun, F. *Proc. Natl. Acad. Sci. U.S.A.* 2017, *114* (23), 5912.
(119) Mühlhäuser, W. W. D.; Fischer, A.; Weber, W.; Radziwill, G. *BBAMCR* 2017, *1864* (2), 280.
(120) Guglielmi, G.; Falk, H. J.; De Renzis, S. *Trends Cell Biol.* 2016, *26* (11), 864.
(121) Möglich, A.; Moffat, K. *Photochem. Photobiol. Sci.* 2010, *9* (10), 1286.
(122) Pudasaini, A.; El-Arab, K. K.; Zoltowski, B. D. *Front. Mol. Biosci.* 2015, *2*, 3129.
(123) Losi, A.; Gardner, K. H.; Möglich, A. *Chem. Rev.* 2018, 1.
(124) Ortiz-Guerrero, J. M.; Polanco, M. C.; Murillo, F. J.; Padmanabhan, S.; Elías-Arnanz, M. *PNAS* 2011, *108* (18), 7565.
(125) Jost, M.; Fernández-Zapata, J.; Polanco, M. C.; Ortiz-Guerrero, J. M.; Chen, P. Y.-T.; Kang, G.; Padmanabhan, S.; Elías-Arnanz, M.; Drennan, C. L. *Nature* 2015, *526* (7574), 536.
(126) Hardman, S. J. O.; Johannissen, L. O.; Bellina, B.; Messiha, H. L.; Ortiz-Guerrero, J. M.; iacute as-Arnanz, El, M.; Padmanabhan, S.; Barran, P.; Scrutton, N. S.; Kutta, R. J.; Jones, A. R. *Nat. Commun.* 2016, *6*, 1.
(127) Kainrath, S.; Stadler, M.; Reichhart, E.; Distel, M.; Janovjak, H. *Angew. Chem.* 2017, *129* (16), 4679.
(128) Harper, S. M.; Neil, L.; Gardner, K. H. *Science* 2003, *301*, 1541.
(129) Strickland, D.; Moffat, K.; Sosnick, T. R. *PNAS* 2008, *105* (31), 10709.
(130) Renicke, C.; Schuster, D.; Usherenko, S.; Essen, L.-O.; Taxis, C. *Chem. Biol.* 2013, *20* (4), 619.
(131) Bonger, K. M.; Rakhit, R.; Payumo, A. Y.; Chen, J. K.; Wandless, T. J. *ACS Chem. Biol.* 2013, *9* (1), 111.
(132) Wong, S.; Mosabbir, A. A.; Truong, K. *PLoS ONE* 2015, *10* (8), e0135965.
(133) Jones, D. C.; Mistry, I. N.; Tavassoli, A. *Mol. BioSyst.* 2016, *12* (4), 1388.
(134) Yumerefendi, H.; Dickinson, D. J.; Wang, H.; Zimmerman, S. P.; Bear, J. E.; Goldstein, B.; Hahn, K.; Kuhlman, B. *PLoS ONE* 2015, *10* (6), e0128443.
(135) Niopek, D.; Benzinger, D.; Roensch, J.; Draebing, T.; Wehler, P.; Eils, R.; Di Ventura, B. *Nat. Commun.* 2014, *5*, 1.
(136) Niopek, D.; Wehler, P.; Roensch, J.; Eils, R.; Di Ventura, B. *Nat. Commun.* 2016, *7*, 1.
(137) Yumerefendi, H.; Lerner, A. M.; Zimmerman, S. P.; Hahn, K.; Bear, J. E.; Strahl, B. D.; Kuhlman, B. *Nat. Chem. Biol.* 2016, *12* (6), 399.

(138) Di Ventura, B.; Kuhlman, B. *Curr. Opin. Chem. Biol.* 2016, *34*, 62.
(139) Spiltoir, J.; Strickland, D.; Glotzer, M.; Tucker, C. *ACS Synth. Biol.* 2015, *5* (7), 1554.
(140) Strickland, D.; Lin, Y.; Wagner, E.; Hope, C. M.; Zayner, J.; Antoniou, C.; Sosnick, T. R.; Weiss, E. L.; Glotzer, M. *Nat Meth* 2012, *9* (4), 379.
(141) van Bergeijk, P.; Adrian, M.; Hoogenraad, C. C.; Kapitein, L. C. *Nature* 2015, *518* (7537), 111.
(142) Wagner, E.; Glotzer, M. *J Cell Biol* 2016, *213* (6), 641.
(143) Oakes, P. W.; Wagner, E.; Brand, C. A.; Probst, D.; Linke, M.; Schwarz, U. S.; Glotzer, M.; Gardel, M. L. *Nat. Commun.* 2017, *8*, 15817.
(144) Witte, K.; Strickland, D.; Glotzer, M. *eLife* 2017, 1.
(145) Wood, L. A.; Larocque, G.; Clarke, N. I.; Sarkar, S.; Royle, S. J. *J Cell Biol* 2017, *216* (12), 4351.
(146) Liao, Z.; Kasirer-Friede, A.; Shattil, S. J. *J. Cell Sci.* 2017, *130* (20), 3532.
(147) Strickland, D.; Lin, Y.; Wagner, E.; Hope, C. M.; Zayner, J.; Antoniou, C.; Sosnick, T. R.; Weiss, E. L.; Glotzer, M. *Nat Meth* 2012, *9* (4), 379.
(148) Lungu, O. I.; Hallett, R. A.; Choi, E. J.; Aiken, M. J.; Hahn, K. M.; Kuhlman, B. *Chem. Biol.* 2012, *19* (4), 507.
(149) Zimmerman, S. P.; Hallett, R. A.; Bourke, A. M.; Bear, J. E.; Kennedy, M. J.; Kuhlman, B. *Biochem.* 2016, *55* (37), 5264.
(150) Guntas, G.; Hallett, R. A.; Zimmerman, S. P.; Williams, T.; Yumerefendi, H.; Bear, J. E.; Kuhlman, B. *Proceedings of the National Academy of Sciences* 2015, *112* (1), 112.
(151) Hallett, R. A.; Zimmerman, S. P.; Yumerefendi, H.; Bear, J. E.; Kuhlman, B. *ACS Synth. Biol.* 2016, *5* (1), 53.
(152) Birch, D. J. S.; Yip, P. In *Fluorescence Spectroscopy and Microscopy: Methods and Protocols*; Engelborghs, Y., Visser, A. J. W. G., Eds.; Fluorescence Spectroscopy and Microscopy: Methods and Protocols; Humana Press: Totowa, NJ, 2014; pp 279–302.
(153) Lakowicz, J. R. In *Principles of Fluorescence Spectroscopy*; Fluorescence Anisotropy; Boston, 2006.
(154) Mart, R. J.; Meah, D.; Allemann, R. K. *ChemBioChem* 2015, *17* (8), 698.
(155) ONeill, P.; Kalyanaraman, V.; Gautam, N. 2016, *27*, 1442.
(156) Zimmerman, S. P.; Asokan, S. B.; Kuhlman, B.; Bear, J. E. *J. Cell Sci.* 2017, *130* (18), 2971.
(157) Ji, C.; Fan, F.; Lou, X. *CellReports* 2017, *20* (6), 1409.
(158) Ma, G.; Liu, J.; Ke, Y.; Liu, X.; Li, M.; Wang, F.; Han, G.; Huang, Y.; Wang, Y.; Zhou, Y. *Angew. Chem. Int. Ed.* 2018, *57* (24), 7019.
(159) Bartelt, S. M.; Chervyachkova, E.; Steinkühler, J.; Ricken, J.; Wieneke, R.; Tampé, R.; Dimova, R.; Wegner, S. V. *Chem. Commun.* 2018, *54* (8), 948.
(160) Chervyachkova, E.; Wegner, S. V. *ACS Synth. Biol.* 2018, *7* (7), 1817.
(161) Wang, H.; Vilela, M.; Winkler, A.; Tarnawski, M.; Schlichting, I.; Yumerefendi, H.; Kuhlman, B.; Liu, R.; Danuser, G.; Hahn, K. M. *Nat Meth* 2016, *13* (9), 755.
(162) van Haren, J.; Charafeddine, R. A.; Ettinger, A.; Wang, H.; Hahn, K. M.; Wittmann, T. *Nat Cell Biol* 2018, *20* (3), 252.
(163) Dagliyan, O.; Tarnawski, M.; Chu, P.-H.; Shirvanyan, D.; Schlichting, I.; Dokholyan, N.; Hahn, K. M. *Science* 2016, *354* (6318), 1441.
(164) Wu, Y. I.; Frey, D.; Lungu, O. I.; Jaehrig, A.; Schlichting, I.; Kuhlman, B.; Hahn, K. M. *Nature* 2009, *461* (7260), 104.
(165) Wang, X.; He, L.; Wu, Y. I.; Hahn, K. M.; Montell, D. J. *Nat Cell Biol* 2010, *12* (6), 591.
(166) *Product Datasheet: Anti-6X His tag® antibody*; Catalog number: Chip Grade ab9108; 2018; pp 1–4.
(167) *Product Datasheet: Recombinant Human Integrin α*; Catalog Number: 3050-V; 2018; pp 1–1.
(168) Renicke, C.; Schuster, D.; Usherenko, S.; Essen, L.-O.; Taxis, C. *Chem. Biol.* 2013, *20* (4), 619.
(169) Niopek, D.; Benzinger, D.; Roensch, J.; Draebing, T.; Wehler, P.; Eils, R.; Di Ventura, B. *Nat. Commun.* 2014, *5* (1), 4404.
(170) Zimmerman, S. P.; Kuhlman, B.; Yumerefendi, H. *Chapter Eight Engineering and Application of LOV2-Based Photoswitches*; 2016; Vol. 580, pp 169–190.
(171) He, L.; Jing, J.; Zhu, L.; Tan, P.; Ma, G.; Zhang, Q.; Nguyen, N. T.; Wang, J.; Zhou, Y.; Huang, Y. *Chemical Science* 2017, *00*, 1.
(172) Strickland, D.; Yao, X.; Gawlak, G.; Rosen, M. K.; Gardner, K. H.; Sosnick, T. R. *Nat Meth* 2010, *7* (8), 623.
(173) Hautanen, A.; Gailit, J.; Mann, D. M.; Ruoslahti, E. *J. Biol. Chem.* 1989, *264* (3), 1437.
(174) Kawano, F.; Aono, Y.; Suzuki, H.; Sato, M. *PLoS ONE* 2013, *8* (12), e82693.
(175) Swartz, T.; Corchnoy, S.; Christie, J. M.; Lewis, J. W.; Szundi, I.; Briggs, W. R.; Bogomolni, R. A. *J. Biol. Chem.* 2001, 1.
(176) Salomon, M.; Christie, J. M.; Knieb, E.; Lempert, U.; Briggs, W. R. *Biochem.* 2000, No. 39, 9401.

(177) Zayner, J. P.; Antoniou, C.; Sosnick, T. R. *J. Mol. Biol.* 2012, *419* (1), 61.
(178) García, A. J.; Schwarzbauer, J. E.; Boettiger, D. *Biochem.* 2002, *41* (29), 9063.
(179) Redick, S.; Settles, D.; Briscoe, G.; Erickson, H. *J Cell Biol* 2000, *149* (2), 521.
(180) Ramos, J.; DeSimone, D. *J Cell Biol* 1996, 227.
(181) Bartelt, S. M.; Chervyachkova, E.; Steinkühler, J.; Ricken, J.; Wieneke, R.; Tampé, R.; Dimova, R.; Wegner, S. V. *Chem. Commun.* 2018, *54* (8), 948.
(182) Lock, S.; Friend, J. *Fd Chem. Toxic.* 1986, *24* (6/7), 789.
(183) Kuse, Y.; Ogawa, K.; Tsuruma, K.; Shimazawa, M.; Hara, H. *Sci. Rep.* 2014, *4*, 5223.
(184) Magidson, V.; Khodjakov, A. *Methods Cell Biol.* 2013, *114*, 545.
(185) Mould, A. P.; Askari, J.; Yamada, K.; Irie, A.; Takada, Y.; Mardon, H. J.; Humphries, M. J. *J. Biol. Chem.* 1997, *272* (28), 17283.
(186) Kong, F.; García, A. J.; Mould, A. P.; Humphries, M. J.; Zhu, C. *J Cell Biol* 2009, *185* (7), 1275.
(187) Brennan, J. R.; Hocking, D. C. *Acta Biomater.* 2016, *32*, 198.
(188) Gee, E. P. S.; Ingber, D. E.; Stultz, C. M. *PLoS ONE* 2008, *3* (6), e2373.
(189) Smith, M. A.; Blankman, E.; Gardel, M. L.; Luettjohann, L.; Waterman, C. M.; Beckerle, M. C. *Dev. Cell.* 2010, *19* (3), 365.
(190) Gallant, N.; Michael, K.; García, A. J. *Mol. Biol. Cell* 2005, *16*, 4329.
(191) Hong, S.; Ergezen, E.; Lec, R.; Barbee, K. A. *Biomaterials* 2006, *27* (34), 5813.
(192) Huang, J.; Gräter, S. V.; Corbellini, F.; Rinck, S.; Bock, E.; Kemkemer, R.; Kessler, H.; Ding, J.; Spatz, J. P. *Nano Lett.* 2009, *9* (3), 1111.

List of Figures

List of Tables

Acronyms

AdoCbl	Vitamin B12
AFM	Atomic Force microscopy
C2C12 cells	Myogenic stem cells
CD	Cyclodextrins
CIBN	CRY-interaction basic helix-loop-helix protein 1
CRY	Cryptochrome
ECM	Extracellular matrix
ePDZ	Engineered PDZ domain
FA	Focal Adhesion
FAK	Focal adhesion kinase
FBS	Fetal bovine serum
FMN	Flavin mononucleotide
GTP	Guanosine triphosphate
GUVs	Giant unilamellar vesicles
HEK cells	Human embryonic kidney cells
HUVEC	Human umbilical vein endothelial cells
ICAMs	Intercellular adhesion molecules
iLID	Improved light-inducible dimers
LOV 2	Light-oxygen voltage domain 2
MCF7	Michigan cancer foundations cells
MEF	Mouse embryonic fibroblasts
mFGFR1	Murine fibroblast growth factor receptor 1
MSCs	Mesenchymal stem cells
MWCO	Molecular weight cut-off
NES	Nuclear export sequences
NIR	Near infrared light

NLS	Nuclear localization sequence
NTA	Nitrilotracetic acid
oLID	Original light-inducible dimer
PAK	P21-activated kinase
PAS	Per-ARNT-Sim
PCR	Polymerase Chain Reaction
PEG	Poly(ethylene)glycol
PHSRN	Pro-His-Ser-Arg-Asp
Phy B	Phytochrome B
PIF 6	Phytochrome interaction factor 6
PLA	Polylactic acid
PNIPAM	Poly(N-isopropylacrylamide)
REDV	Arg-Glu-Asp-Val
RGD	Arg-Gly-Asp
RT	Room temperature
SAM	Self-assembled monolayer
TrpR	Transcription factor repressor
TULIP	Tunable, light-controlled interacting protein tag
U-2 OS cells	Human osteosarcoma cells
UCNP	Upconverting nanoparticles
UV	Ultra violet

Publication List

- S. M. Bartelt, E. Chervyachkova, J. Steinkühler, J. Ricken, R. Wieneke, R. Tampé, S. V. Wegner, Dynamic blue light-switchable protein patterns on giant unilamellar vesicles. In: ***Chem. Commun.***, 2018, **54**, 948-951. DOI: 10.1039/c7cc08758f
- Simge G. Yüz, J. Ricken, S. V. Wegner, Independent Control over Mutiple Cell Types in Space and Time Using Orthogonal Blue and Red Light Switchable Cell Interactions. In: **Adv. Sci**. 2018, **5**, 1800446. DOI: 10.1002/advs.201800446
- F. Chen, J. Ricken, S. V. Wegner, Bacterial Photolithography: Patterning biofilms with high spatiotemporal control using photocleavable adhesion molecules. Accepted **Adv. Biosys.** 2018.
- W. Ye; M. Goetz, S. Celiksoy, L. Tueting, C. Ratzke, J. Prasad, J. Ricken, S. V: Wegner, R. Ahijado-Guzmán, T. Hugel, C. Sönnichsen. Conformational Dynamics of a Single Protein Monitored for 24 Hours at Video Rate. In: **NanoLett.** 2018. DOI: 10.1021/acs.nanolett.8b03342
- J. Ricken, R. Medda, S. V. Wegner, Photo-ECM: A Blue Light Photoswitchable Synthetic Extracellular Matrix Protein for Reversible Control over Cell-Matrix Adhesion. Submitted.
- J. Ricken, S. Bartelt, E. Chervyachkova, S. V. Wegner, Photoswitchable Cell Adhesion. In preparation.
- J. Ricken, S.V. Wegner, A green light cleavable protein to capture and release cells on command. In preparation.

Conference Contributions

- Chemical Biology 2018, poster: "Cell-Matrix Adhesion Mediated By LOV2 Protein Mutants".
- 5th Heidelberg Forum of Young Life Scientists „A Tale of Cells and Organisms" 2017, poster: "Cell-Matrix Adhesion Mediated By LOV2 Protein Mutants"
- Chemical Biology 2016, shared poster with Dr. Simge Yüz: "Reversible Control of Cell Adhesion with Photoswitchable Proteins".
- Embo Non-neuronal optogenetic workshop 2016, flash talk and poster: "Photoswitchable Cell Adhesion Mediated by LOV2 Protein Mutants".
- Kármán Conference 2015, poster: "Photoswitchable Cell Adhesion Mediated by LOV2 Protein Mutants"

EIDESSTATTLICHE VERSICHUNG GEMÄSS §8 DER PROMOTIONSORDNUNG DER NATURWISSENSCHAFLICH-MATHEMATISCHEN GESAMTFAKULTÄT DER UNIVERSITÄT HEIDELBERG

---

1. Bei der eingereichten Dissertation zu dem Thema Photo-Switchable Proteins for Cell-Matrix Adhesion handelt es sich um meine eigenständig erbrachte Leistung.

2. Ich habe nur die angegebenen Quellen und Hilfsmittel benutzt und mich keiner unzulässigen Hilfe Dritter bedient. Insbesondere habe ich wörtliche oder sinngemäß aus anderen Werken übernommene Inhalte als solche kenntlich gemacht.

3. Die Arbeit oder Teile davon habe ich bislang nicht an einer Hochschule des In- oder Auslandes als Bestandteil einer Prüfungs- oder Qualifikationsleistung vorgelegt.

4. Die Richtigkeit der vorstehenden Erklärung bestätige ich.

5. Die Bedeutung der eidesstattlichen Versicherung und die strafrechtlichen Folgen einer unrichtigen oder unvollständigen eidesstattlichen Versicherung sind mir bekannt.

   Ich versichere an Eides statt, dass ich nach bestem Wissen die reine Wahrheit erklärt und nichts verschwiegen habe.

Heidelberg, November 2018

Julia Ricken